Appendix 1. Additional Information

Table of Contents

# Appendix A. Conductivity of Graphene

Conductivity refers to the ability of a material to conduct electric current. The mechanism of conductivity varies depending on whether the material is a metal, or non-metal (semiconductor, insulator, or electrolyte).

Metals are known for their high electrical conductivity, a property that allows them to efficiently conduct electric current.[1] In case of a metal, the outer electrons of atoms are not tightly bound to the individual atoms but are instead free to move throughout the material. The exceptional conductivity can be attributed to the free movement of electrons within the metallic structure. Since the electrons are delocalized, they can move freely throughout the material. This free movement of electrons facilitates the easy flow of electric charge, making metals excellent conductors. However, when an electric field is applied (i.e., when voltage is applied across a metal), these free electrons drift in response to the field, creating an electric current.

Nonmetals, on the other hand, generally exhibit poor electrical conductivity. This is primarily due to their atomic structure. Unlike metals, nonmetals do not have a delocalized electron sea. Instead, electrons in nonmetals are tightly bound to their respective atoms, limiting their ability to move freely. As a result, nonmetals impede the flow of electric current and are considered semiconductors or insulators. However, semiconductors have an intermediate level of conductivity between conductors (like metals) and insulators (non-conductive materials), which can be altered by introducing impurities through a process called doping.[2] Doping introduces additional charge carriers (either electrons or "holes" where electrons are missing) into the semiconductor material.[3] In the presence of an electric field, these charge carriers move, contributing to the electric current. The mobility of charge carriers in semiconductors is influenced by factors such as temperature and the concentration of impurities. On the other hand, insulators are materials that do not conduct electricity easily. The electrons are tightly bound to atoms, and there are only few free charge carriers. When an electric field is applied, very little current flows through insulators.[4] When the electric field becomes strong enough (exceeds the material's dielectric strength), insulators can undergo electrical breakdown starting to conduct. Electrolytes are materials that conduct electricity through the movement of ions. Ions are charged particles that can be positively or negatively charged. In an electrolyte solution, ions are free to move in response to an applied electric field. Positive ions (cations) move toward the negative electrode (cathode), and

negative ions (anions) move toward the positive electrode (anode). The movement of ions constitutes the flow of electric current in electrolytes.[5] In summary, metals rely on the free movement of electrons, semiconductors use doped charge carriers, and electrolytes involve the movement of ions. Insulators, on the other hand, generally resist the flow of electric current.
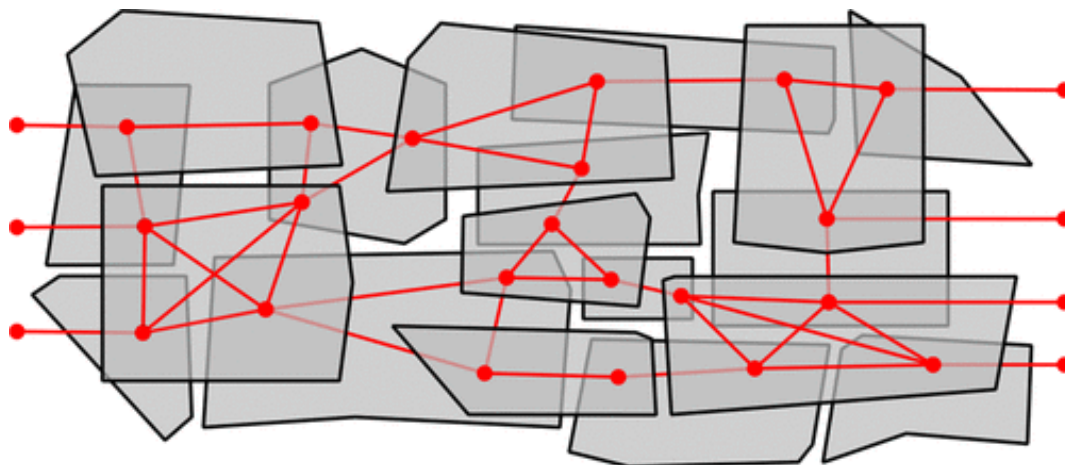
Figure A.1. Top-view schematics of the two layers of graphene flakes and the resulting network graph. Nodes are positioned at overlaps and connected through graphene flakes. Reproduced with permission.[6] Copyright 2018, American Chemical Society.

However, there are exceptions, and some nonmetals can conduct electricity under specific conditions. For instance, graphite, a form of carbon, can conduct electricity due to its unique layered structure that allows electrons to move along the planes. Macroscopic graphene can outperform copper in electrical conductivity. Literature suggests that there are two main parameters to obtain a high electrical conductivity for macroscopic graphene. It is crucial to have a high in-plane electrical conductivity in most of the graphene flakes. The value for the in-plane electrical conductivity determines the maximum possible conductivity. Of course, it is also necessary to reach a reasonable out-of-plane electrical conductivity. Nevertheless, the lateral size of graphene flakes compensates a lower out-of-plane conductivity to a certain extent due to the larger overlap area and the lower contact resistance. Rizzi et al.[6] proposed a network model to investigate the electrical characteristics of layered graphene relying on their microscopic properties to compute the macroscopic electrical conductivity. Graphene flakes were modelled as polygons to reproduce the shape of actual graphene flakes produced by liquid exfoliation. A proper edge-to-edge contact between flakes within the same layer is highly unlikely because of the production methods and would have a negligible effect

compared to that of overlapping flakes. For each overlap, a node is created in the corresponding flakes. Nodes that belong to the same overlap or share the same graphene flake are connected (Figure A.1).

Appendix B. Electrochemical performances of supercapacitor

A series of key parameters, and various techniques are used for the evaluation of the electrochemical performance of a SC. Among them, widely used techniques are: Cyclic voltammetry (CV), galvanostatic charge/ discharge (GCD), and electrochemical impedance spectroscopy (EIS). Three fundamental parameters (voltage, current, and time) for SC can be measured by all these techniques. Additionally, other SC performance metrics including capacitance, equivalent series resistance, operating voltage, time constant, energy and power performance can be derived from those parameters.

B.1 Cyclic voltammetry (CV)
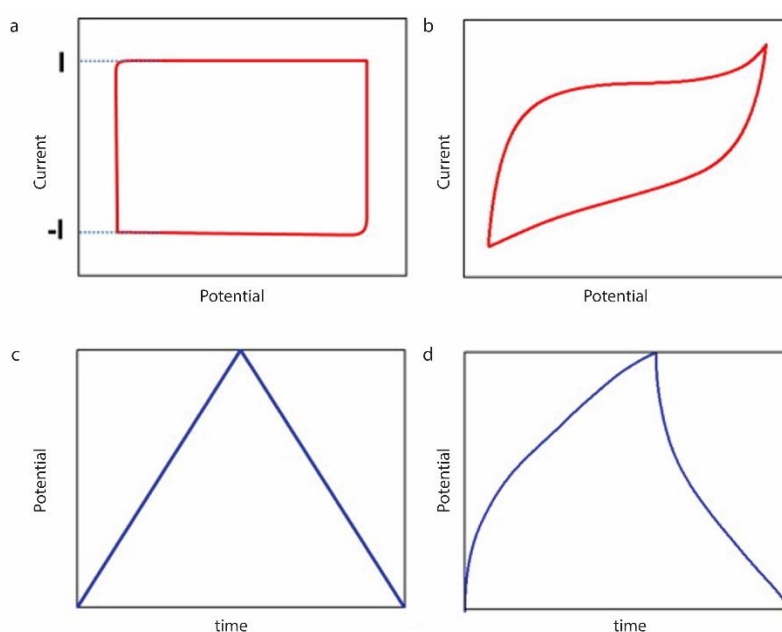
Figure B.1. Typical characterisation parameters of supercapacitors a) CV curves c) GCD curves for ideal supercapacitor; b) CV and d) GCD curve distortion due to faradaic reactions[7]

CV is a powerful and popular electrochemical technique commonly employed to investigate the reduction and oxidation processes of molecular species.[8] Such technique is used to study the electrochemical properties related to electroactive surfaces, and characterize the electrode materials primarily.[9, 10] In this technique, a linearly changed electric potential is applied against time to measure the current. The graphical analysis of a cyclic voltammogram provides redox peaks (reduction and oxidation peaks of the material) and predicts the capacitive behaviour of the electrode. Therefore, the potential at which the material is oxidized and reduced can be found in this technique.[11, 12] A typical cyclic voltammogram for an electrochemically reversible and diffusion-controlled redox process is shown in *Figure*

B.1a. The curves obtained through CV for both EDLCs and pseudocapacitors are evaluated to measure the capacitance (C) of the material deposited over the electrode by using Equation (1). The shape of the resulting CV curves for an ideal SC is rectangular. However, the variation in the shape and size of the plot can occur when the deposited materials over the electrode are dissolved into the electrolyte. It can also happen due to the detachment of the electrode contacts during cyclic repetition, *Figure B.1b*.[13] The gravimetric capacitance (Equation (4)), lengthwise capacitance (Equation (6)), areal capacitance (Equation (8)), volumetric capacitance (Equation (10)), energy density (Equation (12)) of the electrode or total SC cell can be obtained *via* integration of CV curves.[11]

B.2 Galvanostatic charge discharge (GCD)

GCD test is considered as the most accurate and versatile approach, and most widely used method for the capacitance assessment (Equation (2)).[13] The direct current at a constant level is imparted in this method for repetitive charging and discharging of the SC device or the working electrode. A potential *Vs* time plot is obtained from this method, **Figure c**. Additionally, the cyclic stability of SC devices can be studied from GCD. The symmetric curves obtained from the charge discharge through GCD confirms the capacitive behaviour of the device, enlightening capacitance as the function of applied voltage. Additionally, gravimetric capacitance (Equation (5)), lengthwise capacitance (Equation (7)), areal capacitance (Equation (9)), and volumetric capacitance (Equation (11)) for SC materials can also be obtained *via* GCD.[11]

Table B.1. Technical merits and demerits of the CV, GCD, and EIS techniques[13, 14]

Techniques	CV	GCD	EIS
Principle	CV is varying the potential against time and measuring the current	GCD is applying a positive or negative current against time and measuring the voltage	Measuring impedance of a power cell as a function of frequency by applying alternating current (AC)
Merits	- Degradation process - Specific capacitance - Differentiate	- Capacitance calculation - Differentiate between EDL and PC	- Resistance calculation - Specific capacitance calculation - Differentiate between resistive and inductive

			nature
			• Nondestructive technique
			• Relaxation time for recharging
			• Exhibit Degradation behavior
Demerits	• Show only kinetic aspects; thermodynamic aspect is neglected	• Exhibit same triangular shape for all double layer capacitive materials	• Evaluation at small voltage only • Discrete behavior above 10^6 Hz

B.3 Electrochemical impedance spectroscopy (EIS)

EIS, an electroanalytical method, measures the impedance of a power cell as a function of frequency by applying the alternating current (AC) instead of the direct current (DC). The fundamental approach of EIS is the application of a spectrum of small-amplitude sinusoidal AC voltage excitations to the system. The frequency of the AC signal is varied, and the overall impedance of the cell is recorded as a function of frequency. The resulting data are usually expressed graphically in two types of plots: a) the Nyquist plot, which shows imaginary *Vs* real impedance at different frequencies, and b) the Bode plot, which shows absolute impedance *Vs* frequency. For SC materials, EIS testing can be used to study the impedance, charge transfer, mass transport, and charge storage mechanisms as well as to estimate the capacitance (Equation (3)), energy, and power properties.[10, 11] A summary of technical merits and demerits of several characterization techniques are presented in *Table* .

B.4 Key metrics for supercapacitor performances

The key parameters used to evaluate the electrochemical performances of a SC are capacitance, operating voltage, equivalent series resistance, power density, energy density, and time constant. Capacitance is defined as the ratio of the charge stored (or separated) to the potential difference between the conductors.[15] The total charge storage ability of a SC device is termed as the capacitance, which is calculated from the formula stated in **Table B.2** ((*Equation (1)-(3)*). It is noteworthy that, while specifying the capacitance of SC, a more intrinsic specific capacitance is measured in terms of the mass of the electroactive materials or length, area and/or volume of the SC device (*Equation 4-11*). The other two important

parameters for evaluating SC performances are: energy density and power density. Energy density, derived from the *Equation (12)*, denotes the amount of energy that can be delivered from a SC. The power density denotes how faster the energy can be delivered by a SC and can be calculated from the *Equation (13), Equation (14)* or *Equation (15)*.

Table B.2. Key metrics used for the characterization of a supercapacitor

Parameters (Unit)	Information obtained	Measurement formula	Equation
Capacitance (F)	Ability to collect and store energy in the form of electrical charge	$C = \dfrac{\int IdV}{V}$ $C = \dfrac{i\,\Delta V}{\Delta t}$ $2\pi C = \dfrac{d\,(-Z'')}{d\left(\frac{1}{f}\right)}$	Equation 1 Equation 2 Equation 3
Gravimetric capacitance (F g^{-1})	Charge storage ability per unit mass	$C_m = \dfrac{A}{2\,s\,m\,V}$ $C_m = \dfrac{i\,\Delta t}{m\,\Delta V}$	Equation 4 Equation 5
Lengthwise capacitance (F cm^{-1})	Charge storage ability per unit length	$C_l = \dfrac{A}{2\,s\,l\,V}$ $C_l = \dfrac{i\,\Delta t}{l\,\Delta V}$	Equation 6 Equation 7
Areal capacitance (F cm^{-2})	Charge storage ability per unit area	$C_A = \dfrac{A}{2\,s\,a\,V}$ $C_A = \dfrac{i\,\Delta t}{a\,\Delta V}$	Equation 8 Equation 9
Volumetric capacitance (F cm^{-3})	Charge storage ability per unit volume	$C_v = \dfrac{A}{2\,s\,v\,V}$ $C_v = \dfrac{i\,\Delta t}{V\,\Delta V}$	Equation 10 Equation 11
Energy density (Wh kg^{-1})	Amount of energy able to deliver	$E = \frac{1}{2}CV^2 = \dfrac{QV}{2}$	Equation 12
Power density (W kg^{-1})	How faster the energy to deliver	$P = VI$ $P = \dfrac{E}{t}$ $P = \dfrac{V^2}{4\,R}$	Equation 13 Equation 14 Equation 15
Coulombic efficiency	Reversible capacity	$\%E = \dfrac{C_{charging}}{C_{discharging}} \times 100$	Equation 16

[C= capacitance, I= current density, V= voltage window, i=discharging current, Δv=discharge voltage, Δt= discharge time, −Z" = imaginary part of the impedance, A= integrated area of the CV curve, s= scan rate (mV s^{-1}), m= mass of the electroactive material on both electrodes, l=length of the electrode, v=volume of the SC, R= resistance]
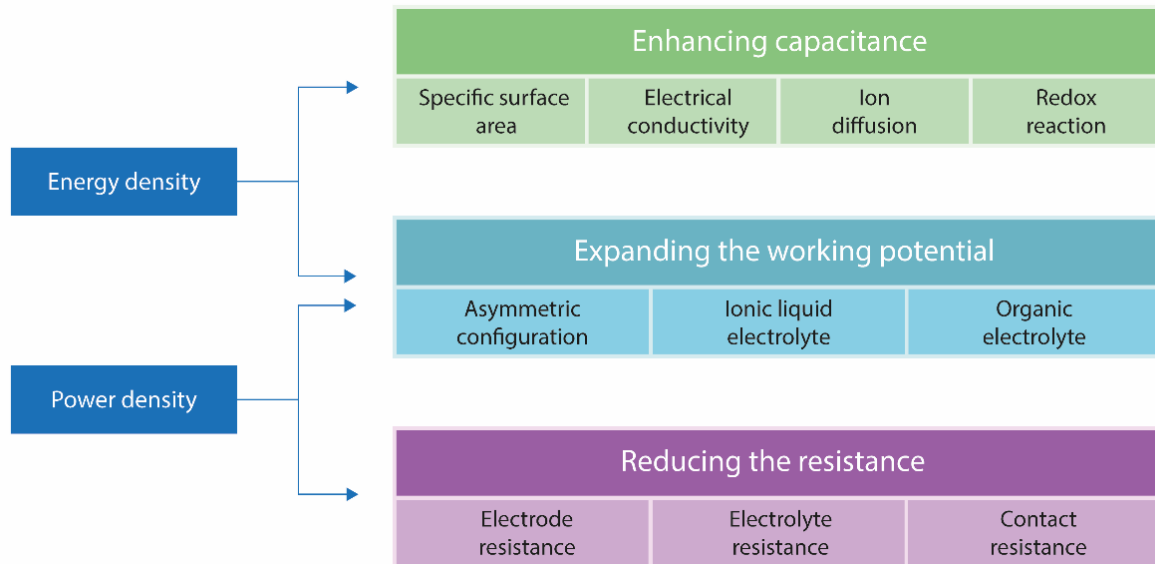
Figure B.2. Approaches for enhancing energy and power densities of supercapacitor[16]

Among the performance metrics for all kinds of energy storage and conversion systems, power density and energy density are the most often used parameters for their performance evaluation for all kind of applications. Compared to batteries, SCs suffer from lower energy density.[17] The energy density depends on the capacitance and working voltage window (V). Therefore, increasing the capacitance or extending operating voltage window will enhance the energy density of a SC. Power density depends on their working voltage window (V) and internal resistance (R). Therefore, in addition to extending the working voltage window, one of the ways to increase the power density is by the reduction of internal resistances of SC components. *Figure B.2* summarizes the approaches to improve the energy and power density of SCs.[16] Additionally, the long cycle life of SC devices is one of the highly desirable characteristics for certain applications. However, the cycle life, when extremely long, is difficult to measure directly. Therefore, the capacitance retention rate is used as an indirect measurement to estimate the cycle life of a SC. By comparing the capacitance after given thousands of cycles with that of the first cycle in GCD test, the capacitance retention value is obtained.[11]

Appendix C. Various type of electrolytes for supercapacitors

C.1. Aqueous electrolytes

The aqueous electrolytes can be categorized into three types: acidic solution (i.e., H_2SO_4 solution), alkaline solution (i.e., KOH solution), and neutral solution (i.e., Li_2SO_4, Na_2SO_4, or KCl solution). Due to high ionic conductivity of acidic aqueous electrolytes, SC electrode materials show better performance in comparison with the neutral aqueous electrolytes.[18] They get dissolved in water, providing high ionic conductivity, and low internal resistance compared with organic electrolytes. Therefore, SCs with an aqueous electrolyte solution may possess a higher capacitance and power than capacitors containing organic electrolytes. The maximum working voltage of aqueous electrolyte is limited to 1.23 V owing to the thermodynamic decomposition of water. In addition, they can be prepared and employed without much tight control of the production process, whereas organic electrolytes require strict preparation procedures to obtain pure electrolytes. Commonly used aqueous electrolytes are inorganic salts (e.g., $LiCl$, $NaCl$) (for Li-ion & SCs), alkali (e.g., KOH) and inorganic acid (e.g., H_2SO_4) in water (for SCs).

C.2 Organic electrolytes

Organic electrolytes allow a much wider voltage window of about 3.5 V resulting in a large advantage with respect to higher energy density. Among the organic electrolytes, propylene carbonate (PC) is the most used solvent, because of their environmentally friendly nature and a wide voltage window with good conductivity. The complex purification and preparation procedures may cause safety problems due to the flammability and toxicity of some of the organic solvents. Furthermore, their low conductivity could lead to lower power and smaller capacitance. Several combinations of organic solvents and lithium salts have been examined as electrolytes for ambient-temperature, rechargeable lithium batteries.[19] Inorganic or organic salts e.g. Lithium hexafluorophosphate ($LiPF_6$); Tetraethylammonium tetrafluoroborate (TEABF4) in organic solvents (carbonates, ethers, sulfones, etc., some of which may be fluorinated) are the common examples of organic electrolytes for SCs.

C.3 Ionic liquids

Ionic liquids (ILs) are salts having uncommonly low melting points, below 100°C, which is usually liquid at room temperature.[20] They are inherent and competitive electrolytes due to their ability to overcome many disadvantages of the conventional aqueous and organic electrolytes,[21] for instance volatility, high thermal and chemical stability, extensive electrochemical stability window between 2 and 6 V, low flammability, nontoxicity and the

wide variety of cation and anion combinations. They are composed entirely of ions, solvent-free and liquids at room temperature, making them attractive "green electrolytes". They are usually highly viscous liquids with low ionic conductivity at ambient temperatures, seriously influencing their electrochemical performance. Salts in ILs (for Li-ion batteries) or pure ILs (for SCs); organic cations (e.g., imidazolium, pyridinium, pyrrolidinium, etc.) with inorganic or organic anions (e.g., H_2SO_4) in water (for SCs) are commonly used ionic liquids.

C.4 Polymer electrolytes

In order to meet the safety (for instance the leakage, flammability and toxicity of organic electrolytes), flexibility and multi-functionality requirements for advanced energy-storage devices (ESDs), polymer electrolytes are considered to be the best candidate to replace liquid electrolytes due to their wide electrochemical window, good thermal stability and less risk with electrolyte solution leakage.[22]

C.4.1 Dry solid polymer electrolytes (Polymer-salt complex electrolytes)

A solid polymer electrolyte is prepared by dissolving inorganic salts into a polar functional polymer, which form a solid electrolyte with ion conducting after drying. With interactions between metal ions and polar groups inside the polymers, electrostatic forces are generated due to the formation of coordinating bonds. Since the coordination of cations to align along the polymer chain is weak, after applying an electric field the cations in the electrolyte may migrate from one coordinated site to another. Various polymers are used to form dry and solid polymer electrolytes including polycarbonate, poly (methyl methacrylate) (PMMA), poly (ethylene oxide) (PEO) and poly (vinyl alcohol) (PVA). For metal ions, various soluble compounds, such as salts containing lithium (Li), sodium (Na) and potassium (K) can be used. Nevertheless, the room ionic conductivities of SPEs ($10^{-8} \sim 10^{-5}$ S cm^{-1}) are lower than the required conductivity of 10^{-3} S cm^{-1} in actual application, limiting their wide practical applications.[22]

C.4.2 Gel polymer electrolytes

The gel polymer electrolytes possess a higher ionic conductivity at room temperature. It has attracted research attention because of the combination of the advantages of high ionic conductivity of liquid-based electrolytes, and the high stability of solid-based electrolytes. This combination superiority is embodied in high ionic conductivity and good interfacial properties from the liquid phase as well as good mechanical properties from the solid component. They are safer to use compared to liquid-based electrolytes. The majority of

GPEs exhibit outstanding ionic conductivity in the order of 10^{-3} S cm^{-1} at ambient temperature, which can boost the electrochemical performance of the cells involving GPEs. Consequently, GPEs have become one of the most desirable alternatives for the fabrication of advanced ESDs with enhanced safety and flexibility.[23, 24]

C.4.3 Plasticized polymer electrolytes

A host polymer with lower molecular weight like poly(ethylene glycol) (PEG), propylene carbonate and ethylene carbonate is used to produce plasticized polymer electrolytes. The rigidity of the polymer structure is decreased with a change in their mechanical and thermomechanical properties. The glass transition temperature of the particular polymer electrolyte system is also decreased. The increase of salt dissociation capability and the reduction of crystallinity results in enhancement of charge carrier transportation.[23] Polymer electrolytes are found to exhibit higher ionic conductivity at higher plasticizer concentration at the cost of their mechanical stability.[25]

C.4.4 Composite polymer electrolytes

The addition of inorganic fillers in polymer electrolytes increase the mechanical strength and interfacial stability of the resulting electrolytes, providing a new branch of polymer electrolytes (Pes) which are known as composite polymer electrolytes (CPEs).[26] By doping different types and amounts of high dielectric constant fillers, especially inorganic inert fillers into the polymer matrix, the electrical properties of polymer electrolytes can be improved. Ceramic materials are one of the most commonly used inorganic dopants. They are fragile and have low dielectric strength. By combining such inorganic dopants with polymers, the new composite electrolytic material can be produced for higher relative permittivity. Since these composite electrolytes consist of ceramic particles, they can be regarded as heterogeneously disordered systems, with electrical properties highly dependent on the relative permittivity and conductivity of the dopants. Moreover, electrical performances of these composite electrolytic materials are affected by the size, shape and volume fraction of the dopants.[23]

Appendix D. Electrochemical performances of textile supercapacitors reported in literature

Table D.1. Summary of Carbon-based supercapacitors or supercapacitor electrodes

1D shaped								
Substrate (Reporting year)	Device Configuration	Device capacitance	Energy density	Power density	Capacitance retention	Flexibility		Ref
Carbon fibre and Gold coated plastic fibre (2012)	Commercial graphite pen ink used as active material and deposited on fibre surface. Spacer wire evenly twisted onto the surface of one fibre electrode, two fibre electrodes placed parallelly in a flexible plastic tube filled with PVA-H_2SO_4 electrolyte	11.9–19.5 mF cm^{-2}	1.76×10^{-6} –2.70×10^{-6} Wh cm^{-2}	Up to 9.07 mW cm^{-2}	Similar after 15,000 cycles	Slight drop at 180°, 360° bending		27
Carbon microfibre bundle (2013)	Carbon microfibre bundle coated with MWCNTs as core electrode in the centre of coaxial SC and carbon nanofibre (CNF) film prepared by electrospinning as outer electrode	6.3 mF cm^{-} (86.8 mF cm^{-2})	0.7 μWh cm^{-1} (9.8 μWh cm^{-2})	583 μW cm^{-1}	94% after 1,000 cycles	Negligible change at 180° bending		28
Carbon fibre (2013)	Electrochemically reduced GO (ERGO) coated carbon fibre followed by acid treatment (ERGO@CF–H) with PVA–H_3PO_4 gel electrolyte	13.5 mF cm^{-1} (307 mF cm^{-2}) at 0.05 mA cm^{-1}	1.9 mW h cm^{-1} (21.4 mW h cm^{-2})	0.74 mW cm^{-1} (8.5 mW cm^{-2})	85% after 5,000 cycles	No decay at bending 0°–180°		29
rGO fibre yarns (2014)	rGO fibre yarns deposited on a titanium current collector and separated by a PVDF membrane	409 Fg^{-1}	14 Wh kg^{-1}	25 kW g^{-1}	No decay after 5,000 cycles			30

Material (year)	Description	Capacitance	Energy density	Power density	Cycling stability	Bending stability	Ref
Carbon nanotube and rGO composite yarn (2014)	Two SWNTs/rGO electrode mounted on a PET substrate using PVA–H_3PO_4 electrolyte	116.3 mF cm^{-2}, 45 F cm^{-3} at 26.7 mA cm^{-3}	6.3 mWh cm^{-3}	1085 mW cm^{-3}	93% after 10,000 cycles	>97% after 1,000 bending cycles at 90°	[31]
GO, CNT and their mixture wet spun filament (2014)	Polyelectrolyte-wrapped carbon nanomaterial (graphene, CNTs and their mixture) core-sheath fibre, RGO@CMC, CNT@CMC, RGO+CNT@CMC, Two coaxial fibres twisted together and coated with PVA electrolyte	269 mF cm^{-2}, 239 F cm^{-3}, 8.0 mF cm^{-1} (liquid electrolyte 1 M H_2SO_4), 177 mF cm^{-2}, 158 F cm^{-3}, 5.3 mF cm^{-1} @ current density of 0.1 mA cm^{-2} (solid electrolyte H_3PO_4/PVA)	3.84 mWh cm^{-2}, 3.5 mWh cm^{-3} (liquid) 5.91 mWh cm^{-2} (solid)		No decay within 2,000 times	Dropped 2% at 200 times of bending and rose persistently up to 111% at 1,000 times of bending	[32]
GO fibre (2014)	Region-specific reduction of GO fibre by laser irradiation, to prepare rGO/GO/rGO single fibre SC with IL electrolyte of 1-butyl-3-mthylimidazolium tetrafluoroborate	1.2 mF cm^{-2} at 80 µA cm^{-2}, 0.45 mF cm^{-2} at 200 µA cm^{-2}	2–5.4×10^{-4} Wh cm^{-2}	3.6–9×10^{-2} W cm^{-2}	No degradation after 1,000 cycles	No decrease after 160 bending cycle	[33]
Carbon fibre yarn (2015)	Two hybrid AC drop casted carbon fibre yarn electrodes, twisted together, dipped in PVA-H_3PO_4 electrolyte, dried	45.2 mF cm^{-1} at 2 mV s^{-1}	6.5 µWh cm^{-1}	27 µWcm^{-1}	86.6% after 10,000 cycle	98% after 1,000 bending	[34]
CNT fibre (2015)	GO sheets coated on CNT fibre, reduced to RGO, forming a core–sheath-structured CNT/RGO composite fibre. Two composite fibres drawn into gel electrolyte consisting of PVA, phosphoric acid, and water, followed by twisting	68.4 F cm^{-3} (126.7 F g^{-1}) at 31 mA cm^{-3}	2.4 mW h cm^{-3}, 3.8 µW h cm^{-2}	0.016 W cm^{-3}, 0.025 mW cm^{-2}	No decay after 10,000	No decrease at bending 180°	[35]

Material (year)	Description	Capacitance	Energy density	Power density	Cycling stability	Flexibility	Ref
Graphene fibre (2015)	Spun-rGO//rGO coaxial all graphene fibre SC with PVA gel coating as separator, a dip-coated cylinder sheath fibre as the other electrode followed by reduction, coating of H_2SO_4-PVA gel electrolyte	205 mF cm^{-2} (182 F g^{-1})	17.5 µWh cm^{-2} (15.5 Wh kg^{-1}), increased to 104 µWh cm^{-2} with organic ionic electrolyte		No decay at 10,000th cycle	92% after 100 times of bending	[36]
Graphene fibre (2015)	Two MWCNTs-rGO fibre electrodes with PVA-H_3PO_4 electrolyte	0.35 mF cm^{-1}, 38.8 F cm^{-3} at 50 mA cm^{-3}	3.4 mWh cm^{-3}	700 mW cm^{-3}	93% after 10,000 cycle	No decrease after knotting	[37]
Porous graphene ribbon (PGRs) (2015)	PGRs freeze-dried for 24 h to obtain dried porous graphene ribbons (DGRs) followed by immersion in H_3PO_4-PVA electrolyte, two pairs of electrodes pressed together	208.7 F g^{-1} (78.3 mF cm^{-2} or 3.12 mF cm^{-1})			99% after 5,000 cycles	No decrease at bending 45°, 90°, 135°, 180°, 95% after 100 cycle bending when woven to glove	[38]
GO fibre (2015)	Region specific reduction of wet spun GO fibre by laser irradiation to prepare alternate rGO-GO electrolyte-free fibre SCs	14.3 mF cm^{-2} at 50 mA cm^{-3}			93% after 1,000 cycles	No decrease after 1,000 cycles	[39]
PVA/RGO hybrid fibres (2016)	Incorporating hydrophilic PVA into a non-liquid-crystalline GO dispersion before wet spinning and chemical reduction, two bundles of PVA/RGO fibres with PVA-H_2SO_4-H_2O gel electrolyte	Fibre 241 F cm^{-3}	5.97 mW h cm^{-3} (5.32 mW h g^{-1})	26.9mW cm^{-3} (23.9 mW g^{-1})	85% after 1,000 cycles	97% retention after cyclic bending between 0 and 180 for 1000 times	[40]
Graphene and few-walled carbon nanotubes composite yarn (2018)	Hybrid fibre based on graphene and few-walled CNTs (G_{10}/CNTs) electrode with 6 M KOH aqueous electrolyte	312.6 F g^{-1} at 200 mA g^{-1}	Varied from 23.46 to 9.66 Wh kg^{-1} at 84.68 to 1134.56 W kg^{-1}		89.6% after 10,000 cycles		[41]

2D shaped							
Substrate (Reporting year)	Device Configuration	Device capacitance	Energy density	Power density	Capacitance retention	Flexibility	Ref
Cotton fabric (2010)	Dipping and drying of cotton with SWNT ink electrodes with $LiPF_6$ electrolyte to form fabric SC	140 Fg^{-1} at 20 $\mu A\,cm^{-2}$, 0.48 F cm^{-2}	20 Wh kg^{-1} at 10 kW kg^{-1}		98% after 130,000 cycles	No decrease @100th 120% strain	[42]
Cotton Stretchable fabric (2010)	Dipping and drying of cotton with SWNT ink electrodes with $LiPF_6$ electrolyte to form fabric SC	62 Fg^{-1} at 1 mA cm^{-2}			<6% decrease after 8,000	Similar after stretched 120% strain 100 times.	[42]
Cotton fabric (2010)	Conformal coating of SWNTs ink with 2 mol L^{-1} Li_2SO_4 electrolyte	70–80 Fg^{-1} at 0.1 mA cm^{-2}			Coulombic efficiency		[43]
Cotton cloth (2012)	Brush-coating of cotton cloth with GO suspension ink as electrode, nickel foam current collector, pure cotton cloth separator with 6 M KOH electrolyte	81.7 Fg^{-1}	7.13 Wh kg^{-1}	1.5 kW kg^{-1}	93.8% after 1,500 cycles		[44]
Cotton woven (2017)	Screen printing of GO, followed by electrochemical reduction to produce rGO-cotton electrode, with PVA-H_2SO_4 gel electrolyte	2.5 mF cm^{-2}, 257 F g^{-1}			97% after 10,000 cycles	95.6% after folding 180° for 2,000 cycles	[45]
Cotton fabric (2019)	Dry-coated and subsequently two step reduced GO coated cotton fabric electrode, raw cotton fabric separator, PVA-H_3PO_4 electrolyte sandwiched	464 F g^{-1} at 0.25 A g^{-1}	27.05 W h kg^{-1}		91.6% after 1,000 cycles	No apparent performance degradation after 0° and 180° bending	[46]

Fabric (year)	Description	Specific capacitance	Energy density	Power density	Cycling stability	Flexibility	Ref
Cotton fabric (2022)	Graphene ink screen-printed on cotton textiles with PVA-H_2SO_4 gel electrolyte	3.2 mF cm^{-2}	0.28 mWh cm^{-2} at 3 mW cm^{-2}		95% after 10,000 cycles		[47]
Polyester fabric (2014)	CNT dip-coated onto PET fabrics electrode	1.4×10^{4} F cm^{-2}					[48]
Polyester fabric (2019)	Sandwiching 2 dip-dried graphene nanoparticle/ polyester electrodes and 1 h-boron nitride/polyester dielectric layer in between to form flexible textile-based capacitor (FTC)	26 pF cm^{-2}				Sustains 100 cycles of repeated bending	[49]
Poly-cotton (65/35) 2/1 twill fabric (2020)	Graphene coated textile electrodes with PVA-H_2SO_4 gel electrolyte	2.7 mF cm^{-2} (electrode)			≈98% after 15,000 cycles	98% after bending 150 cycles at 180°	[50]
Cotton and polyester fabric (2011)	Cotton and polyester screen-printed with AC as SC electrode, polyester separator and Li_2SO_4 and Na_2SO_4 electrolyte	Electrode 0.43 F cm^{-2} at 5 mA cm^{-2} (Na_2SO_4), 85-95 Fg^{-1} at 1-10 mVs^{-1}			92% after 10,000 cycles		[51]
Polypropylene fabric (2019)	Reactive inkjet printing of rGO layers on PP fabric as electrode with PVA-H_3PO_4 gel electrolyte to form flexible solid-state SC	13.3 mF cm^{-2} (79.9 F g^{-1}) at 0.1 mA cm^{-2}	1.18 mWh cm^{-2}	4.6 mW cm^{-2}	Almost 100% after 5,000 cycles		[52]
Carbon fabric (2012)	Entangled carbon nanofibres (CNFs) synthesized on flexible carbon fabric (CF) via water-assisted chemical vapor deposition to form CNF/CF electrode with 0.5 M Na_2SO_4 aqueous solution	140 F g^{-1} at 5 mV s^{-1}			≈95% after 2,000 cycle		[53]

Material	Description	Capacitance	Energy density	Power density	Cyclic stability (cycling)	Cyclic stability (mechanical)	Ref
Carbon fibre knit and woven fabric (2013)	Carbon fabric screen-printed with activated carbon with solid polymer electrolyte	88 Fg^{-1}, 0.51 F cm^{-2} (Knitted), 66 Fg^{-1}, 0.19 F cm^{-2} (Woven)				80% after bending at 90°, 135°, and 180°	54
Carbon cloth (2014)	Electrochemically activated carbon cloth electrode with PVA-H_2SO_4 electrolyte	Electrode 88 mF cm^{-2} (8.8 mFg^{-1}) at 10 mVs^{-1}, SC 15.3 mF cm^{-2} (0.765 mFg^{-1})			95% after 20,000 cycles		55
Activated Carbon fibre felt (2015)	CNTs and graphene (GN) modified composite ACFF textile electrodes, non-woven fabric separator, with KOH electrolyte	3,350 mF cm^{-2}, device 2,700 mFcm^{-2}	112 µW h cm^{-2}	490 µW cm^{-2}	No decay at 1,000 cycles		56
Stainless steel fabric (SSF) (2016)	Two chemically converted graphene (CCG) on SSF electrode with 1 M H_2SO_4 to form flexible solid-state symmetrical SC	730.8 mF cm^{-2} at 2 mA cm^{-2}, 180.4 mF cm^{-2} at 1 mA cm^{-2}	19.2 W h cm^{-2} at 386.2 W cm^{-2}		96.8% after 7,500 cycles	96.4% after 800 stretching-bending cycles	57
Silver fibre fabric (SFF) (2017)	Electrophoretic deposition of graphene on SFF, electrode with KOH 3 M electrolyte	172 mF cm^{-2} at 4 mA cm^{-2}			97% after 5,000 cycles		58

Table D.2 Summary of Conducting polymer-based supercapacitors or supercapacitor electrodes

1D shaped							
Substrate (Reporting year)	**Device Configuration**	**Device capacitance**	**Energy density**	**Power density**	**Capacitance retention**	**Flexibility**	**Ref**
Cotton yarn (2017)	Cotton yarns coated with PPy nanotubes	74.0 mF cm^{-2}	7.5 μWh cm^{-2}			97% after 200 cycles	[59]
Carbon fibre thread (2015)	Carbon fiber thread (CFT) @ PANI as positive and functionalized carbon fiber thread (FCFT) as negative electrode, coated with PVA-H$_3$PO$_4$ gel electrolyte and twisted together	High operating voltage (1.6 V).	2 mWh cm^{-3}	11 W cm^{-3}		Unchanged at 100% strain	[60]
2D shaped							
Substrate (Reporting year)	**Device Configuration**	**Device capacitance**	**Energy density**	**Power density**	**Capacitance retention**	**Flexibility**	**Ref**
Cotton fabric (2013)	PPy-coated cotton fabrics electrode, prepared in mixed surfactants: cetyltrimethylammoni-um bromide (CTAB) and sodium dodecyl benzene sulfonate (SDBS), with NaCl solution	51.7 mAh g^{-1}			Negligible decay after 100 cycles		[61]

Material (Year)	Method	Capacitance	Energy density	Power density	Cycling stability	Other	Ref
Cotton fabric (2013)	In situ oxidation polymerization of pyrrole in presence of lignosulfonate as both template and dopant to prepare PPy/ lignosulfonate (PPy/LGS) coated cotton fabric electrode	304 F g^{-1} at 0.1 A g^{-1}					[62]
Cotton fabric (2015)	PPy nanorods deposited on cotton fabrics via in-situ polymerization	325 F g^{-1}	24.7 Wh kg^{-1} at 0.6 mA cm^{-2}		200 F g^{-1} after 500 cycles		[63]
Cotton fabric (2016)	PPy coated cotton as working, Pt sheet as counter, Ag/AgCl as reference electrode with 1M H$_2$SO$_4$ electrolyte	Knitted 4,117, woven 2,191 and nonwoven fabrics 2,905 mF cm^{-2}	5.94 Wh kg^{-1}	259.55 W kg^{-1}	Stable within 5,000 cycles		[64]
Cotton woven and knit (2019)	In situ polymerization coating of PPy	Woven 1,748, Knitted 4,848 mF cm^{-2} at 1 mA cm^{-2}			88% after 5,000 cycles		[65]
Cotton knit fabric (2019)	In-situ chemical polymerization of PPy on fabric with PVA-H$_2$SO$_4$ gel electrolyte	Electrode 481 and 1,433 mFcm^{-2} at 5 mV s^{-1} and 1 mAcm^{-2} respectively, device 101 and 450 mFcm^{-2} at 5 mV s^{-1}	0.4 Whm^{-2} (2.3 W h kg^{-1} based on total mass of 2 electrodes)	10 W m^{-2} (57.5 W kg^{-1})	30% after 500 cycles (gel electrolyte), above 53% at 5000th cycle (aqueous electrolyte)	Electrode 78%~91% after stretched 1,000 times, device capacitance enhanced to 160% at 5 mA cm^{-2}	[66]

Material (year)	Method	Capacitance	Energy density	Power density	Cycling stability	Stretch stability	Ref
Cotton knit fabric (2019)	PPy-coated fabric electrodes via chemical polymerization with 1 M H_2SO_4 electrolyte	Electrode 5,073 mF cm⁻² at 1 mA cm⁻², device	102.4 µWh cm⁻² at 0.39 mW cm⁻²		90% capacitance after 2,000 cycles		67
Nylon/lycra (80/20) knitted fabric (2012)	Chemical polymerization synthesis of PPy on fabric with 1.0 M NaCl electrolyte	123.3 F g⁻¹ at 10 mV s⁻¹	6.7 Wh kg⁻¹	753.4 W kg⁻¹		90% after stretched to 100% for 1,000 times	68
Polyester fabric (2018)	Repeated spray-coating of PEDOT:PSS solutions containing 5 wt% DMSO	75.30 F g⁻¹ at the scan rate of 20 mVs⁻¹					69
Polyester knitted fabric (2019)	In situ polymerization of PPy on fabric	1,213 mF cm⁻² at 1 mA cm⁻²					65
Polyester fabric (2020)	Electrospun PEDOT: PSS nanofibres deposited on flexible PET substrates to obtain electrodes with PVA-H_3PO_4 polyelectrolyte	1.8 mF cm⁻² and 3.6 F g⁻¹ at 5µA cm⁻²	0.32 Wh kg⁻¹ at 5 µA cm⁻²	11.8 Wkg⁻¹	92% after 1,000 cycles		70
Polyester fabric (2021)	Conductive PET fabric electrode is prepared by in-situ polymerization of aniline and pyrrole	Electrode 1,046 mF cm⁻² at 2 mA cm⁻²	0.043 mWh cm⁻³	0.005 Wcm⁻³	54.2% after 1,000 cycles		71
Cotton/polyester (55/45) fabric (2020)	DMSO-doped PEDOT:PSS-coated cloth as electrode and sweat as electrolyte	Artificial sweat (7.64 F g⁻¹ and 8.45 mF cm⁻² at 0.07 A g⁻¹), real human	Artificial sweat 1.36 Wh kg⁻¹ (1.63 µWh cm⁻²),	Artificial sweat 329.70 W kg⁻¹ (0.40 mW cm⁻²),	75% after 4,000 cycles, 45% after 5,000 cycles		72

Material (year)	Description	Capacitance	Energy density	Power density	Cycling stability	Bending stability	Ref
PP non-woven textile (2021)	Reactive inkjet printing to fabricate PPy layers on textile with direct freezing of inks	72.3 F g^{-1} at 0.6 A g^{-1} at −12 °C	6.12 Wh kg^{-1}	139 W kg^{-1}	55.4% after 2,000 cycles		[73]
Silk woven fabric (2019)	In situ polymerization coating of PPy on fabric	1,349 mF cm^{-2} at 1 mA cm^{-2}					[65]
Wool gauze fabric (2019)	In situ polymerization coating of PPy on fabric	1,007 mF cm^{-2} at 1 mA cm^{-2}					[65]
Fibre glass cloth (2020)	Conductive fibreglass cloth (CFC) derived from gas-phase polymerization of pyrrole, followed by electrochemical polymerization of a layer of PPy attached to the surface of the conductive fibreglass cloth, sandwiching two PPy/CFC composites with PVA-H$_2$SO$_4$ electrolyte	549.6 mF cm^{-2}	48.85 µWh cm^{-2}		92.4% after 10, 000 cycles	96.08% after 1,000 bending cycles	[74]
Carbon fabric (2010)	PEDOT nanofibre electrode, carbon cloths as current collector and electrospun PAN nanofibrous membranes as separator with ionic liquid electrolyte	20 Fg^{-1}			90% after 10,000 cycles		[75]
CNT fibre woven textiles (2014)	Two PANI deposited CNT fibre textile stacked with PVA-H$_3$PO$_4$ gel electrolyte	272.7 Fg^{-1} at 1 Ag^{-1}			No decay after 2,000 cycles	96.4% after 200 cycles bending at 150°	[76]

Table D.3 Summary of Metal-based supercapacitors or supercapacitor electrodes

		1D shaped					
Substrate (Reporting year)	Device Configuration	Device capacitance	Energy density	Power density	Capacitance retention	Flexibility	Ref
Kevlar fibre (2011)	Kevlar fibres and flexible plastic wire substrates for ZnO NW arrays, Plastic wire/ZnO, Kevlar/ZnO/Au electrodes with KNO_3 and PVA-H_3PO_4 electrolyte	0.21 mF cm^{-2} at 100 mV s^{-1} (aqueous) and 2.4 mF cm^{-2} and 0.2 mF cm^{-1} (gel electrolyte)	2.7×10^{-8} Wh cm^{-2} (gel)	1.4×10^{-5} Wcm^{-2} (gel)			[77]
Carbon nanotube (CNT) yarn (2014)	CNT‖CNT, CNT@MnO_2‖CNT, CNT@MnO_2‖ CNT@MnO_2 with aqueous electrolyte	Asymmetric SC CNT@MnO_2 (positive) and CNT (negative) possess a capacitance of 12.5 F g^{-1} at a current density of 0.14 A g^{-1}	1 to 2.12 Wh kg^{-1} (CNT‖CNT), For CNT@MnO_2 ‖ CNT, up to 42.0 Wh kg^{-1} (low power density), and 28.02 Wh kg^{-1} (at high power density)	241.8 to 10 000 W kg^{-1} (CNT‖CNT), for CNT@MnO_2 ‖ CNT, low power density of 483.7 W kg^{-1}, high power density	For CNT@MnO_2 ‖ CNT 98% retention after 500 cycles, in comparison with 99% for CNT‖CNT	For CNT@MnO_2‖ CNT, specific capacitance suffered only 0.5% reduction after 200 cycles of folding and unfolding actions	[78]

Substrate (Reporting year)	Device Configuration	Device capacitance	Energy density	Power density	Capacitance retention	Flexibility	Ref
Carbon nanotube (CNT) yarn (2015)	NiO and Co_3O_4 deposited on spun CNT yarn, two PVA-H_2SO_4 coated CNT, CNT@NiO and CNT@Co_3O_4 yarns placed together and coated with electrolyte again	CNT@Co_3O_4 yarn based SC 52.6 mF cm^{-2} at 0.053 mA cm^{-2}, 87.6 Ag^{-1}, CNT based SC 7.4 mF cm^{-2}, 13.4 Ag^{-1}, CNT@NiO based SC 15.2 mF cm^{-2}, 25.9 Ag^{-1}	CNT@Co_3O_4 yarn based SC 1.1 µWh cm^{-2}	CNT@Co_3O_4 yarn based SC 0.01 mW cm^{-2}	Pure CNT, CNT@NiO and CNT@Co_3O_4 maintain 96%, 94% and 91%, respectively, of original capacitance after 1,000 cycles	No decrease after 100 cycles bending at 90° and 180°	79
Carbon nanofibre (CNF) (2015)	CNFs containing Co_3O_4 nanoparticles electrodes with 6 M KOH	586 Fg^{-1} at 1 Ag^{-1}			74% after 2,000 cycles		80
2D shaped							
Substrate (Reporting year)	**Device Configuration**	**Device capacitance**	**Energy density**	**Power density**	**Capacitance retention**	**Flexibility**	**Ref**
Polyester (2020)	Ni nanoparticle in situ synthesized, two Ni-plated polyester electrodes with PVA-KOH gel electrolyte	450 mF cm^{-2} at 7.5 mA cm^{-2}					81

Substrate (year)	Description	Capacitance	Energy density	Power density	Retention		Ref
Silk fabric (2021)	Graphite coated Berlin (silver coated silk) as negative electrode and Nora Dell (Ni/Cu/Ag coated) fabric as positive electrode with biocompatible PVA-KCl gel electrolyte	32 mF cm^{-2} at 25 mV s^{-1}, 41 mF cm^{-2} at 0.75 mA cm^{-2}	2.8 μ Wh cm^{-2} at 25 mV s^{-1}, 3.6 μ Wh cm^{-2} at 0.75 mA cm^{-2}		45% retention after 1,000 cycles		82
Carbon cloth (2013)	Hydrogenated single-crystal ZnO @ amorphous ZnO-doped MnO$_2$ core-shell nanocables (HZM) on carbon cloth as electrodes with PVA-LiCl electrolyte	26 mF cm^{-2} (325 mF cm^{-3}) at 0.5 mA cm^{-2}	0.04 mWh cm^{-3}	2.44 mW cm^{-3}	87.5% after 10,000 cycles		83
Carbon cloth (2015)	Electrochemically activated carbon cloth (EACC) as anode and TiN@MnO$_2$ on CC as cathode with LiCl electrolyte	2.69 F cm^{-3} at 6 mA cm^{-2}	1.5 mWh cm^{-3}	1.71 W cm^{-3}	No decay at 70,000 cycles		84
Carbon fabric (2016)	Uniform large-area manganese oxide (MnO$_2$) nanosheets on carbon fabric oxidized using O$_2$ plasma treatment (MnO$_2$/O$_2$-carbon fabric) via electrodeposition process with 1 M sodium sulfate (Na$_2$SO$_4$) electrolyte	275 Fg^{-1} at 5 mVs^{-1}			80% of after 10,000 cycles.		85
Carbon cloth (2016)	In-situ electrodeposition of MnO$_2$ on carbon cloth with 1 M Na$_2$SO$_4$ aqueous electrolyte	275 F g^{-1} at 0.2 A g^{-1}					86
Carbon textile (2016)	Zinc sulfide (ZnS) nanospheres hydrothermally grown on flexible carbon textile (CT)	540 F g^{-1} (56.25 F cm^{-2}) at 5 mV s^{-1}	51 W h kg^{-1} at 205 W kg^{-1}		94.6% after 5,000 cycles		87

Substrate (Year)	Method	Capacitance	Energy density	Power density	Cycling stability	Flexibility	Ref
Carbon fibre fabric (2017)	KOH activation of commercial CF threads followed by coated with PVA- H_3PO_4 electrolyte and woven to SC fabric	18.6 F g^{-1} at 2 mV s^{-1}, 300 mF cm^{-2}, 26 F cm^{-3}	2.58 mWh g^{-1} or 3.6 mWh cm^{-3}, 42…		Over 80% after 10,000 at…		88
Carbon fabric (2017)	Fabrication of Co_3O_4 nanowires on flexible carbon fabric electrode (CoNW/CF) with PVA-KOH gel electrolyte	Electrode 3,290 F g^{-1} at 5 mV s^{-1}	6.7 Wh kg^{-1}	5 kW kg^{-1}	95.3% after 5,000 cycles		89
Carbon cloth (2018)	Anodic deposition of MnOx on Pd coated carbon cloth electrode with 0.5 M Na_2SO_4	186 F g^{-1} at 1 mA cm^{-2}					90
Carbon fibre fabric (2020)	Viscose fibre woven fabrics carbonized and activated (ACVF), CeO_2, ZnO hydrothermally deposited, CeO_2-ACVF & ZnO-ACVF electrode, polyester separator, carbon cloth current collector with PVA-H_3PO_4 electrolyte	13.24 mF cm^{-2} at 0.2 mVs^{-1}	4.6×10^{-7} Wh cm^{-2} at 3.31×10^{-6}…		87.6% at 5,000 cycles	Increases by 13.4% after 200 bending cycles	91
Carbon fibre textile (2021)	Crystalline nano-flowers structured zinc oxide (ZnO) directly grown on carbon fibre textile (CFT) via hydrothermal process and fabricated with a binder-free electrode (denoted as ZnO@CFT) for SC	201 Fg^{-1} at 1 Ag^{-1}			90.32% after 3,000 cycles at 10 Ag^{-1}		92

Table D.4 Summary of 2d material-based supercapacitors or supercapacitor electrodes

Substrate (Reporting year)	Device Configuration	Device capacitance	Energy density	Power density	Capacitance retention	Flexibility	Ref
Cotton fabric (2018)	Dipping and drying of cotton into MXene ($Ti_3C_2T_x$) nanosheets	182.70 F g^{-1}					93
Cotton fabric (2020)	3D knitted cotton yarn coated with $Ti_3C_2T_x$ and 1M H_3PO_4-PVA electrolyte	519 mF cm^{-2} at 2 mV s^{-1}, (707 mF cm^{-2} at 2 mV s^{-1} with 1 M H_3PO_4 electrolyte)	25.4 μWh cm^{-2}	0.47 mWcm^{-2}	>100% over 10,000 cycles		94
Carbon cloth (2018)	Hydrothermal growth of MoS_2 nanosheets on carbon fabrics, with Lithium metal counter electrode, and 1.0 M $LiPF_6$ solution with mixture of ethylene carbonate and dimethyl carbonate (EC/DMC, 1:1 in volume) electrolyte	159.38 mF cm^{-2} at 0.5 mA cm^{-2}			80.6% after 15,000 cycles		95
Carbon fabric (2018)	Stacking RuO_2 coated carbon fabric (CF) as positive and $Ti_3C_2T_x$ coated CF as negative electrode with 1 m H_2SO_4 electrolyte	Electrode 416 mF cm^{-2}, 200 F g^{-1}	Device 37 μWh cm^{-2} at 40 mW cm^{-2}		86% after 20,000 cycles		96

Carbon cloth (2021)	Hierarchical flower-like Mn_3O_4@N, P-doped carbon (NPC) composite cathode with an electrochemically reduced porous carbon (PC) anode and a PVA-Na_2SO_4 hydrogel electrolyte	$81.97\,Fg^{-1}$ at $1\,A\,g^{-1}$	$76.96\,Wh\,kg^{-1}$	$26.02\,kW\,kg^{-1}$ at $32.65\,Wh\,kg^{-1}$	92.71% after 10,000 cycles		[97]
Carbon cloth (2021)	MoS_2 drop casted on functionalized carbon cloth; MoS_2/FCC electrodes soaked with 1 M H_2SO_4 electrolyte	$56.525\,F\,g^{-1}$ at $0.2\,A\,g^{-1}$			29% after 1,000 cycles		[98]

Table D.5 Summary of Hybrid material-based supercapacitors or supercapacitor electrodes

1D shaped							
Substrate (Reporting year)	Device Configuration	Device capacitance	Energy density	Power density	Capacitance retention	Flexibility	Ref
Cotton thread (2013)	Two PPy-MnO$_2$ -CNT-cotton thread electrodes, separated with cotton textile wrapping with 0.5 M Na$_2$SO$_4$ electrolyte, transparent silicone pipeline as a package shell	1.49 Fcm^{-2} at 1 mVs^{-1} (electrode)	33 μ Wh cm^{-2} at 0.67 mW cm^{-2}	13 mW cm^{-2} at 14.7 μWh cm^{-2}	87% after 2,000 cycles		[99]
Cellulose yarns (2015)	Yarns (cotton, linen, bamboo, viscose) welded with activated carbon and twisting with stainless steel yarn	120 F g^{-1}, 37 mF cm^{-1} at 2 mV s^{-1}			77% after 3,000 cycles	Some decay at 180° bent, curled, and crumpled	[100]
Cotton yarn (2015)	Electroless deposition of Ni and electrochemical deposition of graphene on commercial cotton yarns (RGO/Ni cotton composite electrodes) with PVA-LiCl electrolyte and separator	0.11 F cm^{-1}	6.1 mWh cm^{-3}	1,400 mW cm^{-3}	82% after 10,000 cycles	No decrease at 45°, 90°, 180° bending, 95% after 4000 cycle at 180°	[101]
Cotton thread (2016)	Twisting 2 strands of PVA-H$_3$PO$_4$ gel electrolyte coated carbon nanoparticles /rGO-cotton thread (CNPs/rGO-CT) together	3.79 mF cm^{-3} at 50 mV s^{-1}	0.084 μWh cm^{-3}		95.23% after 10,000 cycles	92.30% after 2,000 bending cycles	[102]

Material (year)	Description	Capacitance	Energy density	Power density	Cycling stability	Bending stability	Ref
Cotton thread (2016)	Twisting 2 strands of PVA-H_3PO_4 gel electrolyte coated graphene hydrogels/MWCNT-cotton thread (GHs/MWCNTs-CT)	97.73 $\mu F\ cm^{-1}$ at 2 mV s^{-1}	4.79 × 10^{-3} mWh cm^{-1}	1.25 mWcm^{-1}	95.51% after 8,000 cycles	90.75% after 500 bending cycles	102
Cotton thread (2018)	Two cotton/Ni/Co-Ni layered double hydroxide (CT/Ni/Co-Ni LDH) hybrid yarn electrode twisted together and painted with PVA-KOH gel electrolyte	Electrode 1.26 F cm^{-2} at 5 mV s^{-1}, SC 221 mF cm^{-2} at 0.04 mA cm^{-2}	9.3 mWh cm^{-2}	43.99 mW cm^{-2}	79% after 2,000 cycles		103
Cotton yarn (2018)	Cotton electrode by dip-dried in MWCNT followed by interfacial polymerization of PPy, two parallel electrodes embedded in a thin layer of PVA-H_3PO_4 layer	30 F g^{-1}	2.63 mW h g^{-1}	11.33 mW g^{-1}			104
Cotton fibres (2018)	Short-staple length SSFs blended with cotton fibres to spin SSF/cotton blended yarn, PPy deposited on PEDOT:PSS coated composite yarn, followed by coating with PVA-H_3PO_4 electrolyte, placed in parallel and twisted together, followed by coating	1.36 F cm^{-2}	0.16 mWh cm^{-2}		80% over 5,000 cycles		105

Material	Description	Capacitance	Energy density	Power density	Cycling stability	Bending	Ref
Cotton (2019)	GO nanosheets (NSs) modified with ultrathin and large area MoS_2 NSs followed by reduction with PVA-H_3PO_4 electrolyte	134.38 F g^{-1}, 332.85 mF cm^{-2} and 221.9 F cm^{-3} at a current of 50 mA				100% when bent by 30 and 60 degrees	[106]
Cotton fibre (2021)	In-situ growth of PPy and MXene composite, on cotton fibre to prepare fibre electrode	506.6 F g^{-1}, at 1 A g^{-1} and 455.9 mF cm^{-2} at 0.9 mA cm^{-2}			83.3% after 2,000 cycles		[107]
Polyester fibre (2018)	PPy electrochemically deposited on rGO painted $SnCl_2$ modified polyester yarn electrode with PVA-H_2SO_4 electrolyte for SC	Electrode 175.7 mF cm^{-1}, 699.6 mF cm^{-2}, 239.6 F g^{-1}, 35.0 F cm^{-3} at 0.13 mA cm^{-1}, device 85.3 mF cm^{-1}, 339.7 mF cm^{-2}, 116.4 Fg^{-1}, 17.0 F cm^{-3}	0.0472 mWhcm^{-2}	26.5 mWcm^{-2}		Unchanged after 1,000 bending cycles	[108]
Polyaniline fibre (2013)	Two PANI composite fibres incorporated with aligned MWCNT twisted	274 Fg^{-1}, 263 mF cm^{-1} at 2 A g^{-1}			99% after 1,000 cycles	>97% after 50 bending cycles	[109]

Substrate (year)	Description	Capacitance	Energy density	Power density	Cycling stability	Flexibility	Ref
Nylon fibre (2015)	MWCNT helically wrapped around nylon fibres, followed by electrochemical deposition of MnO_2. Two coiled MnO_2/CNT/nylon fibre electrodes placed parallel and coated with PVA-LiCl gel electrolyte	5.4 mF cm⁻¹, 40.9 mF cm⁻², 3.8 F cm⁻³ at 10 mV s⁻¹	2.6 μWh cm⁻²	66.9 μW cm⁻²		90.8% at 12% strain, 50% during large strain	[110]
Elastic fibre (2014)	Elastic fibre/CNTs/PANI	255.5 Fg⁻¹, 0.19 mF cm⁻¹ at 1 A g⁻¹	12.75 Wh kg⁻¹	1494 W kg⁻¹	69% after 10,000 cycles	93.8% after 1,000 cycles bending at 180°	[111]
Shape-memory polyurethane (SMP) substrate (2015)	Wrapping aligned CNT sheets onto shape-memory polyurethane (SMP) substrate as electrode, coated with PVA gel electrolyte followed by winding another layer of aligned CNTs as outer electrode	24 Fg⁻¹, 0.269 mF cm⁻¹ and 42.3 mF cm⁻³			No loss after 12,000 cycles	No decrease after 500 cycles deformation	[112]
Urethane stretchable yarn (2016)	CNTs dipping and PPy electrodeposition on urethane elastic fibre core spun yarns (UY)	69 mF cm⁻²				Nearly unchanged at 80% strain	[113]

Substrate (year)	Method	Capacitance	Energy density	Power density	Cycling stability	Flexibility	Ref
Stretchable substrate (2017)	Electrochemical activation of pristine CNT fibres, coating of PEDOT:PSS followed by electrochemical deposition of MnO_2 to form MnO_2@PEDOT:PSS@OCNTF positive electrode and hydrothermal synthesis of MoS_2 to form MoS_2@CNTF negative electrode with LiCl-PVA electrolyte placed on stretchable substrate	278.6 mF cm^{-2}	125.37 µWh cm^{-2} at 540 µW cm^{-2}			92% after stretching at 100% strain for 3,000 cycles	[114]
Carbon nanotube (CNT) yarn (2013)	PANI nanowire arrays in-situ deposited on CNT yarn, PVA gel coated on CNT yarn or CNT/PANI yarn, two CNT or composite yarns twisted together	At 0.01 mA cm^{-2} CNT/PANI yarn based SC 38 mF cm^{-2}, pure CNT yarn-based SC 2.3 mF cm^{-2}			91% after 800 cycles	No decrease at 45°, 90°, 135°, 180° bending	[115]
Carbon nanotube (CNT) yarn (2014)	Electrochemical deposition of MnO_2 onto CNT yarn, two PVA-KOH coated CNT/MnO_2 composite yarns placed on top of each other, and coated by PVA-KOH	25.4 F cm^{-3} at 10 mV s^{-1}	3.52 mWh cm^{-3}	127 mW cm^{-3}		No decrease after 1,000 bending at 90°	[116]

Material	Description	Specific capacitance	Energy density	Power density	Cyclic stability	Bending/Flexibility	Ref
Carbon nanotube CNT fibre (2017)	MnO nanosheets in situ grown on CNT fiber (positive), polyimide deposited on CNT fiber (negative electrode)		$36.4 \ \mu Wh \ cm^{-2}$ at $0.78 \ mW \ cm^{-2}$)	$15.6 \ mW \ cm^{-2}$ at $30.2 \ \mu Wh \ cm^{-2}$	Well upto 2,000 cycles	Capacitances remains unchanged at bending various degrees (0-180)	[117]
Carbon nanotube (CNT) yarn (2017)	Twisting CNT yarns (n) with Pt filament as current collector, PANI nanowires further deposited in-situ to form the Pt/n-CNT @ PANI with alkaline electrolyte	Pt/5-CNT@PANI FSSC $217.7 \ Fg^{-1}$, $48.27 \ mF \ cm^{-3}$ at $0.2 \ Ag^{-1}$	$30.22 \ Wh \ kg^{-1}$ at $91.88 \ W \ kg^{-1}$		Negligible changes after 5,000 cycles	98.17 % after 3,000 cycles and 95.91 % after 5,000 flexing cycles	[118]
Carbon nanotube (CNT) fibre (2021)	Coating electroactive MoS_2 nanoflakes on a CNT fibre backbone with rGO as adhesion layer	$190.4 \ F \ g^{-1}$, $93.2 \ mF \ cm^{-2}$	$26.4 \ Wh \ Kg^{-1}$	$4,000 \ Wkg^{-1}$	85% after 5,000 cycles	No decay after 1,000 cyclic bending	[119]
Carbon nanotube (CNT) and Polyaniline Nanowire (PANINW) composite yarn (2014)	Spun yarn composed of SWCNTs and PANINWs, coated with PVA-H_2SO_4 electrolyte, twisted together	$2.67 \ mF \ cm^{-2}$ at $0.6 \ A \ g^{-1}$	$0.8 \ \mu Wh \ cm^{-2}$	$150 \ \mu W \ cm^{-2}$	86% after 800 cycles	No decrease at 45°, 90°, 135°, 180° bending	[120]

Material	Description	Capacitance	Energy density	Power density	Rate capability	Bending	Ref
Carbon nanotube (CNT)/MXene yarn (2018)	Yarn electrodes by biscrolling MXene with CNTs, freestanding asymmetric yarn SC prototypes by pairing with biscrolled RuO_2 yarns with 3.0 M H_2SO_4 electrolyte	3,188 mF cm^{-2}, 1,083 F cm^{-3}, 523 F g^{-1} at 2 mA cm^{-2}	61.6 mWh cm^{-3}, 168 µWh cm^{-2}, 8.4 µWh cm^{-1}	5,428 mW cm^{-3}, 14.8 mW cm^{-2}, 741 µW cm^{-1}	~90% at 10,000th cycle		[121]
Graphene fibre (2013)	2 intertwined hierarchical hybrid core–sheath fiber electrode [a core of graphene fibre (GF) covered with a sheath of 3D porous network-like graphene framework, denoted as GF@3D-G], solidified in the H_2SO_4-PVA electrolyte	1.7 mF cm^{-2}, 25-40 F g^{-1}, 20 µF cm^{-1} at 17 µA cm^{-2}	0.4-1.7 × 10^{-7} Wh cm^{-2}	6-100 × 10^{-6} W cm^{-2}	Similar after 500 cycles	No decrease after bending 500 cycles	[122]
Graphene/PPy composite fibre (2014)	Intertwining two G/PPy electrodes pre-coated with H_2SO_4–PVA polyelectrolyte	107 mF cm^{-2} at 0.24 mA cm^{-2}	9.7 µWh cm^{-2}			No decrease after 1,000 bending cycles	[123]
GO/MXene (~88 wt%) fibre (2017)	Wet spinning of GO liquid crystal-assisted MXene fibre with 1 M H_2SO_4 electrolyte	233 mF cm^{-2}, 257 F g^{-1}, 341 F cm^{-3}					[124]

Name	Description	Capacitance	Energy density	Power density	Cycling stability	Flexibility	Ref.
rGO/MXene hybrid fibre (2020)	Electrolyte Mediated hybrid fibre made of rGO and MXene, assembled into fibres via wet spinning with PVA-H_2SO_4 electrolyte	550.96 mF cm^{-2} and 110.89 F g^{-1} at 20 mV s^{-1}	12 μWh cm^{-2} and 9.85 mWh cm^{-3} at 8.8 mW cm^{-2} and 7.1 W cm^{-3}		85% at 10,000 cycle		[125]
rGO/10 wt% MoS$_2$ composite fibre (2021)	Wet spun rGO/10 wt% MoS$_2$ composite fibre with PVA- H_2SO_4 electrolyte	185.3 mF cm^{-2}	3.38 mW h cm^{-3}	0.0936 W cm^{-3}			[126]
rGO/20 wt% MoS$_2$ composite fibre (2021)	Wet spun rGO/20 wt% MoS$_2$ composite fibre with PVA- H_2SO_4 electrolyte	282.6 mF cm^{-2}	4.92 mW h cm^{-3}	0.051 W cm^{-3}	87 % after 1000 cycles		[126]
MXene (70%) /PEDOT:PSS hybrid fibre (2019)	Wet spun fibres using hybrid formulations of Ti$_3$C$_2$T$_x$ MXene nanosheets and PEDOT:PSS with PVA-H_2SO_4 electrolyte	Electrode 676 mF cm^{-2}, 258 F g^{-1}, 615 F cm^{-3}	≈7.13 Wh cm^{-3}	≈8249 mW cm^{-3}	~95% after 10,000 cycle	96% after cyclically stretched to 100% strain	[127]
Carbon fibre tow (CFT) (2015)	Activation of pristine CFTs by oxidative exfoliation by KMnO$_4$/H$_2$SO$_4$, annealing in air and reduction by a mixture of hydrogen iodide (HI) and acetic acid (AcOH), twisting two activated electrodes together after coating with PVA-H_3PO_4 electrolyte	2.55 F cm^{-3} at 10 mV s^{-1}	0.35 mWh cm^{-3}	3000 mW cm^{-3}	91% after 10,000 cycles	No decrease after 1,000 bending at 90°, 135° knotting	[128]

Carbon fibre (2015)	Manganese oxide nanosheet grown on carbon nanoparticle coated carbon fibre (CF@CNPs) and functionalized CF@CNPs are employed as the positive and negative electrode respectively with LiCl-PVA electrolyte	5 F cm^{-3} at 2 mA cm^{-3}	2.1 mWh cm^{-3}	10.22 W cm^{-3}	81.2% afte 10,000 cycles	No decrease after bending at 180°, 360°.	129
Carbon fibre (2013)	PPy deposition on MnO$_2$ nanoflakes coated carbon fibre (CF/MnO$_2$/PPy), two PPy-MnO$_2$-CFs fixed on preservative film substrate and assembled into SC by sandwiching PVA-H$_3$PO$_4$ membrane as separator and electrolyte between electrodes	69.3 F cm^{-3} at 0.1 A cm^{-3}	6.16 mWh cm^{-3}	0.04 W cm^{-3}	86.7% after 1,000 cycles	99.8% after rolling up	130
Carbon fibre (2016)	Carbon fibre bundle @ CNT-NiCo(OH)x (CF@CNC) as positive and carbon fibre bundle @ activated carbon (CF@AC) as negative electrode, immersed in PVA-KOH electrolyte, dried, twisted together	111 mF cm^{-2}, (64.0 mF cm^{-1})	33.0 μWh cm^{-2}, 0.84 mWh cm^{-3}	0.75 mW cm^{-2}, 19.1 mW cm^{-3}	103% after 8,000 cycles	20% decay after 1000 bending times and 107% retention after 1,000 twisting times	131

Carbon fibre (2017)	Braided carbon fiber electrodes coated with MWNT/V_2O_5 nanowires (NWs), a cellulose-based separator, and an ionic-liquid electrolyte of [EMIM][TFSI]/LiCl/Al_2O_3 nanoparticles	10.6 mF cm^{-2} at 0.5 mA cm^{-2}			~100% after > 10,000 cycles	98.7% after 1,000 bending cycles	[132]
Carbon fibre yarn (CFY) (2018)	Sheath-core PANI nanowire array grown on aligned carbon nanofibres/ carbon fibre yarn electrode (CFY@CNFs@PANI NWA), two fibre-shaped electrodes parallelly placed on PET substrate and immersed in PVA-H_2SO_4 electrolyte	234 mF cm^{-2} at 0.1 mA cm^{-2}	21.4 µWh cm^{-2}	at 0.52 mW cm^{-2}	90% after 8,000 cycles		[133]
Carbon fibre (2019)	Dip-coating of mixture of ionic liquid 1-ethyl-3-methylimidazolium bis(trifluoromethylsulfonyl) imide ([EMIM][TFSI]), carbon nanotubes, and electro-polymerization of PPy onto Au coated carbon fiber with propylene carbonate-poly(methyl methacrylate)-[EMIM][TFSI] gel electrolyte to form wire-type SC	38.49 mF cm^{-2} at 0.6 mA cm^{-2}	24.7 µWh cm^{-2}	3.52 mW cm^{-2}		99% after 100 bending cycles, 95.6% capacitance retention at 60 min in water	[134]

Substrate (year)	Description	Capacitance	Energy density	Power density	Cycling stability	Flexibility	Ref
Carbon fibre (2020)	PEDOT:PSS- rGO drop coating and MnO_2 electrodeposition on carbon fibre, MnO_2/PEDOT:PSS-rGO and PEDOT:PSS-rGO as positive and negative electrodes with Na_2SO_4-CMC electrolyte	Electrode 2.92 F cm^{-2} (194 F cm^{-3}, 550 mF cm^{-1}) at 5 mA cm^{-2}	295 µWh cm^{-2} (19 mWh cm^{-3}, 55 µWh cm^{-1})	2900 µW cm^{-2} (190 mW cm^{-3}, 545 µW	96% after 5,000 cycles		[135]
Platinum wire (2013)	PEDOT/MWNT biscrolled yarn with Pt wire with liquid electrolyte (H_2SO_4) or, with 1 M H_2SO_4/PVA gel electrolyte.	At 0.01 Vs^{-1}, ~167 F cm^{-3} (liquid electrolyte), ~180 F cm^{-3} (solid).	1.4 mWh cm^{-3} (Solid)	40 W cm^{-3} (Solid)	98% after 2,000 cycles	98% after 2,000 bending, 92% after 10,000 winding, 99% after 10,000 cycles woven into gloves	[136]
Platinum yarn (2014)	PANI nanowire solution coated on CNT wrapped Pt yarns (Pt wire/CNTs/PANI) with PVA-H_3PO_4 electrolyte	86.2 F g^{-1}, 0.24 mF cm^{-1}, 52.5 mF cm^{-2} at 5 mV s^{-1}	35.27 Wh kg^{-1}	10.69 kW kg^{-1}		No decrease after folding/unfolding 1,000 cycles	[137]
Au wire (2018)	Two wire electrode prepared by layer-by-layer (LbL) assembly of MWCNTs, vanadium oxide (VO_x), wetted with organic electrolyte of propylene carbonate (PC)−acetonitrile (ACN)−lithium perchlorate ($LiClO_4$)−PMMA and twisted together	5.23 mF cm^{-2} at 0.2 mA cm^{-2}	1.86 µ Wh cm^{-2}	8.5 mW cm^{-2}	94% after 10,000 cycles		[138]

Stainless steel yarn (2015)	Two PPy-wrapped Fe_3O_4 deposited SS magnetic electrodes coated with PVA-H_3PO_4 gel electrolyte, dried, twisted and coated with PU	61.4 mF cm^{-2} at 10 mV s^{-1}			77% after 1,000 cycles	Self healing 71.8% at 4 breaking & reconnecting	139
Stainless steel fibre yarn (2015)	PPy@MnO_2@rGO-deposited conductive yarns as both active materials and current collectors, two parallel yarn electrodes coated with PVA-H_3PO_4 electrolyte	36.6 mF cm^{-1} & 486 mF cm^{-2} in aqueous Na_2SO_4 electrolyte (3-electrode cell) or 31 mF cm^{-1} and 411 mF cm^{-2} in PVA / H_3PO_4 (2-electrode cell)	SS SC 0.0092 mWh cm^{-2} & 1.1 mWh cm^{-3}	1.33 mW cm^{-2}, 160 mW cm^{-3}	SS SC 92% over 4,950 cycles	80% after 1,000 cycles at 90 bending, 91% after 1,000 cycles knotting, 103% after 1,000 cycles twisting	140
Stainless steel spring (SSS) (2018)	In-situ synthesis of hierarchical carbon tubular nano structures (hCTNs) and PANI composites onto SSS substrate to form stretchable SC electrode	277.8 F g^{-1} at 1 A g^{-1}, and 402.8 mF cm^{-1} at 1 mA cm^{-1}			75% over 3,000 cycles	100% stretchable	141
Stainless steel filament (2020)	Core-sheath single yarn produced by PVA-H_2SO_4 electrolyte-mediated rGO & MXene fibres twisted around the SS filament core, two-ply yarns made from plying of two single core-sheath yarns, two yarn electrodes plied to obtain SCs	Dual-core YSC 253.01 mF cm^{-2} (43.6 mF cm^{-1} at 20 mV s^{-1})	27.1 µWh cm^{-2} at 2502.6 µW cm^{-2}	2,502.6 µW cm^{-2} at 27.1 µWh cm^{-2}	18% deterioration after 10,000 cycles	90% after 1,000 bending cycles	142

Substrate (Reporting year)	Device Configuration	Device capacitance	Energy density	Power density	Capacitance retention	Flexibility	Ref
Stainless steel filament (2020)	Hydrothermal deposition of nickel-cobalt oxide on stainless steel cables, stainless steel cables @nickel-cobalt oxide electrode	113×10^{-3} mAh cm^{-1} at 0.3 mA cm^{-1}					143
2D shaped							
Cotton fabric (2010)	Deposition of MnO$_2$ after dipping and drying of cotton with SWNT ink electrodes with 2M aqueous Li$_2$SO$_4$ electrolyte	0.41 Fcm^{-2}			Negligible change over 35,000 cycles		42
Non-woven cloth (2011)	Dip coating of nonwoven wiper cloth in the SWCNT ink followed by deposition of PANI nanowire arrays on to obtain the PANI/SWCNT/ cloth composite electrode	390 F g^{-1} at 1 A g^{-1}	26.6 Wh kg^{-1}	7,000 WKg^{-1}	90% after 3,000 cycles	No decrease at 90° bending	144
Cotton t-shirt (2012)	MnO$_2$/ ACT (activated carbon textiles from cotton t-shirt) as positive, ACT as negative electrode, copper foil as current collectors, and Whatman filter paper soaked with 1M Na$_2$SO$_4$ aqueous solution as the separator	120 F g^{-1} at 1 mA cm^{-2}	66.7 Wh kg^{-1}	4.97 kW kg^{-1}	97.5% after 1,000 cycles		145

Cotton stretchable knit fabric (90% cotton/10% Lycra) (2013)	Electrochemical deposition of PPy on pre-strained Au coated cotton fabric with 1.0 M NaCl	255 F g^{-1} at 10 mV s^{-1}				Sustain up to 140% strain without electric failure	[146]
Cotton (2015)	Electrodes prepared by dip coating of cotton on GO dispersion, thermal reduction, and PPy deposition. SC device with 2.0 M NaCl aqueous solution electrolyte	336 F g^{-1}	21.1 Wh kg^{-1} at 0.6 mA cm^{-2}				[147]
Cotton (2015)	PPy coated cotton fabric electrode through in situ chemical polymerization by using CuO nanoparticles template, with 2.0 M NaCl aqueous solution	225 F g^{-1} at 0.6 mA cm^{-2}			92 % after 200 cycles		[148]
Cotton fabric (2015)	PPy conductive polymer coated on top of MnO$_2$ nanoparticles deposited-CNT textile with PEO/Na$_2$SO$_4$ gel electrolyte	461 F g^{-1}	31.1 Wh kg^{-1}	22.1 kW kg^{-1}	93.8% over 10,000 cycles	98.5% upon 21% tensile strain, no capacity change upon 13% bending strain, 96.3% after imposing cyclic bending of 750,000 cycles	[149]

Substrate (Year)	Description	Specific capacitance	Energy density	Power density	Cycling stability	Flexibility	Ref.
Cotton fabric (2015)	Binder-free ternary composites of MnO$_2$ nanoparticles, SWNT, PANI and PEDOT:PSS deposited layer-by-layer by dip coating to prepare cotton electrode with gel electrolyte composed of cetonitrile (ACN): propylenecarbonate (PC): PMMA: tetra-butylammonium hexafluorophosphate (TBAPF6) in a ratio of 70:20:7:3 by weight	MnO$_2$/SWNT/PANI: 294 Fg^{-1}, MnO2/SWNT/PEDOT:PSS ternary composite devices: 246 Fg^{-1}	MnO$_2$/SWNT/PANI: 66.4 Whkg^{-1}, MnO2/SWNT/PEDOT:PSS ternary composite devices: 60.2 Whkg^{-1}	MnO$_2$/SWNT/PANI: 746.5 Wkg^{-1}, MnO2/SWNT/PEDOT:PSS ternary composite devices: 640.5 Wkg^{-1}		<3%, down to a bending angle of 180°	150
Cotton fabric (2016)	Direct electrospinning of MWCNTs on nickel-coated cotton fabrics (Ni–cotton)	973.5 mF cm^{-2} at 2.5 mA cm^{-2}			No decay after 3,000		151
Cotton fabric (2017)	CNT/rGO-coated fabric as negative electrode and PPy-coated fabric as the positive electrode	570 mF cm^{-2} at 1 mA cm^{-2}	0.26 mW hcm^{-2}		91% after 1,000 cycles	Excellent stability under bending 100 times with an angle of 180°.	152
Cotton fabric (2018)	PPy electrochemically deposited on the surface of dip- dried cotton into MXene (Ti$_3$C$_2$T$_x$) nanosheets with H$_2$SO$_4$-PVA electrolyte	Electrode (with 1 M H$_2$SO$_4$ solution) 343.20 F g^{-1}	Device 1.30 mW h g^{-1}	Device 41.1 mW g^{-1}			93

Material	Method						Ref
Cotton fabric (2018)	PPy/TiO$_2$-coated cotton fabric electrode via sol-gel and in-situ chemical oxidation method with 2.0 M NaCl aqueous electrolyte	Electrode 733 F g^{-1} at 0.6 A cm^{-2}	44.4 Wh kg^{-1} at 555 W kg^{-1}				[153]
Cotton fabric (2020)	GO deposited by 'dip and dry' method, chemically reduced into rGO/cotton fabric, MnO$_2$ nanoparticles accumulated on rGO/cotton fabric by in situ chemical deposition, PANI layer coated on rGO/MnO$_2$/cotton fabric by in situ oxidative polymerization technique with 1 M H$_2$SO$_4$ electrolyte solution	888 F g^{-1} and 252 F g^{-1} at 1 A g^{-1} and 25 A g^{-1}, 444 F cm^{-2}				70% after 3,000 cycles at 15 A g^{-1}	[154]
Cotton fabric (2021)	PPy/rGO nanocomposite cotton fabric (NCF) by chemical polymerization	PPy-0.5/rGO NCF electrode 9,300 mF cm^{-2} at 1 mA cm^{-2}	Device 167 μWh cm^{-2}	Device 1.20 mW cm^{-2}	Electrode retention 94.47% after 10,000		[155]

Material	Description	Specific capacitance	Energy density	Power density	Cycling stability	Bending stability	Ref
Cotton fabric (2022)	GO nanosheets fixed on the cotton fabric by vacuum filtration, pyrrole monomers and silver ions (Ag+) adsorbed on the surface of GO/CF by π-π and electrostatic interactions, respectively to form flexible PPy/Ag/GO/CF electrodes with PVA-H_2SO_4 gel electrolyte	Electrode 1,664.0 mF cm^{-2}, 27.0 F cm^{-3}, SC 286.6 mF cm^{-2} (4.7 F cm^{-3})	SC 25.5 µWh cm^{-2}	SC 1149.5 µW cm^{-2}		89.7% after 10,000 bending cycles	[156]
Bamboo fabric (2020)	MnO_2–$NiCo_2O_4$ printed bamboo fabric as positive electrode, and rGO printed bamboo fabric as negative electrode with LiCl-PVA gel electrolyte	2.12 Fcm^{-2} (1,766 F g^{-1}) at 2 mA cm^{-2}	37.8 mW cm^{-3}	2678.4 mWcm^{-3}	92% of after 5,000 cycles		[157]
Polyester fabric (2011)	Graphene/MnO_2-textile as positive and SWNTs-textile as negative electrode in aqueous Na_2SO_4 electrolyte	Hybrid graphene /MnO_2 based textiles, up to 315 F g^{-1}	12.5 Wh kg^{-1}	110 kW kg^{-1}	95% after 5,000 cycles		[158]
Polyester fabric (2011)	MnO_2 nanoflowers electrodeposited onto CNT-enabled conductive textile fibres, MnO_2-CNT-textile as positive electrode, reduced MnO_2-CNT-textile as negative electrode, Whatman filter paper as separator and 0.5 M Na_2SO_4 in water as electrolyte	410 Fg^{-1} at 5 mVs^{-1} and 2.8 F cm^{-2} at 0.05 mV s^{-1}	~5-20 Wh kg^{-1}	~13 000 W kg^{-1}	80% after first 200 cycles, 60% after 10,000 and 50% after 50,000 cycles		[159]

Material (year)	Description	Capacitance	Energy density	Power density	Cycle stability	Flexibility	Ref.
Polyester film (2013)	Directly growing CNTs along graphene fibres with Fe_3O_4 nanoparticles for CVD of the nanotubes, PET films coated with Au layer as supporting substrates and current collectors, filter paper separator soaked with 1 M Na_2SO_4 aqueous electrolyte	200.4 F g^{-1}, 0.98 mF cm^{-2} at 20 mA cm^{-2}				No decrease after 200 bending cycles	[160]
Polyester fabric (2014)	CNT dip-coated onto Cu metallized PET fabrics electrode	8.5×10^{-3} F cm^{-2}					[48]
Polyester fabric (2014)	PANI film deposited on the CNT/Au/PET; with PVA-H_3PO_4 electrolyte	7.1m F cm^{-2} (electrode), (CV)	2.412×10^{-4} W h cm^{-3}		89% after 2,500 cycles	Excellent performance under	[48]
Polyester fabric (2015)	Strip shaped electrode prepared by PANI deposited on aligned CNTs, with PVA-H_3PO_4 gel electrolyte	421.7 F cm^{-3} (343.6 F g^{-1} and 47.8 F cm^{-3} (electrode), at 0.5 A cm^{-2}	9.56 mWh cm^{-3}	2.91 W cm^{-3}	Stable within 10,000 cycles	81% after immersion in water for 48 h	[161]
Polyester fabric (2016)	Two pieces of MnO_2 deposited conductive graphene/polyester composite fabric with PVA-$NaNO_3$ electrolyte	265.8 F g^{-1} at 2 mV s^{-1}				87% after 100 times bending	[162]

Material (year)	Method	Capacitance	Energy density	Power density	Cycling stability	Bending stability	Ref.
Polyester fabric (2018)	PPy electrochemically deposited on rGO painted SnCl$_2$ modified polyester textiles with PVA-H$_2$SO$_4$ electrolyte	Electrode 1,117 mF cm^{-2} at 1 mA cm^{-2}, 329.5 F g^{-1} at 1 mA cm^{-1}, Device 474 mF cm^{-2}	0.0658 mWh cm^{-2} at 1 mA cm^{-2}	25 mW cm^{-2}	100% after 10,000 cycles	98.3% after 1000 bending cycles	[108]
Polyester fabric (2019)	Dipping and drying of PET with GO, followed by chemical reduction of GO and subsequent chemical growth of PPy on PET, composite electrodes of PET/rGO/PPy sandwiched using PVA-H$_2$SO$_4$ gel electrolyte	230 mF cm^{-2} at 1 mV s^{-1}, 5.5 F cm^{-3} at 1.6 mA cm^{-3}	11 µWh cm^{-2}	0.03 mW cm^{-2}	76% after 6,000 cycles		[163]
Polyester fabric (2020)	Pre-treated polyester dip coated in GO, followed by reduction of GO and in situ polymerization of PPy particles on fabric surface with aqueous 1 M H$_2$SO$_4$ solution	Electrode 8,300 mF g^{-1} and 640 mF cm^{-2}					[164]
Polyester fabric (2020)	Silver paste printed on PET, MnHCF-MnOx/GO ink overprinted and reduced to form electrode, PVA-LiCl electrolyte and paper separator	16.8 mF cm^{-2}	0.5 mWh cm^{-2}	0.0023 mW cm^{-2}		Stable while bending to 60°, 90°, and 180° for 100 cycles	[165]

Substrate	Description						
Silk fabric (2016)	Screen-printed current collector and active material layers [MnO-coated hollow carbon microspheres, acetylene black, and binder) mixed in a weight ratio of 7:2:1 as printing ink] on silk fabrics substrate and a PDMS film; after being pasted with gel electrolyte, the PDMS-based electrode transferred on the top of silk fabric electrode	19.23 mF cm^{-2} at 1 mA cm^{-2}			84% after 2,000 cycles	98.5% after 100 times bending and 96.8% after 100 times twisting	[166]
Nylon/PU (67/33) (2021)	Supersonic spraying rGO/SnO$_2$ on fabric with 2 M KOH electrolyte	$1,008$ mF cm^{-2} at 1.5 mA cm^{-2}			93% after 10,000 cycles		[167]
Stretchable textiles (2018)	Fully printed Ag@PPy@MnO$_2$ on Ag cathode electrode and activated carbon on Ag anode electrode with PVA-Na$_2$SO$_4$ electrolyte	426.3 mF cm^{-2} (cathode)	0.0337 mWh cm^{-2} at 0.38 mW cm^{-2}		90.8% after 5,000 cycles	86.2% after 40% stretching strain	[168]
Spandex fabric (2019)	Assembling vertical PPy nanotube (VPPyNT) grown on the carbon nano onions (CNO) @ PPy granula (PPyG)-textile electrodes with a PVA-H$_3$PO$_4$ electrolyte sandwiched structure	64 F g^{-1}	5.7 Wh Kg^{-1}		85% after 1,000 cycles	99% retention after stretching for 500 cycles at a strain of 50%, 88% at a strain of 100%	[169]

Material	Description	Capacitance	Energy density	Power density	Cyclability	Flexibility	Ref
Carbon nanofibre web (2008)	PPy coated on MWCNT-embedded activated carbon nanofibers (PPy/ACNF/CNT) using Ni foil as the current collector with 6 M KOH aqueous electrolyte	333 F g⁻¹ at 1 mA cm⁻², 275 F g⁻¹ at 10 mA cm⁻²			Negligible change after 500 cycles		[170]
Graphene fibre fabric (2017)	Hierarchical graphene fibre fabrics (GFFs) with PVA-H₂SO₄ gel electrolyte	Electrode 244 F g⁻¹, 1,060 mF cm⁻² at thickness of 150 μm,	23.5 μWh cm⁻²	26.3 mW cm⁻²	Good rate capability up to 50,000 cycles	Bendable to 180° without breaking	[171]
Carbon fabric (2012)	Carbon fabric-aligned carbon nanotube/ MnO₂/ conducting polymers (CF-ACNT-MnO₂-PEDOT) with 1 M Na₂SO₄ Composite SC electrodes	1.3 F cm⁻² at 0.1 mV s⁻¹			5% loss after 1,000 cycles		[172]
Carbon cloth (2013)	TiO₂ NWs grown on carbon cloth, hydrogen-treated TiO₂ NWs as core, electrochemically active MnO₂ (H-TiO₂@MnO₂ as positive) and carbon shells (H-TiO₂@C as negative) electrodes with separator, PVA-LiCl gel and LiCl aqueous electrolytes	0.68 F cm⁻³ (PVA/LiCl gel), GCD 0.70 F cm⁻³ at 0.5 mA cm⁻² (139.6 F g⁻¹ at 1.1 A g⁻¹)	0.3 mWh cm⁻³ (59 Wh kg⁻¹)	0.23 W cm⁻³ (45 kW kg⁻¹)	91.2% after 5,000 cycles	No decay in bending & twisting	[173]

Carbon cloth (2015)	MnO$_2$ as cathode, Ti-Fe$_2$O$_3$@PEDOT as anode with NKK separator and PVA-LiCl gel electrolyte	Anode 1.15 F cm^{-2} (311.6 F g^{-1} and 28.8 F cm^{-3} at 1 mA cm^{-2})	0.89 mWh cm^{-3} at 1 mA cm^{-2}	0.44 W cm^{-3}	85.4% after 6,000 cycles		[174]
Carbon cloth (2015)	SnO$_2$@MO$_x$ (SnO$_2$@NiO, SnO$_2$@Co$_3$O$_4$, SnO$_2$@MnO$_2$) heterostructures grown on carbon cloth (CC) with 1 M Na$_2$SO$_4$ aqueous electrolyte (for SnO$_2$ and SnO$_2$@MnO$_2$) and 1 M KOH aqueous electrolyte (for SnO$_2$@NiO and SnO$_2$@Co$_3$O$_4$)	SnO$_2$@MnO$_2$ heterostructure electrode showed the highest discharge areal capacitance (980 mF cm^{-2} at 1 mA cm^{-2})			After 6,000 cycles, SnO$_2$@Co$_3$O$_4$, SnO$_2$@NiO and SnO$_2$@MnO$_2$ electrodes can maintain 58.3%		[175]
Carbon cloth (2015)	Two symmetric freestanding PANI-cobalt-based MOF crystals (PANI-ZIF-67) electrodes with H$_2$SO$_4$-PVA as gel electrolyte	2,146 mF cm^{-2} for PANI-ZIF-67-CC electrode at 10mV s^{-1},	0.0161 mWh cm^{-3} (0.0044 mWh cm^{-2})	0.833 Wcm^{-3} (0.245 Wcm^{-2})	80% after 2,000 cycles		[176]
Carbon cloth (2015)	Assembly of MnO$_2$@carbonized Polypyrole (CPPy) as positive and carbon coated Co$_3$O$_4$ (Co$_3$O$_4$@C) microsheet as negative electrode with PVA-KOH electrolyte	59.5 F cm^{-3} at 20 mA cm^{-2}	27.0 mWh cm^{-3}	1.31 W cm^{-3}	96 % after 5,000 cycles	97 % after 500 bending cycles	[177]

Substrate (Year)	Description	Capacitance	Energy density	Power density	Cycle stability	Flexibility	Ref.
Carbon cloth (2015)	Hierarchical structure of ALD Co_3O_4 nanolayer deposited on CVD derived carbon cloth (CNT/CC), (CNTs@Co_3O_4/CC) with 2M KOH electrolyte	Highest 416.7 mF cm^{-2}			No capacity fading even after 50,000 cycles		178
Carbon cloth (2016)	In-situ electrodeposition of MnO_2 and PPy composite on carbon cloth with 1 M Na_2SO_4 aqueous electrolyte	Electrode 325 F g^{-1} at 0.2 A g^{-1}, 228 mF cm^{-2} at 0.14 mA cm^{-2}			~96% after 1,000 cycles		86
Carbon cloth (2017)	SnO_2 nanoparticles, CNTs, ethyl cellulose, and terpineol composite ink screen-printed onto carbon cloth. Furnace-calcined SnO_2/CNT electrodes sandwiched with PVA-H_2SO_4 gel electrolyte	5.61 mF cm^{-2} (flat) and 5.68 mF cm^{-2} (bent)					179
Carbon cloth (2018)	Solvothermal MoO_2 coating of carbon fibres followed by covered and interconnect by rGO film to form electrode with 1 mol L^{-1} H_2SO_4 aqueous electrolyte	Electrode 8,132 mF cm^{-2} at 2 mV s^{-1}	143 μWh cm^{-2} at 10 mA cm^{-2}	15,022 μW cm^{-2} at 100 mA cm^{-2}	95% after 30,000 cycles at 120 mA cm^{-2}	77% after 6,000 times folding	180

Material	Description	Capacitance	Energy density	Power density	Cycling stability		Ref
Carbon cloth (2018)	MnO_2/cotton derived carbon cloth (CDCC) as positive, CDCC as negative electrode attached by nickel foams, cotton woven separator sandwiched with 1 M Na_2SO_4 aqueous electrolyte	202 mF cm^{-2} at 0.1 mA cm^{-2}	30.1 mWh cm^{-2} at 0.15 mW cm^{-2}		87.7% after 5,000 cycles		[181]
Carbon cloth (2019)	Hydrothermal incorporation of Pt into MoS_2 nanosheets grown on carbon cloth as electrode in 1 M Na_2SO_4 solution, Pt-doped MoS_2 and activated carbon electrodes with PVA-H_3PO_4 electrolyte	250 F g^{-1} at 0.5 A g^{-1} (electrode), 42 F g^{-1} at 0.4 A g^{-1} (device)			87.96% after 3,000 cycles		[182]
Carbon fibre textile (CFT) (2019)	Activated porous CFT (APCFT) electrode as anode and TiN@MnO_2 on CFT as cathode with PVA-LiCl electrolyte	Anode 1.2 F cm^{-2} at 4 mA cm^{-2}	4.70 mWh cm^{-3}	2.29 W cm^{-3}	No decay after 25,000 cycles		[183]
Carbon fabric (2019)	Two, RGO enfolded cobalt (II, III) oxide nanowires on flexible carbon fabric substrate (CONW-RGO) electrodes with PVA/KOH gel electrolyte and filter paper as a separator	Electrode 1,110 F g^{-1} at 1 A g^{-1}, SC 111.35 F g^{-1}, 33.4 mF cm^{-2} and 685 mF cm^{-3}	34.78 Wh kg^{-1} or 0.0104 mWh cm^{-2}	3.6 kW kg^{-1} or 1.2 mW cm^{-2} or 23 mW cm^{-3} at 24.68 Wh kg^{-1}	Electrode 94.2% after 2,000 cyclics		[184]

Carbon cloth (2020)	One-step hydrothermal method to prepare NiMnO3 nanosheets on a carbon cloth (CC) with 6M KOH was the electrolyte	2,330 F g^{-1} at 1 A g^{-1}				67.8% after 1,000 cycles at 10 A g^{-1}	[185]
Carbon cloth (2021)	MoS$_2$/PANI composite material drop casted on functionalized carbon cloth; MoS$_2$/PANI/FCC electrodes soaked with 1 M H$_2$SO$_4$ electrolyte	452.25 F g^{-1} at 0.2 A g^{-1} (electrode), 72.8 F g^{-1} at 0.2 A g^{-1} (device)				87% after 1,000 cycles at 10 A g^{-1} (electrode)	[98]
Carbon fabric (2022)	Cobalt doped MoS$_2$ (Co-MoS$_2$) nanoflower electrode with 1 M KOH electrolyte	86 F g^{-1}	4.30 Wh kg^{-1}	0.6 KW kg^{-1}	98.5% after 10,000 cycles		[186]
Multidimensional hirerarchial fabric (2019)	Graphene nanosheets (GNS) and PEDOT: PSS deposited on hierarchical fabric via spraying method to fabricate flexible SCs with PVA/H$_2$SO$_4$ electrolyte	245.5 mFcm^{-2} at 1 mVcm^{-2}	21.82 µWhcm^{-2} at 0.4 mWcm^{-2}		83.9% after 10,000 cycles	mere loss under different bending states	[187]

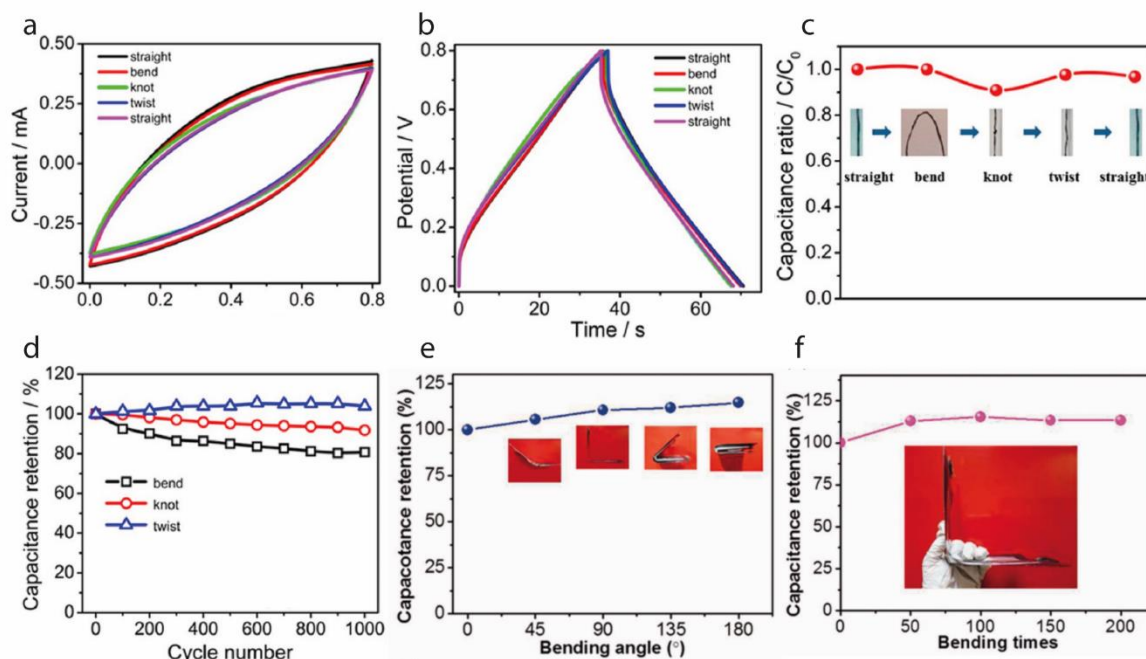# Appendix E. Other key properties of SCs for wearable applications

E.1 Flexibility

Figure E.1 Flexibility tests of PPy@MnO₂@rGO-deposited conductive yarns measured in the two-electrode cell a) CV curves of the all-solid-state yarn supercapacitor undergoing consecutive deformations at a scan rate of 100 mV/s b) GCD curves of the all-solid-state yarn supercapacitor undergoing consecutive deformations at a current density of 80 mA/cm³ c) Capacitance ratio under various deformations d) Capacitance retention of the all-solid-state yarn supercapacitor after each deformation. Reproduced with permission.[140] Copyright 2015, American Chemical Society. Influence of bending deformation on CeO₂-ACVF capacitive performance; specific capacitance e) under various bending angles; and f) after different bending cycles. ACVF: activated viscose fabric. Reproduced with permission.[91] Copyright 2020, SAGE Publications.

To be considered as wearable, a SC device must be flexible and durable under the physical movement of the body. The bending of SC devices for hundred to several hundred cycles are performed at various angles to evaluate the flexibility of a SC device. Additionally, twisting, winding, and other deformations are also assessed. Yu et al.,[31] reported more than 97% capacitance retention after 1000 bending cycles at 90° angle of hierarchically structured carbon nanotube-graphene fibre-based micro SCs. Chen et al.[111] reported an electrochromic fibre-shaped SC composed of elastic fibre/CNTs/PANI retaining capacitance of 93.8% after 1000 bending cycles at 180°. Choi et al.[116] reported a flexible SC made of carbon nanotube

yarn with MnO_2 exhibiting no decrease of capacitance even after 1000 bending at 90°. Ding et al.[123] fabricated a graphene/PPy composite fibres for all-solid-state, flexible fibre form SC that exhibiting similar performance.

In addition to bending, the flexibility of SCs for other mechanical deformations was reported by some research groups. For example, a yarn-based SC was developed by Lee et al.,[136] composed of Pt/MWCNTs/PEDOT retained 98% of its initial capacitance after 2,000 bending, 92% after 10,000 winding, and 99% after 10,000 cycles when woven into a glove. Huang et al.[140] reported yarn-based SC of rGO/MnO_2/PPy that retained 80% capacitance after 1,000 cycles at 90° bending, 91% after 1,000 cycles knotting, and 103% after 1,000 cycles twisting, revealing the enhancement of the capacitive performance, *Figure (a-d)*. Similarly, the capacitance was increased (107% retention) after 1,000 cycles of twisting for an asymmetric fibre-shaped solid-state SC based on carbon fibre bundle.[131] Additionally, several other articles have reported higher bending cycles. For example, Ye et al.[102] reported a fibre-shaped SC by introducing rGO and carbon nanoparticles (CNPs) on commercial cotton threads (CT) using dip-coating technique combined with low-temperature vapour reduction, which resulted in 92.30% capacitance retention after 2000 bending cycles. Liu et al.[101] examined their 1D-shaped flexible yarn SC composed of rGO/Ni cotton composite electrodes with PVA/LiCl gel as electrolyte and separator for 4000 cycles, and found 95% of retention after at 180° bending angle. Furthermore, Wu et al.[118] reported a flexible fiber-shaped SCs (FSSCs) by twisting a number of CNT yarns (n) with a Pt filament as current collector and PANI nanowires. They obtained a capacitance retention of 98.17 % after 3,000 cycles and 95.91 % after 5,000 flexing cycles.

For 2D-shaped SC devices, shorter bending cycles were used for testing capacitance retention of textiles SCs. Zhang et al.[166] reported a silk fabric-based SC which retained 98.5% after 100 bending cycles and 96.8% after 100 twisting cycles. Lee et al.[177] developed an asymmetric SC by assembling MnO_2@CPPy and carbon coated Co_3O_4 microsheet (Co_3O_4@C)-decorated carbon cloths with a solid-state PVA/KOH electrolyte, which retained 97% capacitance after 500 bending cycles. Luo et al.[91] reported an increase of 13.4% capacitance after 200 bending cycles for an all-fabric solid-state flexible SC, made of activated carbon fibre fabric, *Figure* (e,f). The capacitance of a solid-state stretchable SC, prepared by assembling VPPyNTs/CNOs@PPyG-textile electrodes with a PVA/H_3PO_4 gel electrolyte into a sandwiched structure, was nearly unchanged after stretching for 500 cycles at a strain of 50%.

However, the capacitance retention ratio decreased slightly to 88% as the strain% was increased to 100%.[169]

E.2 Safety issue

To be wearable, the flexible SC device components must be non-toxic to avoid any health concern as well as for the environment when disposed of. The concerns with wearable SCs is raised due to the toxic nanoparticles or metal particles of all sizes entering or generated during manufacturing stages as well as during usage. In addition, the effect of electromagnetic fields, accidental electric shock, and the inability to activate the emergency shut-off in case of malfunctioning are also matter of concerns.[188] In addition, wearable SCs and other wearable electronic devices have limited lifetimes. Therefore, it is also critical to ensure that the waste generated by the SCs does not create new hazards for health and the environment.

A report was published revealing that more than 8 billion batteries enter the US and European markets annually. Also 3 billion alkaline units get discarded each year in North America alone.[189] Another report projected a generation of more than 130 g of battery waste per person each year.[190] Besides battery, increasing usage of mobile, computing and other autonomous electrical devices increases the production and disposal of SC devices exponentially.[189] An estimated 20,000 tonnes of old household batteries end up in landfill every year.[191] The challenges of such disposal to the environment is due to the presence of a large number of toxic metals (e.g., Cd, Ni, Pb), F-containing electrolytes and device components, corrosive fluids (e.g., H_2SO_4 and H_3PO_4), and fire hazards from organic electrolytes, which may have negative environmental impacts and may induce numerous health problems such as acute or long-term exposure. The principal issue of the release of metals into landfills is the potential to contaminate the groundwater. Incineration of them may also pose two major potential environmental concerns; the release of metals (mostly mercury, cadmium and lead) into the ambient air and the concentration of metals in the ashes which must be landfilled. The F-containing electrolyte salts (tetraethylammonium tetrafluoroborate, Net_4BF_4), carbon particle binder (such as PTFE or PVDF), and electrode separator (often PTFE) are likely to generate volatile fluorocarbons during traditional incineration, which are highly toxic to organisms and are likely to damage incinerators and nearby structures. Acetonitrile solvents, commonly implemented in high-performance devices, are flammable, carcinogenic, and may decompose into highly toxic cyanides upon heating. Some ions commonly used in promising ionic liquids, such as bis(trifluoromethanesulfonyl)imide (TFSI), have been shown to inhibit

cellular respiration. Although some aqueous electrolytes that implement Li_2SO_4 or Na_2SO_4 are expected to be benign to the environment, they still emit SO_2, contributing to acid rain when released during incineration. Although SCs, unlike fuel cells and batteries, contain no noble or heavy metals that are particularly difficult to dispose of, conventional collectors and packaging materials, such as steel and Al, are incombustible and cannot be fully burned without leaving ash residue. Thus, the disposal of SCs not only generates harmful substances but also incombustible waste materials that need to be stored in landfill.[190]

E.3 Washability
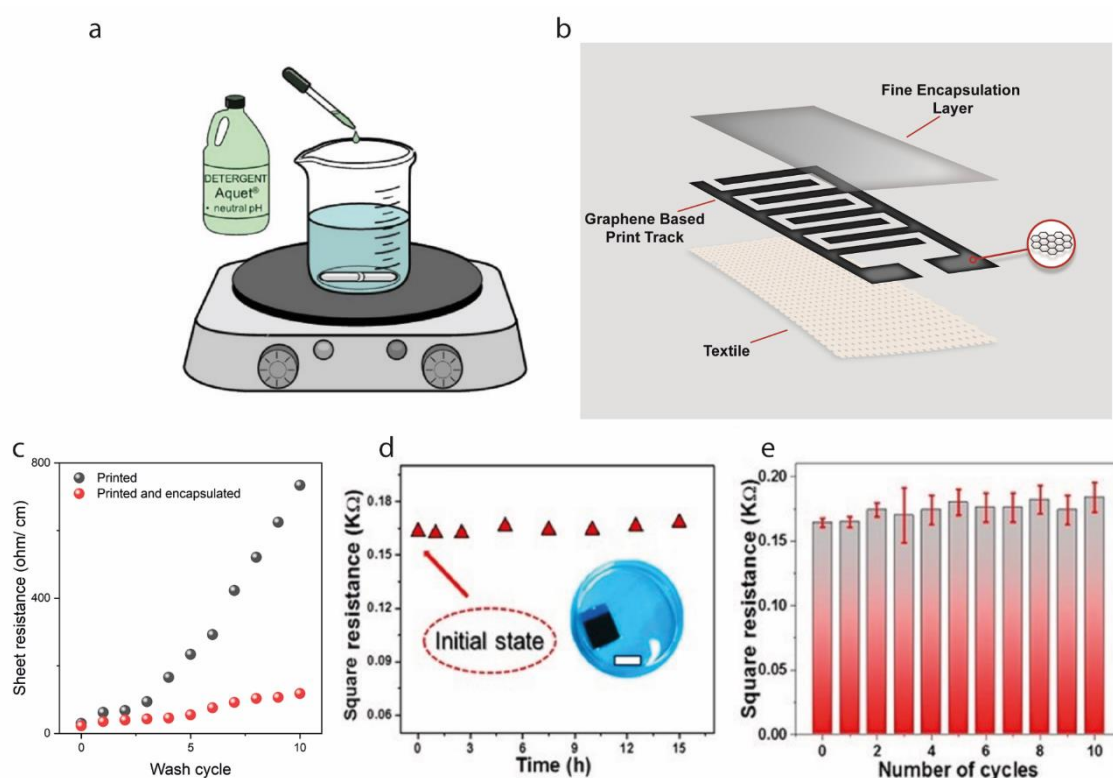
Figure E.2 a) Schematic diagram of washing test. Reproduced with permission.[192] Copyright 2019, The Royal Society of Chemistry. b) Illustration of graphene-based ink pattern and encapsulation layer on textile substrate c) The change in electrical resistance with number of washing cycles of graphene-based ink printed (without encapsulation) and graphene-based ink-printed (with encapsulation) cotton fabric. Reproduced with permission.[47] Copyright Copyright 2022, Elsevier. d) Resistances of electrode after being immersed in water for different times. The inset is the photograph of electrode immersed in water for 1 week (scale bar: 20 mm) e) Resistances of same electrode on nylon substrate after being immersed in

water for different times and 2 h for each time. Reproduced with permission.[193] Copyright 2018, American Chemical Society.

Washability is a product's ability to withstand a predetermined number of cycles of a specified washing process, able to adequately clean the product without loss of functionality and/or serviceability and without resulting security risks for the user.[194] Most e-textiles still suffer from the poor wash ability, reducing the reliability of e-textiles to be ready for the market. Many of experimental wearable e-textiles are not suitable for real life applications because of this problem. The hydrophobic textile substrate, due to capillary effect, can still absorb water in the textile bulk making the device fail. Also, the mechanical stresses incorporated by the washing cycles may destroy the electrical contacts between the conductive thread and the electronic wearable device. Thus, the electric impedance becomes uncontrollable after several washing cycles, making the wearable device unstable and often stops functioning.[195] Therefore, there remains a need for the technology that can provide better wash stability for conductive textiles.

Wash ability is usually reported by the retention of performance after several washing cycles. We encapsulated screen-printed graphene-based conductive pattern on textiles to protect it from being washed away, ***Figure b***. [47] The sheet resistance before and after encapsulation of the printed pattern was evaluated. It was found that the bare pattern had an increase of 10 times resistance, whereas the encapsulated pattern exhibited only 3.5 times increase in the sheet resistance after 10 wash cycle, ***Figure c***. Cao et al.[193] also reported a screen-printed washable e-textile electrodes, which were tested after being immersed in water for different times, showed very negligible variation, after soaking in water repeatedly and for longer duration, ***Figure (d,e)***. A KAIST research team, fabricated a self-powered washable textile-based wearable display module on real textiles that integrate polymer solar cells (PSCs) with organic light emitting diodes (OLEDs), exhibiting little change in characteristics after 10 minutes-long 20 washings cycles.[192] Qiang et al.[49] demonstrated a super-hydrophobic conducting fabric with graphene and hexagonal boron nitride inks. The different fabrics were then integrated to engineer an all-textile-based capacitive heterostructure that sustained 20 cycles of repeated washing. Barazekhi et al.[164] also reported a negligible decrease in conductivity after 20 laundry cycles for rGO - PPy based polyester textile SC.

Appendix F. Supporting information of Chapter 3. Fully printed and multifunctional graphene-based wearable e-textiles for personalized healthcare applications

**F1. Characterization of screen-print ink**
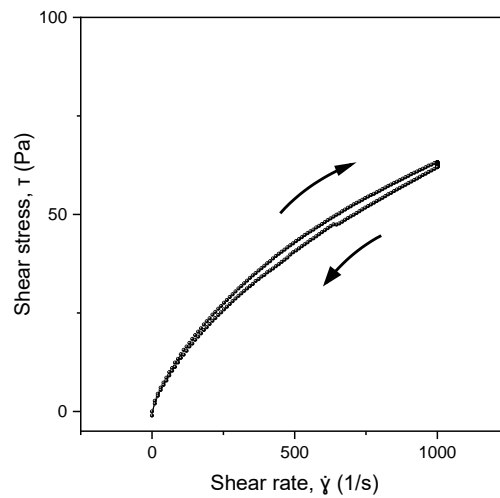
Figure F1. Thixotropic behaviour of the graphene-based print ink.

F2. Effect of annealing of fabric

Table F1. Comparison of tensile properties of annealed substrate in comparison with the untreated substrate according to EN ISO 13934-1.

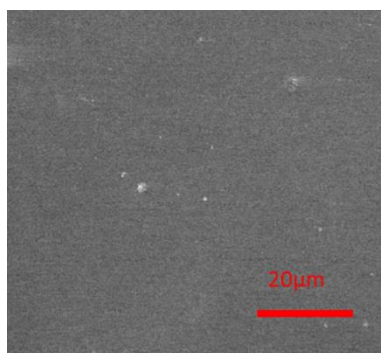| Parameters	Un-treated substrate	Annealed (at 170°C)	% Change
Breaking force (N)	613.30	596.18	-2.79
Standard deviation	46.73	52.76	-
Elongation (mm)	34.63	33.43	-3.47
Standard deviation	1.55	1.61	-
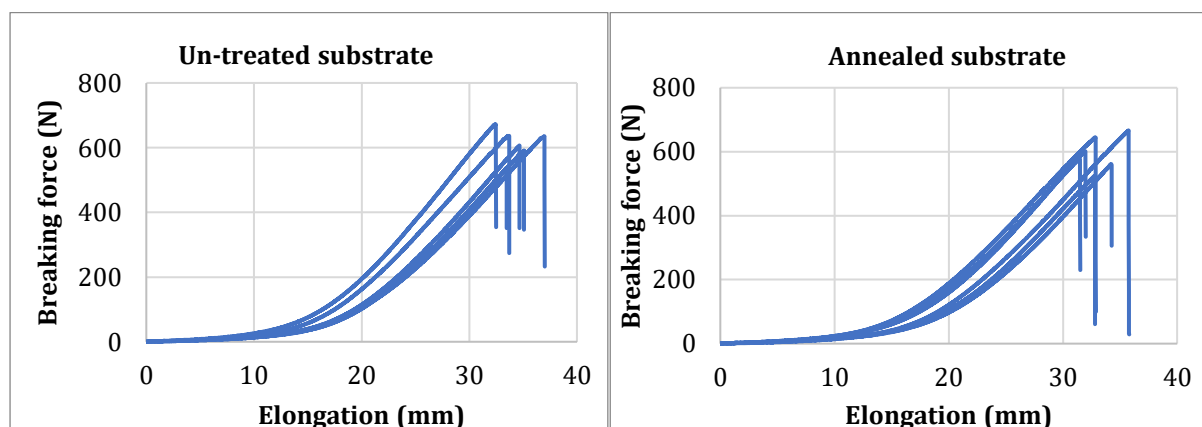
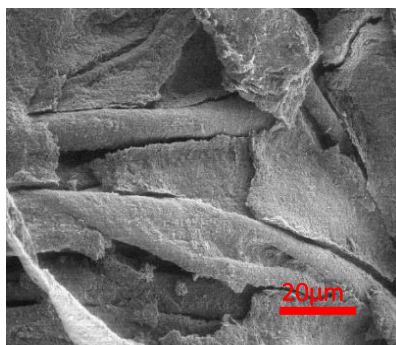**Figure F2**. Force-elongation curves for untreated and annealed substrate.

F3. Scanning electron microscope (SEM) images
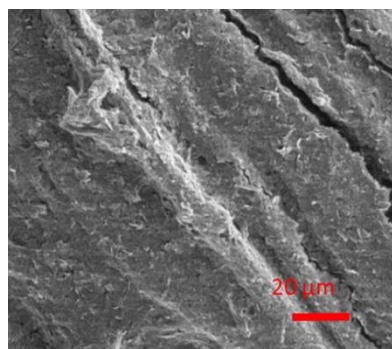
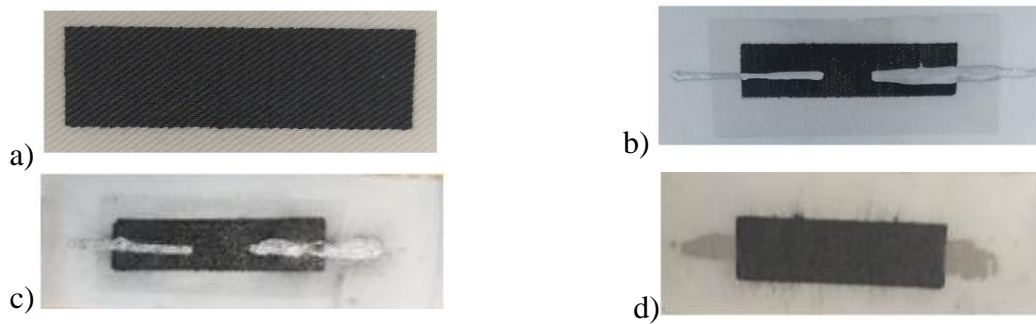**Figure F3.** SEM image of graphene-ink printed (1 layer) fabric (×2000).

Figure F4. SEM image of graphene-ink printed (4 layer) and encapsulated fabric (×2000).


Figure F5. SEM image of graphene-ink printed and washed cotton fabric without encapsulation (×1000).

**F4. Digital photographs of graphene-based textiles**

a) b) c) d)

Figure F6. Digital photograph of a) printed (4 layer), b) encapsulated, c) washed without encapsulation, and d) washed after encapsulation of graphene-ink printed cotton fabric.
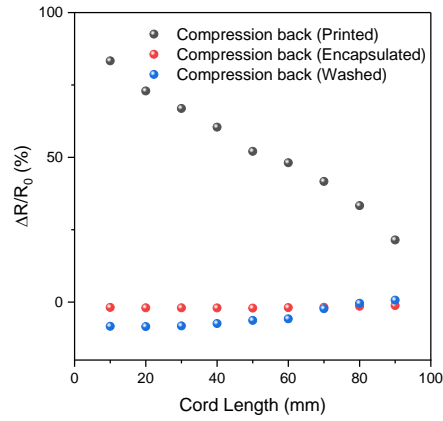
F5. Flexibility tests of graphene-based textiles

Bending
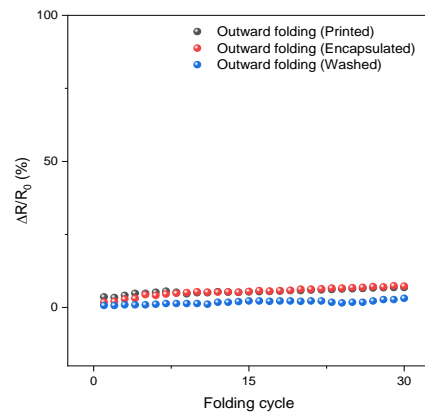
C

C

Compression
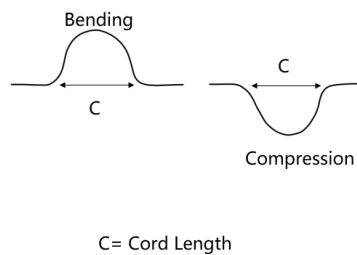
C= Cord Length

Figure F7. The cord lengths during bending (concave down) and compression (concave upward) of graphene-ink printed textiles.
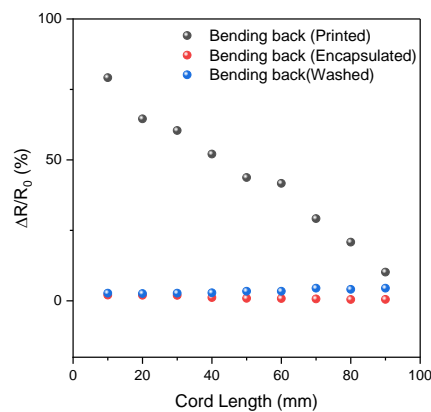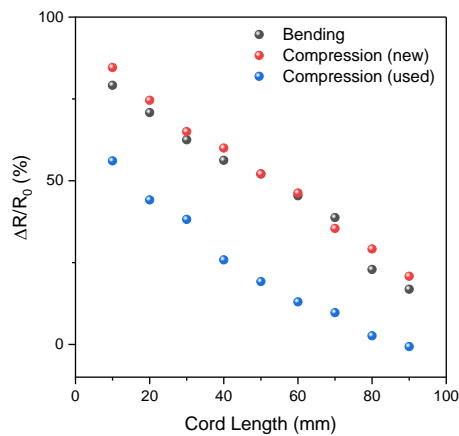

Figure F8. The variation in resistance of the bending sensor in backward (bending back) direction.
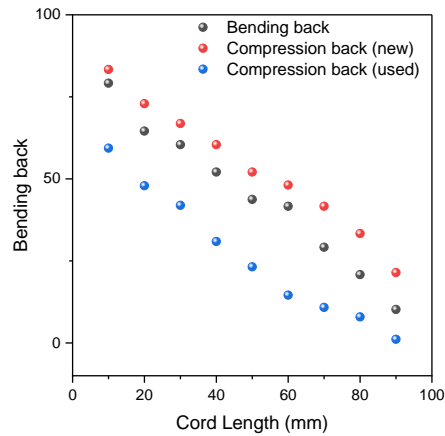
Figure F9. The variation in resistance of the compression sensor in backward (compression back) direction.

Figure F10. The variation in resistance under 30 outward (printed pattern outside) folding−releasing cycles.

Figure F11. The variation in resistance of the compression sensor (forward direction) while used as new sample versus a bended sample.

Figure F12. The variation in resistance of the compression sensor (backward direction) while used as new sample versus a bended sample.

F5. Digital photographs of activity monitoring
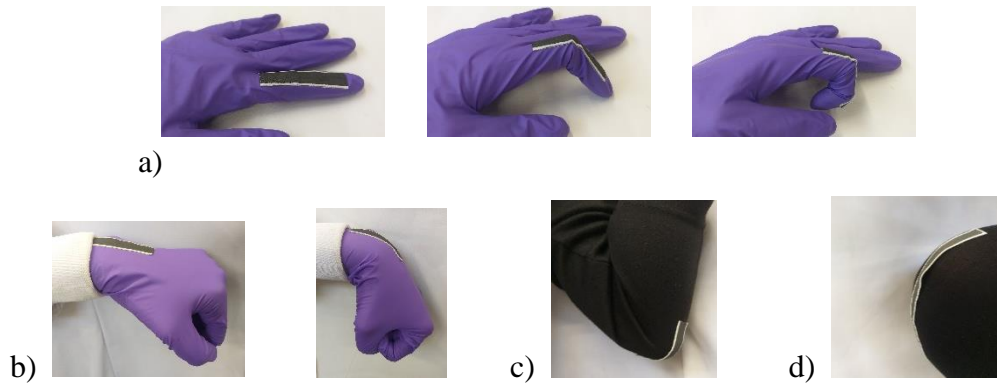
Figure F13. Activity monitoring with the printed sensors a) finger bending b) wrist bending c) elbow bending and d) knee bending.

F6. Schematic of interdigitated supercapacitor pattern
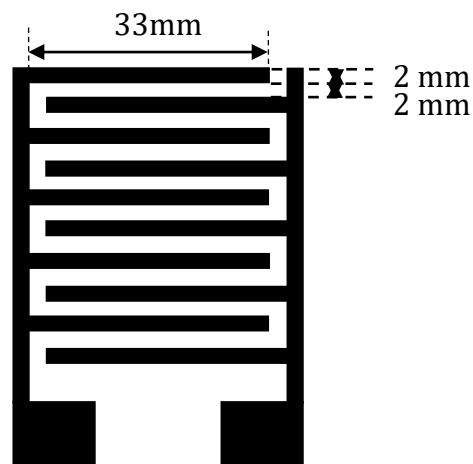
Figure F14. Schematic of graphene-ink printed supercapacitor device.

F6. Comparison of capacitance performance with literature

Table F2. Comparison of the electrochemical performance of the graphene-ink printed energy storage textile with others reported in the literature.

Sl.	Assembly of energy storage textiles	performance	Energy and power density	Device retention	Flexibility	Ref.
1	Screen printed rGO on cotton followed by reduction with PVA-H_2SO_4 solid electrolyte	2.5 mF cm^{-2}	-	97 % after 10000 cycle	95.6% after folding 180° for 2000 cycles	[45]
2	Graphene film with PVA-H_2SO_4 solid electrolyte	2.7 mF cm^{-2}	-	-	-	[196]
3	Textiles fully printed Ag@PPy@MnO_2 on Ag cathode electrode and activated carbon on Ag anode electrode with PVA-Na_2SO_4 electrolyte	426.3 mF cm^{-2} (cathode)	0.0337 mWh cm^{-2} at 0.38 mWcm^{-2}	90.8% retention after 5000 cycles	86.2% retention after 40% stretching strain	[168]
4	PPy electrochemically deposited on rGO painted $SnCl_2$ modified polyester textiles with PVA/H_2SO_4 gel electrolyte	1117 mF cm^{-2} at a current density of 1 mA cm^{-2}	0.0658 mWh cm^{-2} at 1 mA cm^{-2} and 0.5 mW cm^{-2}	100% after 10 000 cycles	98.3% after 1000 bending cycles	[108]
5	Coating of poly-cotton textiles with graphene ink	2.7 mF cm^{-2}	-	98% after 15 000 cycles	98% after 150 cycles of bending at 180°	[50]
6	Kevlar fibres, coated in gold, and then grew ZnO nanowires with PVA- H_3PO_4 electrolyte	Areal capacitance 2.4 mF cm^{-2}	2.7×10^{-5} mWh cm^{-2}	-	-	[197]
7	CNT on Ti wire with PVA-H_2SO_4 solid electrolyte	Areal capacitance 1.84 mF cm^{-3}	0.16×10^{-3} mW h cm^{-3} and 0.01 mW cm^{-3}	80 % after 1000 cycles	-	[198]
8	SnS/S doped graphene on PET with PVA/H_2SO_4 solid	Areal capacitance	-	99% after 10000 cycle	-	[199]

|		electrolyte	2.98 mF cm^{-2}				
9	N-Doped rGO on PET with PVA-H$_3$PO$_4$ solid electrolyte	Areal capacitance 3.4 mF cm^{-2}	0.3 mWh cm^{-3} at 0.2 W cm^{-3}	98% after 2000 cycles	-		[200]
10	Graphene ink screen printed on cotton textiles with PVA-H$_2$SO$_4$ gel electrolyte	3.2 mFcm^{-2}	0.28 mWh cm^{-2} at 3 mW cm^{-2}.	95% after 10000 cycles	-		This work

Appendix G. Supporting Information of Chapter 4. Scalable production of 2D material heterostructure-based wearable textile supercapacitors

G1. Configuration of coating samples

Table G1. Graphene (G)- MoS₂ (M) – Graphene (G) layer deposition

Configurations	G-M-G	G-M-G	G-M-G	G-M-G	G-M-G
Graphene coating layers	1-0-0	2-0-0	3-0-0	4-0-0	5-0-0
	6-0-0	7-0-0	8-0-0	9-0-0	10-0-0
MoS₂ coating layers	0-1-0	0-2-0	0-3-0	0-4-0	0-5-0
	0-6-0	0-7-0	0-8-0	0-9-0	0-10-0
MoS₂-graphene bi-layers	0-1-1	0-2-1	0-3-1	0-4-1	0-5-1
	0-1-2	0-2-2	0-3-2	0-4-2	0-5-2
	0-1-3	0-2-3	0-3-3	0-4-3	0-5-3
	0-1-4	0-2-4	0-3-4	0-4-4	0-5-4
	0-1-5	0-2-5	0-3-5	0-4-5	0-5-5
Graphene-MoS₂-graphene tri-layers	1-1-1	1-2-1	1-3-1	1-4-1	1-5-1
	2-1-2	2-2-2	2-3-2	2-4-2	2-5-2
	3-1-3	3-2-3	3-3-3	3-4-3	3-5-3
	4-1-4	4-2-4	4-3-4	4-4-4	4-5-4
	5-1-5	5-2-5	5-3-5	5-4-5	5-5-5

G2. Scanning Electron Microscope images of the coated textiles
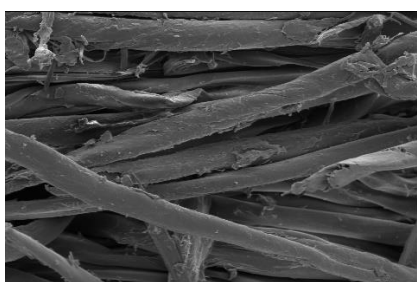
a. Un-coated cotton textiles (x 1000)
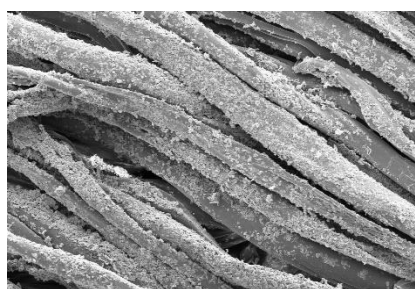
b. MoS$_2$ 1 coated textiles, M1 (x 1000)
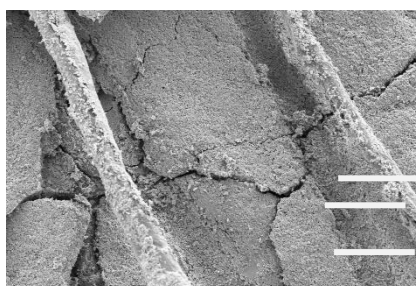
c. MoS$_2$ 10 coated textiles, M10 (x 1000)

Figure G1. *Scanning electron microscope (SEM) image of the a. Un-coated cotton textiles, b. MoS$_2$ 1layer coated textiles c. MoS$_2$ 10 layer coated textiles (Scale bar: 40 μm)*

G3. Flexibility of coated textiles
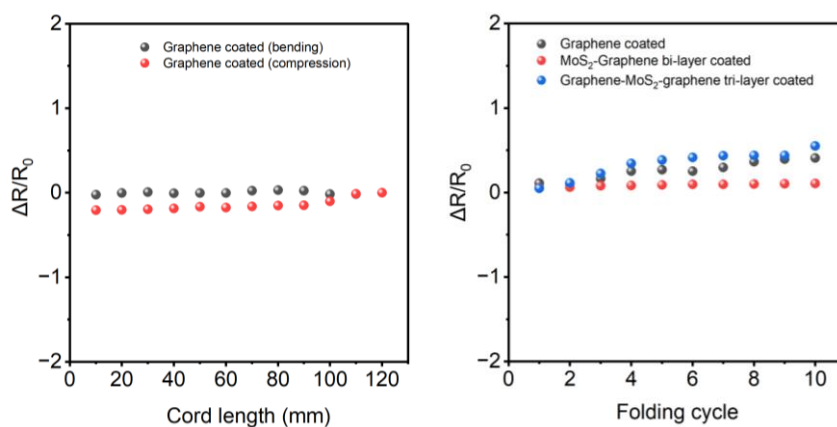
a. The variation in resistance of graphene coated textiles during bending and compression (left) and the variation in resistance of graphene coated, MoS$_2$-graphene coated and graphene-MoS$_2$-graphene coated textiles during 10 folding−releasing cycles (right)
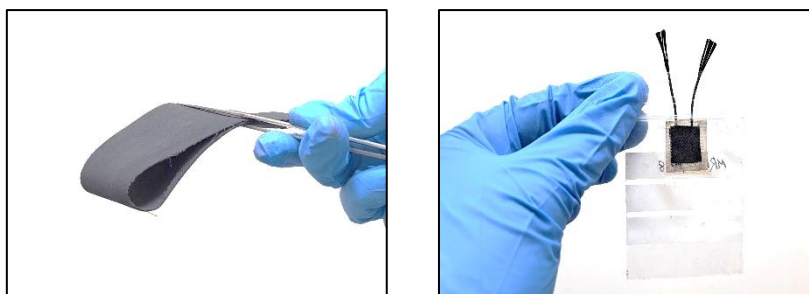
b. Graphene coated textiles and fabricated supercapacitor (1 cm × 1cm)
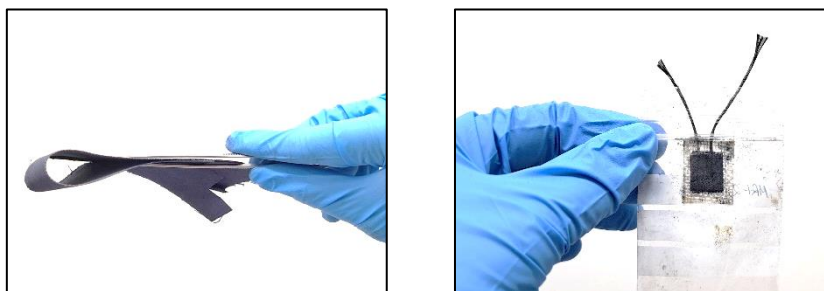
c. MoS₂ coated textiles and fabricated supercapacitor (1 cm × 1cm)
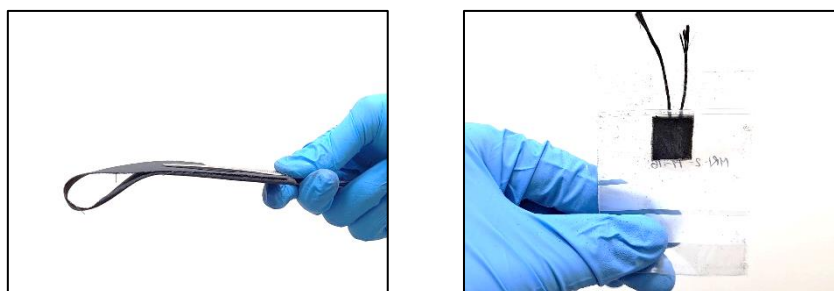
d. MoS₂-graphene bi-layer coated textiles and fabricated supercapacitor (1 cm × 1cm)
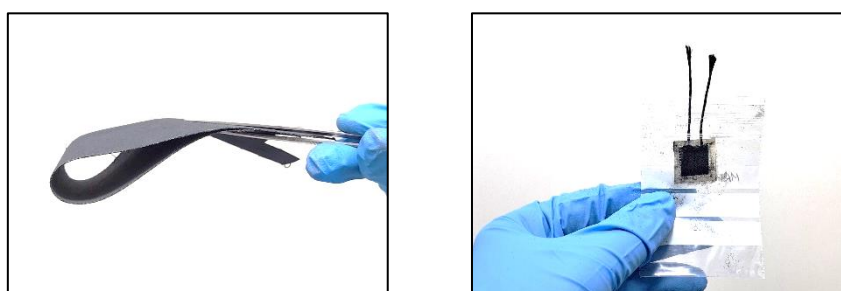
e. Graphene-MoS₂-graphene tri-layer coated textiles and fabricated supercapacitor

(1 cm × 1cm)

Figure G2. *Flexibility of the 2D materials-heterostructure coated textiles and as-fabricated supercapacitors*

G4. Electrochemical characterization of graphene-based textile supercapacitors
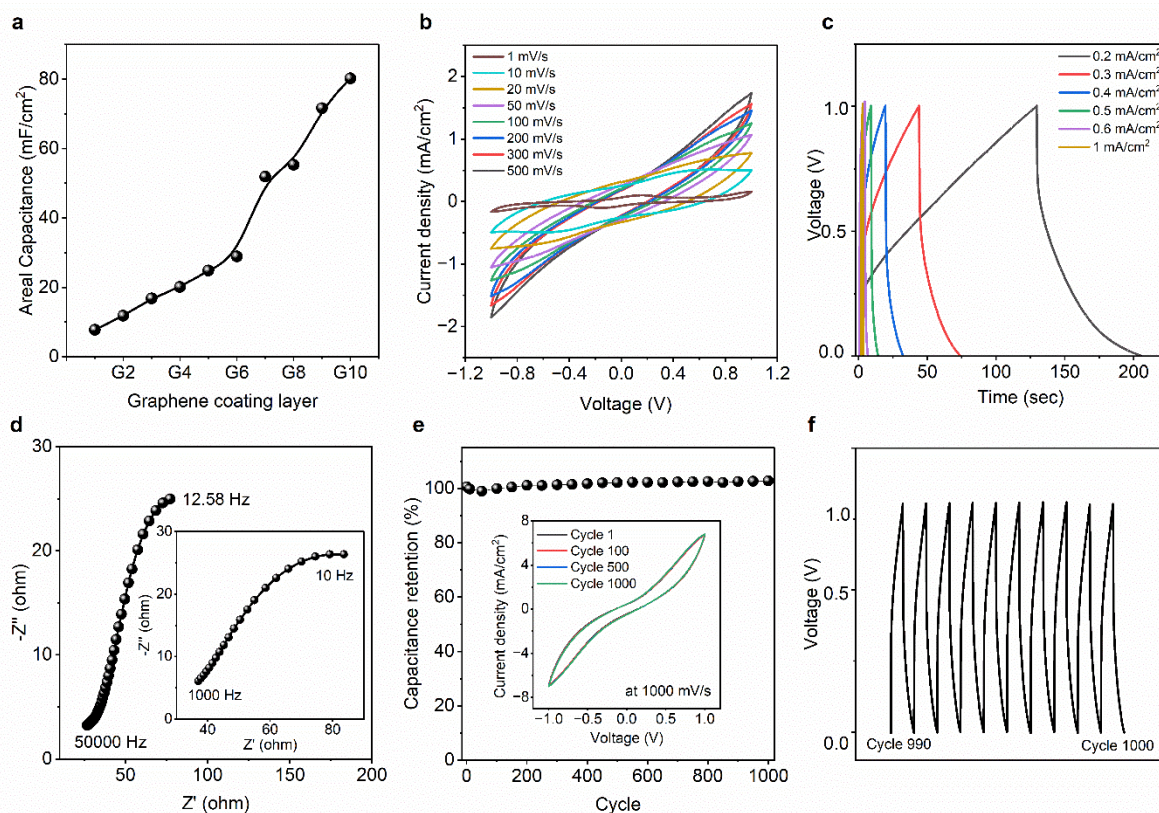
Figure G3. *Graphene-coated textile supercapacitor a. Change of areal capacitance with increase of graphene coating layers b. Cyclic voltammetry curves of the G10 coated textile supercapacitor at various scan rates c. Charge-discharge profile of the G10 coated textile supercapacitor at different current densities d. Electrical impedance spectroscopy of the device at high frequency range (inset shows the response of the supercapacitor device at low frequency range) e. Capacitance retention of the G10 coated textile supercapacitor device up to 1000 cycles, inset shows the CV curves at 1st, 100th, 500th and 1000th cycles and f. cyclic test of the supercapacitor (from 990th to 1000th cycles).*

G5. Electrochemical characterization of MoS₂-textile supercapacitors
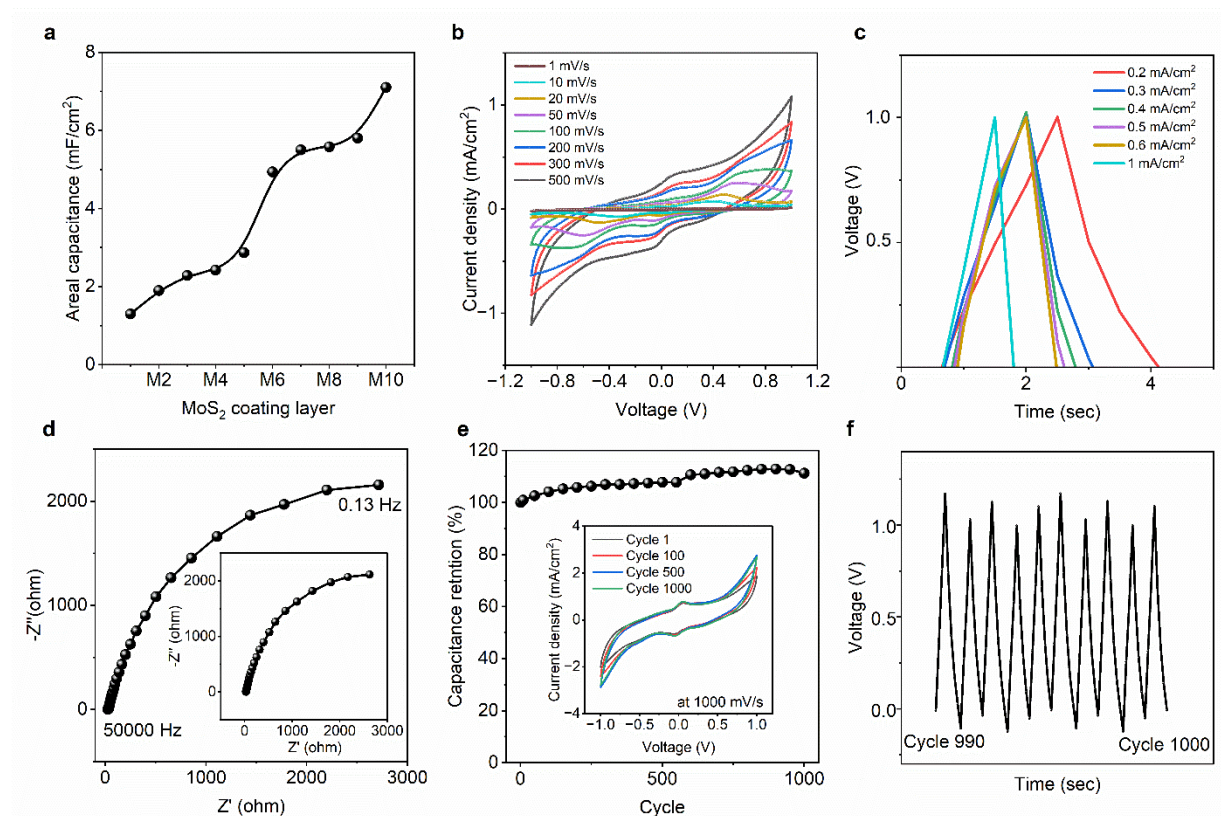
Figure G4. *MoS₂-coated textile supercapacitor a. Change of areal capacitance with increase of MoS₂ coating layers b. Cyclic voltammetry curves of the M10 coated textile supercapacitor at various scan rates c. Charge-discharge profile of the M10 coated textile supercapacitor at different current densities d. Electrical impedance spectroscopy of the device at high frequency range (inset shows the response of the supercapacitor device at low frequency range) e. Capacitance retention of the M10 coated textile supercapacitor device up to 1000 cycles, inset shows the CV curves at 1st, 100th, 500th and 1000th cycles and f. cyclic test of the supercapacitor (from 990th to 1000th cycles).*

G6. Comparison of capacitance performance of the heterostructure supercapacitors

Table G2. Overview of capacitance comparison of some reported supercapacitors in the literature

Electrode	Electrolyte	Areal capacitance	Energy and Power density	Ref
Graphene	PVA-H_2SO_4	3.2 mFcm^{-2}	0.28 mWh cm^{-2} and 3 mWcm^{-2}	[201]
NiO/MoS2/rGO	1 M KCl	7.38 mFcm^{-2} (at 25 mVs^{-1})		[202]
rGO-GO-rGO	0.1 M NaClO$_4$	2 mFcm^{-2}	2–5.4×10^{-4} Whcm^{-2} and 3.6–9×10^{-2} Wcm^{-2}	[33]
Light scribed GO	PVA-H_2SO_4	2.9 mFcm^{-2} (at 50 mVs^{-1})		[203]
rGO-CNT	3 M KCl	6.1 mFcm^{-2} (at 10 mVs^{-1})	0.68 mWhcm^{-3} and 77 Wcm^{-3}	[204]
CNT/MoO3	1 M HCl	4.86 mFcm^{-2} (at 10 mVs^{-1})	2.70 µWhcm^{-2} and 0.53 mWcm^{-2}	[205]
Graphite oxide	1 M Na$_2$SO$_4$	0.51 mFcm^{-2} (at 20 mVs^{-1})		[206]
MoS$_2$ nanoparticles	0.5 M H_2SO_4	29 µFcm^{-2} (at 0.5 mVs^{-1})		[207]
Graphene/CNT	1 M Na$_2$SO$_4$	2.16 mFcm^{-2} (at 100 mA cm^{-2})	2.42 mWhcm^{-3} and 115 Wcm^{-3}	[208]
Exfoliated MoS$_2$	6 M KOH	2 mFcm^{-2} (at 10 mVs^{-1})		[209]
Graphene/textile	PVA-H_2SO_4	80.185 mFcm^{-2} (at 1 mVs^{-1})	44.547 µWhcm^{-2} and 581.05 µWcm^{-2}	This study
MoS$_2$/textile	PVA-H_2SO_4	7.1 mFcm^{-2} (at 1 mVs^{-1})	3.944 µWhcm^{-2} and 3550 µWcm^{-2}	This study
MoS$_2$-graphene bi-layer/textile	PVA-H_2SO_4	63.73 mFcm^{-2} (at 1 mVs^{-1})	35.405 µWhcm^{-2} and 8497.333 µWcm^{-2}	This study
Graphene-MoS$_2$-graphene tri-layer/textile	PVA-H_2SO_4	105.08 mFcm^{-2} (at 1 mVs^{-1})	58.377 µWhcm^{-2} and 1604.274 µWcm^{-2}	This study

Appendix H. Supporting information of Chapter 5. ████████████████████████
██
████████

██

(Image redacted for copyright reason)

██

(Image redacted for copyright reason)

██

(Image redacted for copyright reason)

(Image redacted for copyright reason)

(Image redacted for copyright reason)

(Image redacted for copyright reason)

(Image redacted for copyright reason)

(Image redacted for copyright reason)

(Image redacted for copyright reason)

(Image redacted for copyright reason)

███████	████████████████████			
██████████████████	■	■	■	■
	■	■	■	
████████████████ ████	██████	███████	███████	██████
████████████████ ████	██████	███████	███████	██████
██████████████████ ██████	██████	███████	███████	

(Text redacted for copyright reason)

(Image redacted for copyright reason)

(Image redacted for copyright reason)

(Image redacted for copyright reason)

(Image redacted for copyright reason)

(Image redacted for copyright reason)

(Image redacted for copyright reason)

(Image redacted for copyright reason)

(Image redacted for copyright reason)

(Image redacted for copyright reason)

(Image redacted for copyright reason)

(Image redacted for copyright reason)

(Image redacted for copyright reason)

(Image redacted for copyright reason)

(Image redacted for copyright reason)

(Image redacted for copyright reason)

(Image redacted for copyright reason)

(Image redacted for copyright reason)

(Image redacted for copyright reason)

(Image redacted for copyright reason)

(Image redacted for copyright reason)

(Image redacted for copyright reason)

(Image redacted for copyright reason)

References

(1) Tehrani, M. Advanced Electrical Conductors: An Overview and Prospects of Metal Nanocomposite and Nanocarbon Based Conductors. *physica status solidi (a)* **2021**, *218* (8), 2000704. DOI: https://doi.org/10.1002/pssa.202000704.

(2) Spann, B. T.; Weber, J. C.; Brubaker, M. D.; Harvey, T. E.; Yang, L.; Honarvar, H.; Tsai, C.-N.; Treglia, A. C.; Lee, M.; Hussein, M. I.; et al. Semiconductor Thermal and Electrical Properties Decoupled by Localized Phonon Resonances. *Advanced Materials* **2023**, *35* (26), 2209779. DOI: https://doi.org/10.1002/adma.202209779.

(3) Salzmann, I.; Heimel, G.; Oehzelt, M.; Winkler, S.; Koch, N. Molecular Electrical Doping of Organic Semiconductors: Fundamental Mechanisms and Emerging Dopant Design Rules. *Accounts of Chemical Research* **2016**, *49* (3), 370-378. DOI: 10.1021/acs.accounts.5b00438.

(4) Feng, L.-C.; Xie, N.; Shao, W.-Z.; Lu, L.-X.; Zhen, L.; Zhao, J. Thermal conductivity determination of conductor/insulator composites by fractal: Geometrical tortuosity and percolation. *Composites Part B: Engineering* **2016**, *92*, 377-383. DOI: https://doi.org/10.1016/j.compositesb.2016.02.046.

(5) Zhang, W.; Chen, X.; Wang, Y.; Wu, L.; Hu, Y. Experimental and Modeling of Conductivity for Electrolyte Solution Systems. *ACS Omega* **2020**, *5* (35), 22465-22474. DOI: 10.1021/acsomega.0c03013.

(6) Rizzi, L.; Zienert, A.; Schuster, J.; Köhne, M.; Schulz, S. E. Electrical Conductivity Modeling of Graphene-based Conductor Materials. *ACS Applied Materials & Interfaces* **2018**, *10* (49), 43088-43094. DOI: 10.1021/acsami.8b16361.

(7) Azman, N. H. N.; Mamat @ Mat Nazir, M. S.; Ngee, L. H.; Sulaiman, Y. Graphene-based ternary composites for supercapacitors. *International Journal of Energy Research* **2018**, *42* (6), 2104-2116. DOI: 10.1002/er.4001.

(8) Elgrishi, N.; Rountree, K. J.; McCarthy, B. D.; Rountree, E. S.; Eisenhart, T. T.; Dempsey, J. L. A Practical Beginner's Guide to Cyclic Voltammetry. *Journal of Chemical Education* **2018**, *95* (2), 197-206. DOI: 10.1021/acs.jchemed.7b00361.

(9) Asthana, N.; Pal, K. Chapter 14 - Polymerized hybrid nanocomposite implementations of energy conversion cells device. In *Nanofabrication for Smart Nanosensor Applications*, Pal, K., Gomes, F. Eds.; Elsevier, 2020; pp 349-397.

(10) Nnamchi, P. S.; Obayi, C. S. Chapter 4 - Electrochemical Characterization of Nanomaterials. In *Characterization of Nanomaterials*, Mohan Bhagyaraj, S., Oluwafemi, O. S., Kalarikkal, N., Thomas, S. Eds.; Woodhead Publishing, 2018; pp 103-127.

(11) Zhang, S.; Pan, N. Supercapacitors Performance Evaluation. *Advanced Energy Materials* **2015**, *5* (6), 1401401, https://doi.org/10.1002/aenm.201401401. DOI: 10.1002/aenm.201401401 (acccessed 2021/03/10).

(12) Choudhary, Y. S.; Jothi, L.; Nageswaran, G. Chapter 2 - Electrochemical Characterization. In *Spectroscopic Methods for Nanomaterials Characterization*, Thomas, S., Thomas, R., Zachariah, A. K., Mishra, R. K. Eds.; Elsevier, 2017; pp 19-54.

(13) Iqbal, M. Z.; Faisal, M. M.; Ali, S. R. Integration of supercapacitors and batteries towards high-performance hybrid energy storage devices. *International Journal of Energy Research* **2021**, *45* (2), 1449-1479. DOI: 10.1002/er.5954.

(14) Raza, W.; Ali, F.; Raza, N.; Luo, Y.; Kim, K.-H.; Yang, J.; Kumar, S.; Mehmood, A.; Kwon, E. E. Recent advancements in supercapacitor technology. *Nano Energy* **2018**, *52*, 441-473. DOI: 10.1016/j.nanoen.2018.08.013.

(15) Diaz, R. E. 2 - Electrostatics. In *The Electrical Engineering Handbook*, Chen, W.-K. Ed.; Academic Press, 2005; pp 499-512.

(16) Zhai, S.; Karahan, H. E.; Wang, C.; Pei, Z.; Wei, L.; Chen, Y. 1D Supercapacitors for Emerging Electronics: Current Status and Future Directions. *Advanced Materials* **2020**, *32* (5), 1902387, https://doi.org/10.1002/adma.201902387. DOI: 10.1002/adma.201902387 (acccessed 2021/09/25).

(17) Yan, J.; Wang, Q.; Wei, T.; Fan, Z. Recent Advances in Design and Fabrication of Electrochemical Supercapacitors with High Energy Densities. *Advanced Energy Materials* **2014**, *4* (4), 1300816. DOI: 10.1002/aenm.201300816.

(18) Iqbal, M. Z.; Zakar, S.; Haider, S. S. Role of aqueous electrolytes on the performance of electrochemical energy storage device. *Journal of Electroanalytical Chemistry* **2020**, *858*, 113793. DOI: 10.1016/j.jelechem.2019.113793.

(19) Matsuda, Y.; Morita, M. Organic electrolyte solutions for rechargeable lithium batteries. *Journal of Power Sources* **1987**, *20* (3), 273-278. DOI: 10.1016/0378-7753(87)80123-4.

(20) Jónsson, E. Ionic liquids as electrolytes for energy storage applications – A modelling perspective. *Energy Storage Materials* **2020**, *25*, 827-835. DOI: 10.1016/j.ensm.2019.08.030.

(21) Yu, L.; Chen, G. Z. Ionic Liquid-Based Electrolytes for Supercapacitor and Supercapattery. *Frontiers in Chemistry* **2019**, *7* (272), Review. DOI: 10.3389/fchem.2019.00272.

(22) Zhu, M.; Wu, J.; Wang, Y.; Song, M.; Long, L.; Siyal, S. H.; Yang, X.; Sui, G. Recent advances in gel polymer electrolyte for high-performance lithium batteries. *Journal of Energy Chemistry* **2019**, *37*, 126-142. DOI: 10.1016/j.jechem.2018.12.013.

(23) Hui, C.-y.; Kan, C.-w.; Mak, C.-l.; Chau, K.-h. Flexible Energy Storage System—An Introductory Review of Textile-Based Flexible Supercapacitors. *Processes* **2019**, *7* (12). DOI: 10.3390/pr7120922.

(24) Cheng, X.; Pan, J.; Zhao, Y.; Liao, M.; Peng, H. Gel Polymer Electrolytes for Electrochemical Energy Storage. *Advanced Energy Materials* **2018**, *8* (7), 1702184, https://doi.org/10.1002/aenm.201702184. DOI: 10.1002/aenm.201702184 (acccessed 2021/03/12).

(25) Arunkumar, R.; Babu, R. S.; Usha Rani, M.; Rajendran, S. Influence of plasticizer on ionic conductivity of PVC-PBMA polymer electrolytes. *Ionics* **2017**, *23* (11), 3097-3109. DOI: 10.1007/s11581-017-2101-2.

(26) Boaretto, N.; Meabe, L.; Martinez-Ibañez, M.; Armand, M.; Zhang, H. Review— Polymer Electrolytes for Rechargeable Batteries: From Nanocomposite to Nanohybrid. *Journal of The Electrochemical Society* **2020**, *167* (7), 070524. DOI: 10.1149/1945-7111/ab7221.

(27) Fu, Y.; Cai, X.; Wu, H.; Lv, Z.; Hou, S.; Peng, M.; Yu, X.; Zou, D. Fiber Supercapacitors Utilizing Pen Ink for Flexible/Wearable Energy Storage. *Advanced Materials* **2012**, *24* (42), 5713-5718, https://doi.org/10.1002/adma.201202930. DOI: https://doi.org/10.1002/adma.201202930 (acccessed 2021/03/13).

(28) Le, V. T.; Kim, H.; Ghosh, A.; Kim, J.; Chang, J.; Vu, Q. A.; Pham, D. T.; Lee, J.-H.; Kim, S.-W.; Lee, Y. H. Coaxial Fiber Supercapacitor Using All-Carbon Material Electrodes. *ACS Nano* **2013**, *7* (7), 5940-5947. DOI: 10.1021/nn4016345.

(29) Cao, Y.; Zhu, M.; Li, P.; Zhang, R.; Li, X.; Gong, Q.; Wang, K.; Zhong, M.; Wu, D.; Lin, F.; et al. Boosting supercapacitor performance of carbon fibres using electrochemically reduced graphene oxide additives. *Physical Chemistry Chemical Physics* **2013**, *15* (45), 19550-19556, 10.1039/C3CP54017K. DOI: 10.1039/C3CP54017K.

(30) Aboutalebi, S. H.; Jalili, R.; Esrafilzadeh, D.; Salari, M.; Gholamvand, Z.; Aminorroaya Yamini, S.; Konstantinov, K.; Shepherd, R. L.; Chen, J.; Moulton, S. E.; et al. High-performance multifunctional Graphene yarns: Toward wearable all-carbon energy storage textiles. *ACS Nano* **2014**, *8* (3), 2456-2466. DOI: 10.1021/nn406026z.

(31) Yu, D.; Goh, K.; Wang, H.; Wei, L.; Jiang, W.; Zhang, Q.; Dai, L.; Chen, Y. Scalable synthesis of hierarchically structured carbon nanotube–graphene fibres for capacitive energy storage. *Nature Nanotechnology* **2014**, *9* (7), 555-562. DOI: 10.1038/nnano.2014.93.

(32) Kou, L.; Huang, T.; Zheng, B.; Han, Y.; Zhao, X.; Gopalsamy, K.; Sun, H.; Gao, C. Coaxial wet-spun yarn supercapacitors for high-energy density and safe wearable electronics. *Nature Communications* **2014**. DOI: 10.1038/ncomms4754.

(33) Hu, Y.; Cheng, H.; Zhao, F.; Chen, N.; Jiang, L.; Feng, Z.; Qu, L. All-in-one graphene fiber supercapacitor. *Nanoscale* **2014**, *6* (12), 6448-6451, 10.1039/C4NR01220H. DOI: 10.1039/C4NR01220H.

(34) Zhai, S.; Jiang, W.; Wei, L.; Karahan, H. E.; Yuan, Y.; Ng, A. K.; Chen, Y. All-carbon solid-state yarn supercapacitors from activated carbon and carbon fibers for smart textiles. *Materials Horizons* **2015**, *2* (6), 598-605, 10.1039/C5MH00108K. DOI: 10.1039/C5MH00108K.

(35) Wang, B.; Fang, X.; Sun, H.; He, S.; Ren, J.; Zhang, Y.; Peng, H. Fabricating Continuous Supercapacitor Fibers with High Performances by Integrating All Building Materials and Steps into One Process. *Adv Mater* **2015**, *27* (47), 7854-7860. DOI: 10.1002/adma.201503441 From NLM.

(36) Zhao, X.; Zheng, B.; Huang, T.; Gao, C. Graphene-based single fiber supercapacitor with a coaxial structure. *Nanoscale* **2015**, *7* (21), 9399-9404, 10.1039/C5NR01737H. DOI: 10.1039/C5NR01737H.

(37) Ma, Y.; Li, P.; Sedloff, J. W.; Zhang, X.; Zhang, H.; Liu, J. Conductive Graphene Fibers for Wire-Shaped Supercapacitors Strengthened by Unfunctionalized Few-Walled Carbon Nanotubes. *ACS Nano* **2015**, *9* (2), 1352-1359. DOI: 10.1021/nn505412v.

(38) Huang, G.; Hou, C.; Shao, Y.; Zhu, B.; Jia, B.; Wang, H.; Zhang, Q.; Li, Y. High-performance all-solid-state yarn supercapacitors based on porous graphene ribbons. *Nano Energy* **2015**, *12*, 26-32. DOI: 10.1016/j.nanoen.2014.11.056.

(39) Liang, Y.; Wang, Z.; Huang, J.; Cheng, H.; Zhao, F.; Hu, Y.; Jiang, L.; Qu, L. Series of in-fiber graphene supercapacitors for flexible wearable devices. *Journal of Materials Chemistry A* **2015**, *3* (6), 2547-2551, 10.1039/C4TA06574C. DOI: 10.1039/C4TA06574C.

(40) Chen, S.; Ma, W.; Xiang, H.; Cheng, Y.; Yang, S.; Weng, W.; Zhu, M. Conductive, tough, hydrophilic poly(vinyl alcohol)/graphene hybrid fibers for wearable supercapacitors. *Journal of Power Sources* **2016**, *319*, 271-280. DOI: 10.1016/j.jpowsour.2016.04.030.

(41) Jia, Y.; Zhou, L.; Shao, J. Electrochemical performance of flexible graphene-based fibers as electrodes for wearable supercapacitors. *Synthetic Metals* **2018**, *246*, 108-114. DOI: https://doi.org/10.1016/j.synthmet.2018.09.016.

(42) Hu, L.; Pasta, M.; La Mantia, F.; Cui, L.; Jeong, S.; Deshazer, H. D.; Choi, J. W.; Han, S. M.; Cui, Y. Stretchable, Porous, and Conductive Energy Textiles. *Nano Letters* **2010**, *10* (2), 708-714. DOI: 10.1021/nl903949m.

(43) Pasta, M.; La Mantia, F.; Hu, L.; Deshazer, H. D.; Cui, Y. Aqueous supercapacitors on conductive cotton. *Nano Research* **2010**, *3* (6), 452-458. DOI: 10.1007/s12274-010-0006-8.

(44) Liu, W.-w.; Yan, X.-b.; Lang, J.-w.; Peng, C.; Xue, Q.-j. Flexible and conductive nanocomposite electrode based on graphene sheets and cotton cloth for supercapacitor. *Journal of Materials Chemistry* **2012**, *22* (33), 17245-17253, 10.1039/C2JM32659K. DOI: 10.1039/C2JM32659K.

(45) Abdelkader, A. M.; Karim, N.; Vallés, C.; Afroj, S.; Novoselov, K. S.; Yeates, S. G. Ultraflexible and robust graphene supercapacitors printed on textiles for wearable electronics applications. *2D Materials* **2017**, *4* (3). DOI: 10.1088/2053-1583/aa7d71.

(46) Li, Y.; Zhang, Y.; Zhang, H.; Xing, T.-l.; Chen, G.-q. A facile approach to prepare a flexible sandwich-structured supercapacitor with rGO-coated cotton fabric as electrodes. *RSC Advances* **2019**, *9* (8), 4180-4189, 10.1039/C9RA00171A. DOI: 10.1039/C9RA00171A.

(47) Islam, M. R.; Afroj, S.; Beach, C.; Islam, M. H.; Parraman, C.; Abdelkader, A.; Casson, A. J.; Novoselov, K. S.; Karim, N. Fully printed and multifunctional graphene-based wearable e-textiles for personalized healthcare applications. *iScience* **2022**, 103945. DOI: https://doi.org/10.1016/j.isci.2022.103945.

(48) Li, W. C.; Mak, C. L.; Kan, C. W.; Hui, C. Y. Enhancing the capacitive performance of a textile-based CNT supercapacitor. *RSC Advances* **2014**, *4* (110), 64890-64900, 10.1039/C4RA10450A. DOI: 10.1039/C4RA10450A.

(49) Qiang, S.; Carey, T.; Arbab, A.; Song, W.; Wang, C.; Torrisi, F. Wearable solid-state capacitors based on two-dimensional material all-textile heterostructures. *Nanoscale* **2019**, *11* (20), 9912-9919, 10.1039/C9NR00463G. DOI: 10.1039/C9NR00463G.

(50) Afroj, S.; Tan, S.; Abdelkader, A. M.; Novoselov, K. S.; Karim, N. Highly Conductive, Scalable, and Machine Washable Graphene-Based E-Textiles for Multifunctional Wearable Electronic Applications. *Advanced Functional Materials* **2020**. DOI: 10.1002/adfm.202000293.

(51) Jost, K.; Perez, C. R.; McDonough, J. K.; Presser, V.; Heon, M.; Dion, G.; Gogotsi, Y. Carbon coated textiles for flexible energy storage. *Energy & Environmental Science* **2011**, *4* (12), 5060-5067, 10.1039/C1EE02421C. DOI: 10.1039/C1EE02421C.

(52) Stempien, Z.; Khalid, M.; Kozicki, M.; Kozanecki, M.; Varela, H.; Filipczak, P.; Pawlak, R.; Korzeniewska, E.; Sąsiadek, E. In-situ deposition of reduced graphene oxide layers on

textile surfaces by the reactive inkjet printing technique and their use in supercapacitor applications. *Synthetic Metals* **2019**, *256*, 116144. DOI: 10.1016/j.synthmet.2019.116144.

(53) Gao, Y.; Pandey, G. P.; Turner, J.; Westgate, C. R.; Sammakia, B. Chemical vapor-deposited carbon nanofibers on carbon fabric for supercapacitor electrode applications. *Nanoscale Research Letters* **2012**, *7* (1), 651. DOI: 10.1186/1556-276X-7-651.

(54) Jost, K.; Stenger, D.; Perez, C. R.; McDonough, J. K.; Lian, K.; Gogotsi, Y.; Dion, G. Knitted and screen printed carbon-fiber supercapacitors for applications in wearable electronics. *Energy & Environmental Science* **2013**, *6* (9), 2698-2705, 10.1039/C3EE40515J. DOI: 10.1039/C3EE40515J.

(55) Wang, G.; Wang, H.; Lu, X.; Ling, Y.; Yu, M.; Zhai, T.; Tong, Y.; Li, Y. Solid-State Supercapacitor Based on Activated Carbon Cloths Exhibits Excellent Rate Capability. *Advanced Materials* **2014**, *26* (17), 2676-2682, https://doi.org/10.1002/adma.201304756. DOI: https://doi.org/10.1002/adma.201304756 (acccessed 2021/03/14).

(56) Dong, L.; Xu, C.; Yang, Q.; Fang, J.; Li, Y.; Kang, F. High-performance compressible supercapacitors based on functionally synergic multiscale carbon composite textiles. *Journal of Materials Chemistry A* **2015**, *3* (8), 4729-4737, 10.1039/C4TA06494A. DOI: 10.1039/C4TA06494A.

(57) Yu, J.; Wu, J.; Wang, H.; Zhou, A.; Huang, C.; Bai, H.; Li, L. Metallic Fabrics as the Current Collector for High-Performance Graphene-Based Flexible Solid-State Supercapacitor. *ACS Applied Materials & Interfaces* **2016**, *8* (7), 4724-4729. DOI: 10.1021/acsami.5b12180.

(58) Mehrabi-Matin, B.; Shahrokhian, S.; Iraji-Zad, A. Silver Fiber Fabric as the Current Collector for Preparation of Graphene-Based Supercapacitors. *Electrochimica Acta* **2017**, *227*, 246-254. DOI: 10.1016/j.electacta.2017.01.031.

(59) Wei, C.; Xu, Q.; Chen, Z.; Rao, W.; Fan, L.; Yuan, Y.; Bai, Z.; Xu, J. An all-solid-state yarn supercapacitor using cotton yarn electrodes coated with polypyrrole nanotubes. *Carbohydrate Polymers* **2017**, *169*, 50-57. DOI: https://doi.org/10.1016/j.carbpol.2017.04.002.

(60) Jin, H.; Zhou, L.; Mak, C. L.; Huang, H.; Tang, W. M.; Chan, H. L. W. High-performance fiber-shaped supercapacitors using carbon fiber thread (CFT)@polyanilne and functionalized CFT electrodes for wearable/stretchable electronics. *Nano Energy* **2015**, *11*, 662-670. DOI: https://doi.org/10.1016/j.nanoen.2014.11.055.

(61) Liang, G.; Zhu, L.; Xu, J.; Fang, D.; Bai, Z.; Xu, W. Investigations of poly(pyrrole)-coated cotton fabrics prepared in blends of anionic and cationic surfactants as flexible electrode. *Electrochimica Acta* **2013**, *103*, 9-14. DOI: 10.1016/j.electacta.2013.04.065.

(62) Zhu, L.; Wu, L.; Sun, Y.; Li, M.; Xu, J.; Bai, Z.; Liang, G.; Liu, L.; Fang, D.; Xu, W. Cotton fabrics coated with lignosulfonate-doped polypyrrole for flexible supercapacitor electrodes. *RSC Advances* **2014**, *4* (12), 6261-6266, 10.1039/C3RA47224H. DOI: 10.1039/C3RA47224H.

(63) Xu, J.; Wang, D.; Fan, L.; Yuan, Y.; Wei, W.; Liu, R.; Gu, S.; Xu, W. Fabric electrodes coated with polypyrrole nanorods for flexible supercapacitor application prepared via a reactive self-degraded template. *Organic Electronics* **2015**, *26*, 292-299. DOI: 10.1016/j.orgel.2015.07.054.

(64) Liu, L.; Weng, W.; Zhang, J.; Cheng, X.; Liu, N.; Yang, J.; Ding, X. Flexible supercapacitor with a record high areal specific capacitance based on a tuned porous fabric. *Journal of Materials Chemistry A* **2016**, *4* (33), 12981-12986, 10.1039/C6TA04911G. DOI: 10.1039/C6TA04911G.

(65) Lv, J.; Zhou, P.; Zhang, L.; Zhong, Y.; Sui, X.; Wang, B.; Chen, Z.; Xu, H.; Mao, Z. High-performance textile electrodes for wearable electronics obtained by an improved in situ polymerization method. *Chemical Engineering Journal* **2019**, *361*, 897-907. DOI: 10.1016/j.cej.2018.12.083.

(66) Wang, B.; Song, W.; Gu, P.; Fan, L.; Yin, Y.; Wang, C. A stretchable and hydrophobic polypyrrole/knitted cotton fabric electrode for all-solid-state supercapacitor with excellent strain capacitance. *Electrochimica Acta* **2019**, *297*, 794-804. DOI: 10.1016/j.electacta.2018.12.042.

(67) Lv, J.; Zhang, L.; Zhong, Y.; Sui, X.; Wang, B.; Chen, Z.; Feng, X.; Xu, H.; Mao, Z. High-performance polypyrrole coated knitted cotton fabric electrodes for wearable energy storage. *Organic Electronics* **2019**, *74*, 59-68. DOI: 10.1016/j.orgel.2019.06.027.

(68) Yue, B.; Wang, C.; Ding, X.; Wallace, G. G. Polypyrrole coated nylon lycra fabric as stretchable electrode for supercapacitor applications. *Electrochimica Acta* **2012**, *68*, 18-24. DOI: 10.1016/j.electacta.2012.01.109.

(69) Gong, F.; Meng, C.; He, J.; Dong, X. Fabrication of highly conductive and multifunctional polyester fabrics by spray-coating with PEDOT:PSS solutions. *Progress in Organic Coatings* **2018**, *121*, 89-96. DOI: 10.1016/j.porgcoat.2018.04.006.

(70) Cárdenas-Martínez, J.; España-Sánchez, B. L.; Esparza, R.; Ávila-Niño, J. A. Flexible and transparent supercapacitors using electrospun PEDOT:PSS electrodes. *Synthetic Metals* **2020**, *267*, 116436. DOI: 10.1016/j.synthmet.2020.116436.

(71) Xie, X.; Xin, B.; Chen, Z.; Xu, Y. Preparation and characterization of PANI-PPY/PET fabric conductive composite for supercapacitors. *The Journal of The Textile Institute* **2021**, 1-8. DOI: 10.1080/00405000.2021.1992848.

(72) Manjakkal, L.; Pullanchiyodan, A.; Yogeswaran, N.; Hosseini, E. S.; Dahiya, R. A Wearable Supercapacitor Based on Conductive PEDOT:PSS-Coated Cloth and a Sweat Electrolyte. *Advanced Materials* **2020**, *32* (24), 1907254. DOI: 10.1002/adma.201907254.

(73) Stempien, Z.; Khalid, M.; Kozanecki, M.; Filipczak, P.; Wrzesińska, A.; Korzeniewska, E.; Sąsiadek, E. Inkjet Printing of Polypyrrole Electroconductive Layers Based on Direct Inks Freezing and Their Use in Textile Solid-State Supercapacitors. *Materials (Basel)* **2021**, *14* (13), 3577. DOI: 10.3390/ma14133577 PubMed.

(74) Liu, Q.; Qiu, J.; Yang, C.; Zang, L.; Zhang, G.; Sakai, E. High-performance textile electrode enhanced by surface modifications of fiberglass cloth with polypyrrole tentacles for flexible supercapacitors. *International Journal of Energy Research* **2020**, *44* (11), 9166-9176. DOI: 10.1002/er.5558.

(75) Laforgue, A. All-textile flexible supercapacitors using electrospun poly(3,4-ethylenedioxythiophene) nanofibers. *Journal of Power Sources* **2011**, *196* (1), 559-564. DOI: 10.1016/j.jpowsour.2010.07.007.

(76) Pan, S.; Lin, H.; Deng, J.; Chen, P.; Chen, X.; Yang, Z.; Peng, H. Novel Wearable Energy Devices Based on Aligned Carbon Nanotube Fiber Textiles. *Advanced Energy Materials* **2015**, *5* (4), 1401438, https://doi.org/10.1002/aenm.201401438. DOI: 10.1002/aenm.201401438 (acccessed 2021/03/13).

(77) Bae, J.; Song, M. K.; Park, Y. J.; Kim, J. M.; Liu, M.; Wang, Z. L. Fiber Supercapacitors Made of Nanowire-Fiber Hybrid Structures for Wearable/Flexible Energy Storage. *Angewandte Chemie International Edition* **2011**, *50* (7), 1683-1687, https://doi.org/10.1002/anie.201006062. DOI: 10.1002/anie.201006062 (acccessed 2021/03/13).

(78) Su, F.; Miao, M. Asymmetric carbon nanotube–MnO2two-ply yarn supercapacitors for wearable electronics. *Nanotechnology* **2014**, *25* (13), 135401. DOI: 10.1088/0957-4484/25/13/135401.

(79) Su, F.; Lv, X.; Miao, M. High-Performance Two-Ply Yarn Supercapacitors Based on Carbon Nanotube Yarns Dotted with Co3O4 and NiO Nanoparticles. *Small* **2015**, *11* (7), 854-

861, https://doi.org/10.1002/smll.201401862. DOI: 10.1002/smll.201401862 (acccessed 2021/03/13).

(80) Abouali, S.; Akbari Garakani, M.; Zhang, B.; Xu, Z.-L.; Kamali Heidari, E.; Huang, J.-q.; Huang, J.; Kim, J.-K. Electrospun Carbon Nanofibers with in Situ Encapsulated Co3O4 Nanoparticles as Electrodes for High-Performance Supercapacitors. *ACS Applied Materials & Interfaces* **2015**, *7* (24), 13503-13511. DOI: 10.1021/acsami.5b02787.

(81) Shahidi, S.; Kalaoglu, F. In situ deposition of nickel nano particles on polyester fabric and its application as a flexible electrode in supercapacitor. *Journal of Industrial Textiles* **2020**, *0* (0), 1528083720944252. DOI: 10.1177/1528083720944252.

(82) Pullanchiyodan, A.; Manjakkal, L.; Dahiya, R. Metal Coated Fabric Based Asymmetric Supercapacitor for Wearable Applications. *IEEE Sensors Journal* **2021**, *21* (23), 26208-26214. DOI: 10.1109/JSEN.2021.3058894.

(83) Yang, P.; Xiao, X.; Li, Y.; Ding, Y.; Qiang, P.; Tan, X.; Mai, W.; Lin, Z.; Wu, W.; Li, T.; et al. Hydrogenated ZnO Core–Shell Nanocables for Flexible Supercapacitors and Self-Powered Systems. *ACS Nano* **2013**, *7* (3), 2617-2626. DOI: 10.1021/nn306044d.

(84) Wang, W.; Liu, W.; Zeng, Y.; Han, Y.; Yu, M.; Lu, X.; Tong, Y. A Novel Exfoliation Strategy to Significantly Boost the Energy Storage Capability of Commercial Carbon Cloth. *Adv Mater* **2015**, *27* (23), 3572-3578. DOI: 10.1002/adma.201500707 From NLM.

(85) Zhang, J.; Chen, M.; Ge, Y.; Liu, Q. Manganese Oxide on Carbon Fabric for Flexible Supercapacitors. *Journal of Nanomaterials* **2016**, *2016*, 2870761. DOI: 10.1155/2016/2870761.

(86) Fan, X.; Wang, X.; Li, G.; Yu, A.; Chen, Z. High-performance flexible electrode based on electrodeposition of polypyrrole/MnO2 on carbon cloth for supercapacitors. *Journal of Power Sources* **2016**, *326*, 357-364. DOI: 10.1016/j.jpowsour.2016.05.047.

(87) Javed, M. S.; Chen, J.; Chen, L.; Xi, Y.; Zhang, C.; Wan, B.; Hu, C. Flexible full-solid state supercapacitors based on zinc sulfide spheres growing on carbon textile with superior charge storage. *Journal of Materials Chemistry A* **2016**, *4* (2), 667-674, 10.1039/C5TA08752J. DOI: 10.1039/C5TA08752J.

(88) Shen, C.; Xie, Y.; Zhu, B.; Sanghadasa, M.; Tang, Y.; Lin, L. Wearable woven supercapacitor fabrics with high energy density and load-bearing capability. *Scientific Reports* **2017**, *7* (1), 14324. DOI: 10.1038/s41598-017-14854-3.

(89) Howli, P.; Das, S.; Sarkar, S.; Samanta, M.; Panigrahi, K.; Das, N. S.; Chattopadhyay, K. K. Co3O4 Nanowires on Flexible Carbon Fabric as a Binder-Free Electrode for All Solid-

State Symmetric Supercapacitor. *ACS Omega* **2017**, *2* (8), 4216-4226. DOI: 10.1021/acsomega.7b00702.

(90) Babkova, T. A.; Fei, H.; Kazantseva, N. E.; Sapurina, I. Y.; Saha, P. Enhancing the supercapacitor performance of flexible MnOxCarbon cloth electrodes by Pd-decoration. *Electrochimica Acta* **2018**, *272*, 1-10. DOI: 10.1016/j.electacta.2018.03.143.

(91) Luo, W.; Li, X.; Chen, J. Y. All-fabric flexible supercapacitor for energy storage. *Journal of Industrial Textiles* **2018**, *49* (8), 1061-1077. DOI: 10.1177/1528083718804208 (acccessed 2021/03/14).

(92) Abbas, Q.; Javed, M. S.; Ahmad, A.; Siyal, S. H.; Asim, I.; Luque, R.; Albaqami, M. D.; Tighezza, A. M. ZnO Nano-Flowers Assembled on Carbon Fiber Textile for High-Performance Supercapacitor's Electrode. *Coatings* **2021**, *11* (11), 1337. DOI: 10.3390/coatings11111337.

(93) Yan, J.; Ma, Y.; Zhang, C.; Li, X.; Liu, W.; Yao, X.; Yao, S.; Luo, S. Polypyrrole–MXene coated textile-based flexible energy storage device. *RSC Advances* **2018**, *8* (69), 39742-39748, 10.1039/C8RA08403C. DOI: 10.1039/C8RA08403C.

(94) Levitt, A.; Hegh, D.; Phillips, P.; Uzun, S.; Anayee, M.; Razal, J. M.; Gogotsi, Y.; Dion, G. 3D knitted energy storage textiles using MXene-coated yarns. *Materials Today* **2020**, *34*, 17-29. DOI: https://doi.org/10.1016/j.mattod.2020.02.005.

(95) Yin, H.; Liu, Y.; Yu, N.; Qu, H.-Q.; Liu, Z.; Jiang, R.; Li, C.; Zhu, M.-Q. Graphene-like MoS2 Nanosheets on Carbon Fabrics as High-Performance Binder-free Electrodes for Supercapacitors and Li-Ion Batteries. *ACS Omega* **2018**, *3* (12), 17466-17473. DOI: 10.1021/acsomega.8b02446.

(96) Jiang, Q.; Kurra, N.; Alhabeb, M.; Gogotsi, Y.; Alshareef, H. N. All Pseudocapacitive MXene-RuO2 Asymmetric Supercapacitors. *Advanced Energy Materials* **2018**, *8* (13), 1703043. DOI: 10.1002/aenm.201703043.

(97) Ding, Y.; Dai, L.; Wang, R.; Wang, H.; Zhang, H.; Jiang, W.; Tang, J.; Zang, S.-Q. Bio-inspired Mn3O4@N, P-doped carbon cathode for 2. V flexible aqueous asymmetric supercapacitors. *Chemical Engineering Journal* **2021**, *407*, 126874. DOI: 10.1016/j.cej.2020.126874.

(98) Wang, Y.; Lv, X.; Zou, S.; Lin, X.; Ni, Y. MoS2/polyaniline/functionalized carbon cloth electrode materials for excellent supercapacitor performance. *RSC Advances* **2021**, *11* (18), 10941-10950, 10.1039/D0RA09126J. DOI: 10.1039/D0RA09126J.

(99) Liu, N.; Ma, W.; Tao, J.; Zhang, X.; Su, J.; Li, L.; Yang, C.; Gao, Y.; Golberg, D.; Bando, Y. Cable-Type Supercapacitors of Three-Dimensional Cotton Thread Based Multi-Grade

Nanostructures for Wearable Energy Storage. *Advanced Materials* **2013**, *25* (35), 4925-4931, https://doi.org/10.1002/adma.201301311. DOI: 10.1002/adma.201301311 (acccessed 2021/03/13).

(100) Jost, K.; Durkin, D. P.; Haverhals, L. M.; Brown, E. K.; Langenstein, M.; De Long, H. C.; Trulove, P. C.; Gogotsi, Y.; Dion, G. Natural Fiber Welded Electrode Yarns for Knittable Textile Supercapacitors. *Advanced Energy Materials* **2015**, *5* (4), 1401286, https://doi.org/10.1002/aenm.201401286. DOI: 10.1002/aenm.201401286 (acccessed 2021/03/13).

(101) Liu, L.; Yu, Y.; Yan, C.; Li, K.; Zheng, Z. Wearable energy-dense and power-dense supercapacitor yarns enabled by scalable graphene–metallic textile composite electrodes. *Nature Communications* **2015**, *6* (1), 7260. DOI: 10.1038/ncomms8260.

(102) Ye, X.; Zhou, Q.; Jia, C.; Tang, Z.; Wan, Z.; Wu, X. A Knittable Fibriform Supercapacitor Based on Natural Cotton Thread Coated with Graphene and Carbon Nanoparticles. *Electrochimica Acta* **2016**, *206*, 155-164. DOI: https://doi.org/10.1016/j.electacta.2016.04.100.

(103) Wang, H. T.; Jin, C.; Liu, Y. N.; Kang, X. H.; Bian, S. W.; Zhu, Q. Cotton yarns modified with three-dimensional metallic Ni conductive network and pseudocapacitive Co-Ni layered double hydroxide nanosheet array as electrode materials for flexible yarn supercapacitors. *Electrochimica Acta* **2018**, *283*, 1789-1797. DOI: 10.1016/j.electacta.2018.07.090.

(104) Lima, R.; Alcaraz-Espinoza, J. J.; da Silva, F. A. G., Jr.; de Oliveira, H. P. Multifunctional Wearable Electronic Textiles Using Cotton Fibers with Polypyrrole and Carbon Nanotubes. *ACS Appl Mater Interfaces* **2018**, *10* (16), 13783-13795. DOI: 10.1021/acsami.8b04695 From NLM.

(105) Ma, Y.; Wang, Q.; Liang, X.; Zhang, D.; Miao, M. Wearable supercapacitors based on conductive cotton yarns. *Journal of Materials Science* **2018**, *53* (20), 14586-14597. DOI: 10.1007/s10853-018-2655-z.

(106) Li, J.; Shao, Y.; Jiang, P.; Zhang, Q.; Hou, C.; Li, Y.; Wang, H. 1T-Molybdenum disulfide/reduced graphene oxide hybrid fibers as high strength fibrous electrodes for wearable energy storage. *Journal of Materials Chemistry A* **2019**, *7* (7), 3143-3149, 10.1039/C8TA09328H. DOI: 10.1039/C8TA09328H.

(107) Yang, L.; Lin, F.; Zabihi, F.; Yang, S.; Zhu, M. High specific capacitance cotton fiber electrode enhanced with PPy and MXene by in situ hybrid polymerization. *International*

Journal of Biological Macromolecules **2021**, *181*, 1063-1071. DOI: 10.1016/j.ijbiomac.2021.04.112.

(108) Li, X.; Liu, R.; Xu, C.; Bai, Y.; Zhou, X.; Wang, Y.; Yuan, G. High-Performance Polypyrrole/Graphene/SnCl2 Modified Polyester Textile Electrodes and Yarn Electrodes for Wearable Energy Storage. *Advanced Functional Materials* **2018**, *28* (22), 1800064. DOI: 10.1002/adfm.201800064.

(109) Cai, Z.; Li, L.; Ren, J.; Qiu, L.; Lin, H.; Peng, H. Flexible, weavable and efficient microsupercapacitor wires based on polyaniline composite fibers incorporated with aligned carbon nanotubes. *Journal of Materials Chemistry A* **2013**, *1* (2), 258-261, 10.1039/C2TA00274D. DOI: 10.1039/C2TA00274D.

(110) Choi, C.; Kim, S. H.; Sim, H. J.; Lee, J. A.; Choi, A. Y.; Kim, Y. T.; Lepró, X.; Spinks, G. M.; Baughman, R. H.; Kim, S. J. Stretchable, Weavable Coiled Carbon Nanotube/MnO2/Polymer Fiber Solid-State Supercapacitors. *Scientific Reports* **2015**, *5* (1), 9387. DOI: 10.1038/srep09387.

(111) Chen, X.; Lin, H.; Deng, J.; Zhang, Y.; Sun, X.; Chen, P.; Fang, X.; Zhang, Z.; Guan, G.; Peng, H. Electrochromic Fiber-Shaped Supercapacitors. *Advanced Materials* **2014**, *26* (48), 8126-8132, https://doi.org/10.1002/adma.201403243. DOI: 10.1002/adma.201403243 (acccessed 2021/03/12).

(112) Deng, J.; Zhang, Y.; Zhao, Y.; Chen, P.; Cheng, X.; Peng, H. A Shape-Memory Supercapacitor Fiber. *Angewandte Chemie International Edition* **2015**, *54* (51), 15419-15423, https://doi.org/10.1002/anie.201508293. DOI: https://doi.org/10.1002/anie.201508293 (acccessed 2021/03/14).

(113) Sun, J.; Huang, Y.; Fu, C.; Wang, Z.; Huang, Y.; Zhu, M.; Zhi, C.; Hu, H. High-performance stretchable yarn supercapacitor based on PPy@CNTs@urethane elastic fiber core spun yarn. *Nano Energy* **2016**, *27*, 230-237. DOI: https://doi.org/10.1016/j.nanoen.2016.07.008.

(114) Zhang, Q.; Sun, J.; Pan, Z.; Zhang, J.; Zhao, J.; Wang, X.; Zhang, C.; Yao, Y.; Lu, W.; Li, Q.; et al. Stretchable fiber-shaped asymmetric supercapacitors with ultrahigh energy density. *Nano Energy* **2017**, *39*, 219-228. DOI: 10.1016/j.nanoen.2017.06.052.

(115) Wang, K.; Meng, Q.; Zhang, Y.; Wei, Z.; Miao, M. High-performance two-ply yarn supercapacitors based on carbon nanotubes and polyaniline nanowire arrays. *Adv Mater* **2013**, *25* (10), 1494-1498. DOI: 10.1002/adma.201204598 From NLM.

(116) Choi, C.; Lee, J. A.; Choi, A. Y.; Kim, Y. T.; Lepró, X.; Lima, M. D.; Baughman, R. H.; Kim, S. J. Flexible supercapacitor made of carbon nanotube yarn with internal pores. *Adv Mater* **2014**, *26* (13), 2059-2065. DOI: 10.1002/adma.201304736 From NLM.

(117) Huang, G.; Zhang, Y.; Wang, L.; Sheng, P.; Peng, H. Fiber-based MnO2/carbon nanotube/polyimide asymmetric supercapacitor. *Carbon* **2017**, *125*, 595-604. DOI: https://doi.org/10.1016/j.carbon.2017.09.103.

(118) Wu, Y.; Wang, Q.; Li, T.; Zhang, D.; Miao, M. Fiber-shaped Supercapacitor and Electrocatalyst Containing of Multiple Carbon Nanotube Yarns and One Platinum Wire. *Electrochimica Acta* **2017**, *245*, 69-78. DOI: https://doi.org/10.1016/j.electacta.2017.05.117.

(119) Jian, X.; Li, H.; Li, H.; Li, Y.; Shang, Y. Flexible and freestanding MoS2/rGO/CNT hybrid fibers for high-capacity all-solid supercapacitors. *Carbon* **2021**, *172*, 132-137. DOI: 10.1016/j.carbon.2020.09.095.

(120) Meng, Q.; Wang, K.; Guo, W.; Fang, J.; Wei, Z.; She, X. Thread-like supercapacitors based on one-step spun nanocomposite yarns. *Small* **2014**, *10* (15), 3187-3193. DOI: 10.1002/smll.201303419 From NLM.

(121) Wang, Z.; Qin, S.; Seyedin, S.; Zhang, J.; Wang, J.; Levitt, A.; Li, N.; Haines, C.; Ovalle-Robles, R.; Lei, W.; et al. High-Performance Biscrolled MXene/Carbon Nanotube Yarn Supercapacitors. *Small* **2018**, *14* (37), 1802225. DOI: 10.1002/smll.201802225.

(122) Meng, Y.; Zhao, Y.; Hu, C.; Cheng, H.; Hu, Y.; Zhang, Z.; Shi, G.; Qu, L. All-graphene core-sheath microfibers for all-solid-state, stretchable fibriform supercapacitors and wearable electronic textiles. *Adv Mater* **2013**, *25* (16), 2326-2331. DOI: 10.1002/adma.201300132 From NLM.

(123) Ding, X.; Zhao, Y.; Hu, C.; Hu, Y.; Dong, Z.; Chen, N.; Zhang, Z.; Qu, L. Spinning fabrication of graphene/polypyrrole composite fibers for all-solid-state, flexible fibriform supercapacitors. *Journal of Materials Chemistry A* **2014**, *2* (31), 12355-12360, 10.1039/C4TA01230E. DOI: 10.1039/C4TA01230E.

(124) Seyedin, S.; Yanza, E. R. S.; Razal, Joselito M. Knittable energy storing fiber with high volumetric performance made from predominantly MXene nanosheets. *Journal of Materials Chemistry A* **2017**, *5* (46), 24076-24082, 10.1039/C7TA08355F. DOI: 10.1039/C7TA08355F.

(125) He, N.; Patil, S.; Qu, J.; Liao, J.; Zhao, F.; Gao, W. Effects of Electrolyte Mediation and MXene Size in Fiber-Shaped Supercapacitors. *ACS Applied Energy Materials* **2020**, *3* (3), 2949-2958. DOI: 10.1021/acsaem.0c00024.

(126) Roy, A. K.; Faisal, S. N.; Spickenheuer, A.; Scheffler, C.; Wang, J.; Harris, A. T.; Minett, A. I.; Islam, M. S. Loading dependency of 2D MoS2 nanosheets in the capacitance of

3D hybrid microfibre-based energy storage devices. *Carbon Trends* **2021**, *5*, 100097. DOI: 10.1016/j.cartre.2021.100097.

(127) Zhang, J.; Seyedin, S.; Qin, S.; Wang, Z.; Moradi, S.; Yang, F.; Lynch, P. A.; Yang, W.; Liu, J.; Wang, X.; et al. Highly Conductive Ti3C2Tx MXene Hybrid Fibers for Flexible and Elastic Fiber-Shaped Supercapacitors. *Small* **2019**, *15* (8), 1804732. DOI: 10.1002/smll.201804732.

(128) Yu, D.; Zhai, S.; Jiang, W.; Goh, K.; Wei, L.; Chen, X.; Jiang, R.; Chen, Y. Transforming Pristine Carbon Fiber Tows into High Performance Solid-State Fiber Supercapacitors. *Adv Mater* **2015**, *27* (33), 4895-4901. DOI: 10.1002/adma.201501948 From NLM.

(129) Jin, H.; Zhou, L.; Mak, C. L.; Huang, H.; Tang, W. M.; Wa Chan, H. L. Improved performance of asymmetric fiber-based micro-supercapacitors using carbon nanoparticles for flexible energy storage. *Journal of Materials Chemistry A* **2015**, *3* (30), 15633-15641, 10.1039/C5TA03576G. DOI: 10.1039/C5TA03576G.

(130) Tao, J.; Liu, N.; Ma, W.; Ding, L.; Li, L.; Su, J.; Gao, Y. Solid-State High Performance Flexible Supercapacitors Based on Polypyrrole-MnO2-Carbon Fiber Hybrid Structure. *Scientific Reports* **2013**, *3* (1), 2286. DOI: 10.1038/srep02286.

(131) Lu, X.; Bai, Y.; Wang, R.; Sun, J. A high-performance flexible and weavable asymmetric fiber-shaped solid-state supercapacitor enhanced by surface modifications of carbon fibers with carbon nanotubes. *Journal of Materials Chemistry A* **2016**, *4* (46), 18164-18173, 10.1039/C6TA08233E. DOI: 10.1039/C6TA08233E.

(132) Kim, D.; Keum, K.; Lee, G.; Kim, D.; Lee, S.-S.; Ha, J. S. Flexible, water-proof, wire-type supercapacitors integrated with wire-type UV/NO2 sensors on textiles. *Nano Energy* **2017**, *35*, 199-206. DOI: 10.1016/j.nanoen.2017.03.044.

(133) Mao, N.; Chen, W.; Meng, J.; Li, Y.; Zhang, K.; Qin, X.; Zhang, H.; Zhang, C.; Qiu, Y.; Wang, S. Enhanced electrochemical properties of hierarchically sheath-core aligned carbon nanofibers coated carbon fiber yarn electrode-based supercapacitor via polyaniline nanowire array modification. *Journal of Power Sources* **2018**, *399*, 406-413. DOI: 10.1016/j.jpowsour.2018.07.022.

(134) Song, C.; Yun, J.; Keum, K.; Jeong, Y. R.; Park, H.; Lee, H.; Lee, G.; Oh, S. Y.; Ha, J. S. High performance wire-type supercapacitor with Ppy/CNT-ionic liquid/AuNP/carbon fiber electrode and ionic liquid based electrolyte. *Carbon* **2019**, *144*, 639-648. DOI: https://doi.org/10.1016/j.carbon.2018.12.100.

(135) Naderi, L.; Shahrokhian, S.; Soavi, F. Fabrication of a 2.8 V high-performance aqueous flexible fiber-shaped asymmetric micro-supercapacitor based on MnO2/PEDOT:PSS-reduced graphene oxide nanocomposite grown on carbon fiber electrode. *Journal of Materials Chemistry A* **2020**, *8* (37), 19588-19602, 10.1039/D0TA06561G. DOI: 10.1039/D0TA06561G.

(136) Lee, J. A.; Shin, M. K.; Kim, S. H.; Cho, H. U.; Spinks, G. M.; Wallace, G. G.; Lima, M. D.; Lepró, X.; Kozlov, M. E.; Baughman, R. H.; et al. Ultrafast charge and discharge biscrolled yarn supercapacitors for textiles and microdevices. *Nat Commun* **2013**, *4*, 1970. DOI: 10.1038/ncomms2970 From NLM.

(137) Zhang, D.; Miao, M.; Niu, H.; Wei, Z. Core-spun carbon nanotube yarn supercapacitors for wearable electronic textiles. *ACS Nano* **2014**, *8* (5), 4571-4579. DOI: 10.1021/nn5001386 From NLM.

(138) Keum, K.; Lee, G.; Lee, H.; Yun, J.; Park, H.; Hong, S. Y.; Song, C.; Kim, J. W.; Ha, J. S. Wire-Shaped Supercapacitors with Organic Electrolytes Fabricated via Layer-by-Layer Assembly. *ACS Appl Mater Interfaces* **2018**, *10* (31), 26248-26257. DOI: 10.1021/acsami.8b07113 From NLM.

(139) Huang, Y.; Huang, Y.; Zhu, M.; Meng, W.; Pei, Z.; Liu, C.; Hu, H.; Zhi, C. Magnetic-Assisted, Self-Healable, Yarn-Based Supercapacitor. *ACS Nano* **2015**, *9* (6), 6242-6251. DOI: 10.1021/acsnano.5b01602.

(140) Huang, Y.; Hu, H.; Huang, Y.; Zhu, M.; Meng, W.; Liu, C.; Pei, Z.; Hao, C.; Wang, Z.; Zhi, C. From Industrially Weavable and Knittable Highly Conductive Yarns to Large Wearable Energy Storage Textiles. *ACS Nano* **2015**, *9* (5), 4766-4775. DOI: 10.1021/acsnano.5b00860.

(141) Chu, X.; Zhang, H.; Su, H.; Liu, F.; Gu, B.; Huang, H.; Zhang, H.; Deng, W.; Zheng, X.; Yang, W. A novel stretchable supercapacitor electrode with high linear capacitance. *Chemical Engineering Journal* **2018**, *349*, 168-175. DOI: https://doi.org/10.1016/j.cej.2018.05.090.

(142) He, N.; Liao, J.; Zhao, F.; Gao, W. Dual-Core Supercapacitor Yarns: An Enhanced Performance Consistency and Linear Power Density. *ACS Appl Mater Interfaces* **2020**, *12* (13), 15211-15219. DOI: 10.1021/acsami.0c00182 From NLM.

(143) Zhang, T.; Wang, Z.; Zhu, A.; Ran, F. Flexible, twistable and plied electrode of stainless steel Cables@Nickel–Cobalt oxide with high electrochemical performance for wearable electronic textiles. *Electrochimica Acta* **2020**, *348*, 136312. DOI: 10.1016/j.electacta.2020.136312.

(144) Wang, K.; Zhao, P.; Zhou, X.; Wu, H.; Wei, Z. Flexible supercapacitors based on cloth-supported electrodes of conducting polymer nanowire array/SWCNT composites. *Journal of Materials Chemistry* **2011**, *21* (41), 16373-16378, 10.1039/C1JM13722K. DOI: 10.1039/C1JM13722K.

(145) Bao, L.; Li, X. Towards Textile Energy Storage from Cotton T-Shirts. *Advanced Materials* **2012**, *24* (24), 3246-3252, https://doi.org/10.1002/adma.201200246. DOI: 10.1002/adma.201200246 (acccessed 2021/03/14).

(146) Yue, B.; Wang, C.; Ding, X.; Wallace, G. G. Electrochemically synthesized stretchable polypyrrole/fabric electrodes for supercapacitor. *Electrochimica Acta* **2013**, *113*, 17-22. DOI: 10.1016/j.electacta.2013.09.024.

(147) Xu, J.; Wang, D.; Yuan, Y.; Wei, W.; Duan, L.; Wang, L.; Bao, H.; Xu, W. Polypyrrole/reduced graphene oxide coated fabric electrodes for supercapacitor application. *Organic Electronics* **2015**, *24*, 153-159. DOI: 10.1016/j.orgel.2015.05.037.

(148) Xu, J.; Wang, D.; Yuan, Y.; Wei, W.; Gu, S.; Liu, R.; Wang, X.; Liu, L.; Xu, W. Polypyrrole-coated cotton fabrics for flexible supercapacitor electrodes prepared using CuO nanoparticles as template. *Cellulose* **2015**, *22* (2), 1355-1363. DOI: 10.1007/s10570-015-0546-x.

(149) Yun, T. G.; Hwang, B. i.; Kim, D.; Hyun, S.; Han, S. M. Polypyrrole–MnO2-Coated Textile-Based Flexible-Stretchable Supercapacitor with High Electrochemical and Mechanical Reliability. *ACS Applied Materials & Interfaces* **2015**, *7* (17), 9228-9234. DOI: 10.1021/acsami.5b01745.

(150) Yuksel, R.; Unalan, H. E. Textile supercapacitors-based on MnO2/SWNT/conducting polymer ternary composites. *International Journal of Energy Research* **2015**, *39* (15), 2042-2052. DOI: 10.1002/er.3439.

(151) Huang, Q.; Liu, L.; Wang, D.; Liu, J.; Huang, Z.; Zheng, Z. One-step electrospinning of carbon nanowebs on metallic textiles for high-capacitance supercapacitor fabrics. *Journal of Materials Chemistry A* **2016**, *4* (18), 6802-6808, 10.1039/C5TA09309K. DOI: 10.1039/C5TA09309K.

(152) Liang, Y.; Weng, W.; Yang, J.; Liu, L.; Zhang, Y.; Yang, L.; Luo, X.; Cheng, Y.; Zhu, M. Asymmetric fabric supercapacitor with a high areal energy density and excellent flexibility. *RSC Advances* **2017**, *7* (77), 48934-48941, 10.1039/C7RA08703A. DOI: 10.1039/C7RA08703A.

(153) Xu, Q.; Wei, C.; Fan, L.; Rao, W.; Xu, W.; Liang, H.; Xu, J. Polypyrrole/titania-coated cotton fabrics for flexible supercapacitor electrodes. *Applied Surface Science* **2018**, *460*, 84-91. DOI: 10.1016/j.apsusc.2017.12.128.

(154) Etana, B. B.; Ramakrishnan, S.; Dhakshnamoorthy, M.; Saravanan, S.; C Ramamurthy, P.; Demissie, T. A. Functionalization of textile cotton fabric with reduced graphene oxide/MnO2/polyaniline based electrode for supercapacitor. *Materials Research Express* **2020**, *6* (12), 125708. DOI: 10.1088/2053-1591/ab669d.

(155) Xu, S.; Hao, H.; Chen, Y.; Li, W.; Shen, W.; Shearing, P. R.; Brett, D. J. L.; He, G. Flexible all-solid-state supercapacitors based on PPy/rGO nanocomposite on cotton fabric. *Nanotechnology* **2021**, *32* (30), 305401. DOI: 10.1088/1361-6528/abf9c4.

(156) Liang, C.; Zang, L.; Shi, F.; Yang, C.; Qiu, J.; Liu, Q.; Chen, Z. High-performance cotton fabric-based supercapacitors consisting of polypyrrole/Ag/graphene oxide nanocomposite prepared via UV-induced polymerization. *Cellulose* **2022**. DOI: 10.1007/s10570-022-04454-4.

(157) Sundriyal, P.; Bhattacharya, S. Textile-based supercapacitors for flexible and wearable electronic applications. *Scientific Reports* **2020**, *10* (1), 13259. DOI: 10.1038/s41598-020-70182-z.

(158) Yu, G.; Hu, L.; Vosgueritchian, M.; Wang, H.; Xie, X.; McDonough, J. R.; Cui, X.; Cui, Y.; Bao, Z. Solution-Processed Graphene/MnO2 Nanostructured Textiles for High-Performance Electrochemical Capacitors. *Nano Letters* **2011**, *11* (7), 2905-2911. DOI: 10.1021/nl2013828.

(159) Hu, L.; Chen, W.; Xie, X.; Liu, N.; Yang, Y.; Wu, H.; Yao, Y.; Pasta, M.; Alshareef, H. N.; Cui, Y. Symmetrical MnO2–Carbon Nanotube–Textile Nanostructures for Wearable Pseudocapacitors with High Mass Loading. *ACS Nano* **2011**, *5* (11), 8904-8913. DOI: 10.1021/nn203085j.

(160) Cheng, H.; Dong, Z.; Hu, C.; Zhao, Y.; Hu, Y.; Qu, L.; Chen, N.; Dai, L. Textile electrodes woven by carbon nanotube–graphene hybrid fibers for flexible electrochemical capacitors. *Nanoscale* **2013**, *5* (8), 3428-3434, 10.1039/C3NR00320E. DOI: 10.1039/C3NR00320E.

(161) Cheng, X.; Fang, X.; Chen, P.; Doo, S. G.; Son, I. H.; Huang, X.; Zhang, Y.; Weng, W.; Zhang, Z.; Deng, J.; et al. Designing one-dimensional supercapacitors in a strip shape for high performance energy storage fabrics. *Journal of Materials Chemistry A* **2015**. DOI: 10.1039/c5ta06317e.

(162) Guo, M.-X.; Bian, S.-W.; Shao, F.; Liu, S.; Peng, Y.-H. Hydrothermal synthesis and electrochemical performance of MnO2/graphene/polyester composite electrode materials for flexible supercapacitors. *Electrochimica Acta* **2016**, *209*, 486-497. DOI: 10.1016/j.electacta.2016.05.082.

(163) Barakzehi, M.; Montazer, M.; Sharif, F.; Norby, T.; Chatzitakis, A. A textile-based wearable supercapacitor using reduced graphene oxide/polypyrrole composite. *Electrochimica Acta* **2019**, *305*, 187-196. DOI: 10.1016/j.electacta.2019.03.058.

(164) Barakzehi, M.; Montazer, M.; Sharif, F. Electrically and Electrochemically Active Composite Based on Polyester/Reduced Graphene Oxide/Polypyrrole with Remarkable Washing Durability. *Journal of Textiles and Polymers* **2020**, *8* (2), 15-22.

(165) Liang, J.; Tian, B.; Li, S.; Jiang, C.; Wu, W. All-Printed MnHCF-MnOx-Based High-Performance Flexible Supercapacitors. *Advanced Energy Materials* **2020**, *10* (12), 2000022. DOI: 10.1002/aenm.202000022.

(166) Zhang, H.; Qiao, Y.; Lu, Z. Fully Printed Ultraflexible Supercapacitor Supported by a Single-Textile Substrate. *ACS Applied Materials & Interfaces* **2016**, *8* (47), 32317-32323. DOI: 10.1021/acsami.6b11172.

(167) Kim, T.; Samuel, E. P.; Park, C.; Kim, Y.-I.; Aldalbahi, A.; Alotaibi, F.; Yoon, S. S. Wearable fabric supercapacitors using supersonically sprayed reduced graphene and tin oxide. *Journal of Alloys and Compounds* **2021**, *856*, 157902. DOI: 10.1016/j.jallcom.2020.157902.

(168) Liu, L.; Tian, Q.; Yao, W.; Li, M.; Li, Y.; Wu, W. All-printed ultraflexible and stretchable asymmetric in-plane solid-state supercapacitors (ASCs) for wearable electronics. *Journal of Power Sources* **2018**, *397*, 59-67. DOI: https://doi.org/10.1016/j.jpowsour.2018.07.013.

(169) Wang, L.; Zhang, C.; Jiao, X.; Yuan, Z. Polypyrrole-based hybrid nanostructures grown on textile for wearable supercapacitors. *Nano Research* **2019**, *12* (5), 1129-1137. DOI: 10.1007/s12274-019-2360-5.

(170) Ju, Y.-W.; Choi, G.-R.; Jung, H.-R.; Lee, W.-J. Electrochemical properties of electrospun PAN/MWCNT carbon nanofibers electrodes coated with polypyrrole. *Electrochimica Acta* **2008**, *53* (19), 5796-5803. DOI: 10.1016/j.electacta.2008.03.028.

(171) Li, Z.; Huang, T.; Gao, W.; Xu, Z.; Chang, D.; Zhang, C.; Gao, C. Hydrothermally Activated Graphene Fiber Fabrics for Textile Electrodes of Supercapacitors. *ACS Nano* **2017**, *11* (11), 11056-11065. DOI: 10.1021/acsnano.7b05092.

(172) Lv, P.; Feng, Y. Y.; Li, Y.; Feng, W. Carbon fabric-aligned carbon nanotube/MnO2/conducting polymers ternary composite electrodes with high utilization and mass loading of MnO2 for super-capacitors. *Journal of Power Sources* **2012**, *220*, 160-168. DOI: 10.1016/j.jpowsour.2012.07.073.

(173) Lu, X.; Yu, M.; Wang, G.; Zhai, T.; Xie, S.; Ling, Y.; Tong, Y.; Li, Y. H-TiO2@MnO2//H-TiO2@C Core–Shell Nanowires for High Performance and Flexible Asymmetric Supercapacitors. *Advanced Materials* **2013**, *25* (2), 267-272, https://doi.org/10.1002/adma.201203410. DOI: 10.1002/adma.201203410 (acccessed 2021/03/14).

(174) Zeng, Y.; Han, Y.; Zhao, Y.; Zeng, Y.; Yu, M.; Liu, Y.; Tang, H.; Tong, Y.; Lu, X. Advanced Ti-Doped Fe2O3@PEDOT Core/Shell Anode for High-Energy Asymmetric Supercapacitors. *Advanced Energy Materials* **2015**, *5* (12), 1402176, https://doi.org/10.1002/aenm.201402176. DOI: 10.1002/aenm.201402176 (acccessed 2021/03/14).

(175) Liu, Y.; Jiao, Y.; Yin, B.; Zhang, S.; Qu, F.; Wu, X. Enhanced electrochemical performance of hybrid SnO2@MOx (M = Ni, Co, Mn) core–shell nanostructures grown on flexible carbon fibers as the supercapacitor electrode materials. *Journal of Materials Chemistry A* **2015**, *3* (7), 3676-3682, 10.1039/C4TA06339B. DOI: 10.1039/C4TA06339B.

(176) Wang, L.; Feng, X.; Ren, L.; Piao, Q.; Zhong, J.; Wang, Y.; Li, H.; Chen, Y.; Wang, B. Flexible Solid-State Supercapacitor Based on a Metal–Organic Framework Interwoven by Electrochemically-Deposited PANI. *Journal of the American Chemical Society* **2015**, *137* (15), 4920-4923. DOI: 10.1021/jacs.5b01613.

(177) Lee, J. S.; Shin, D. H.; Jang, J. Polypyrrole-coated manganese dioxide with multiscale architectures for ultrahigh capacity energy storage. *Energy & Environmental Science* **2015**, *8* (10), 3030-3039, 10.1039/C5EE02076J. DOI: 10.1039/C5EE02076J.

(178) Guan, C.; Qian, X.; Wang, X.; Cao, Y.; Zhang, Q.; Li, A.; Wang, J. Atomic layer deposition of Co3O4 on carbon nanotubes/carbon cloth for high-capacitance and ultrastable supercapacitor electrode. *Nanotechnology* **2015**, *26* (9), 094001. DOI: 10.1088/0957-4484/26/9/094001.

(179) Kuok, F.-H.; Liao, C.-Y.; Chen, C.-W.; Hao, Y.-C.; Yu, I.-S.; Chen, J.-Z. Screen-printed SnO2/CNT quasi-solid-state gel-electrolyte supercapacitor. *Materials Research Express* **2017**, *4* (11), 115501. DOI: 10.1088/2053-1591/aa9405.

(180) Zhu, J.; Zhao, S.-X.; Wu, X.; Wang, Y.-F.; Yu, L.; Nan, C.-W. Wrapping RGO/MoO2/carbon textile as supercapacitor electrode with enhanced flexibility and areal capacitance. *Electrochimica Acta* **2018**, *282*, 784-791. DOI: 10.1016/j.electacta.2018.06.089.

(181) Wan, C.; Jiao, Y.; Liang, D.; Wu, Y.; Li, J. A high-performance, all-textile and spirally wound asymmetric supercapacitors based on core–sheath structured MnO2 nanoribbons and cotton-derived carbon cloth. *Electrochimica Acta* **2018**, *285*, 262-271. DOI: https://doi.org/10.1016/j.electacta.2018.07.036.

(182) Shao, J.; Li, Y.; Zhong, M.; Wang, Q.; Luo, X.; Li, K.; Zhao, W. Enhanced-performance flexible supercapacitor based on Pt-doped MoS2. *Materials Letters* **2019**, *252*, 173-177. DOI: 10.1016/j.matlet.2019.05.124.

(183) Han, Y.; Lu, Y.; Shen, S.; Zhong, Y.; Liu, S.; Xia, X.; Tong, Y.; Lu, X. Enhancing the Capacitive Storage Performance of Carbon Fiber Textile by Surface and Structural Modulation for Advanced Flexible Asymmetric Supercapacitors. *Advanced Functional Materials* **2019**, *29* (7), 1806329, https://doi.org/10.1002/adfm.201806329. DOI: https://doi.org/10.1002/adfm.201806329 (acccessed 2021/03/14).

(184) Howli, P.; Panigrahi, K.; Mitra, A.; Das, N. S.; Chattopadhyay, K. K. Textile-based RGO-muffled cobalt (II, III) oxide hybrid nano-architectures for flexible energy storage device. *Applied Surface Science* **2019**, *485*, 238-246. DOI: https://doi.org/10.1016/j.apsusc.2019.04.216.

(185) Mu, F.; Zhao, J.; Gu, C. Ultrathin porous NiMnO3 nanosheets on carbon cloth for use as supercapacitor electrode. *AIP Advances* **2020**, *10* (6), 065002. DOI: 10.1063/5.0009246.

(186) Rohith, R.; Manuraj, M.; Jafri, R. I.; Rakhi, R. B. Co-MoS2 nanoflower coated carbon fabric as a flexible electrode for supercapacitor. *Materials Today: Proceedings* **2022**, *50*, 1-6. DOI: 10.1016/j.matpr.2020.12.1054.

(187) Li, Z.; Ma, Y.; Wang, L.; Du, X.; Zhu, S.; Zhang, X.; Qu, L.; Tian, M. Multidimensional Hierarchical Fabric-Based Supercapacitor with Bionic Fiber Microarrays for Smart Wearable Electronic Textiles. *ACS Applied Materials & Interfaces* **2019**, *11* (49), 46278-46285. DOI: 10.1021/acsami.9b19078.

(188) Dolez, P. I.; Decaens, J.; Buns, T.; Lachapelle, D.; Vermeersch, O. Applications of smart textiles in occupational health and safety. *IOP Conference Series: Materials Science and Engineering* **2020**, *827* (1), 012014. DOI: 10.1088/1757-899x/827/1/012014.

(189) Dyatkin, B.; Presser, V.; Heon, M.; Lukatskaya, M. R.; Beidaghi, M.; Gogotsi, Y. Development of a Green Supercapacitor Composed Entirely of Environmentally Friendly

Materials. *ChemSusChem* **2013**, *6* (12), 2269-2280, https://doi.org/10.1002/cssc.201300852. DOI: 10.1002/cssc.201300852 (acccessed 2021/03/14).

(190) Bernardes, A. M.; Espinosa, D. C. R.; Tenório, J. A. S. Recycling of batteries: a review of current processes and technologies. *Journal of Power Sources* **2004**, *130* (1), 291-298. DOI: 10.1016/j.jpowsour.2003.12.026.

(191) Hall, M. Brits throw away 600 million batteries each year. businesswaste.co.uk waste management: 2021.

(192) Jeong, E. G.; Jeon, Y.; Cho, S. H.; Choi, K. C. Textile-based washable polymer solar cells for optoelectronic modules: toward self-powered smart clothing. *Energy & Environmental Science* **2019**, *12* (6), 1878-1889, 10.1039/C8EE03271H. DOI: 10.1039/C8EE03271H.

(193) Cao, R.; Pu, X.; Du, X.; Yang, W.; Wang, J.; Guo, H.; Zhao, S.; Yuan, Z.; Zhang, C.; Li, C.; et al. Screen-Printed Washable Electronic Textiles as Self-Powered Touch/Gesture Tribo-Sensors for Intelligent Human–Machine Interaction. *ACS Nano* **2018**, *12* (6), 5190-5196. DOI: 10.1021/acsnano.8b02477.

(194) Rotzler, S.; Kallmayer, C.; Dils, C.; von Krshiwoblozki, M.; Bauer, U.; Schneider-Ramelow, M. Improving the washability of smart textiles: influence of different washing conditions on textile integrated conductor tracks. *The Journal of The Textile Institute* **2020**, *111* (12), 1766-1777. DOI: 10.1080/00405000.2020.1729056.

(195) Tao, X.; Koncar, V.; Huang, T.-H.; Shen, C.-L.; Ko, Y.-C.; Jou, G.-T. How to Make Reliable, Washable, and Wearable Textronic Devices. *Sensors* **2017**, *17* (4). DOI: 10.3390/s17040673.

(196) Chen, Q.; Li, X.; Zang, X.; Cao, Y.; He, Y.; Li, P.; Wang, K.; Wei, J.; Wu, D.; Zhu, H. Effect of different gel electrolytes on graphene-based solid-state supercapacitors. *RSC Advances* **2014**, *4* (68), 36253-36256, 10.1039/C4RA05553E. DOI: 10.1039/C4RA05553E.

(197) Bae, J.; Song, M. K.; Park, Y. J.; Kim, J. M.; Liu, M.; Wang, Z. L. Fiber supercapacitors made of nanowire-fiber hybrid structures for wearable/flexible energy storage. *Angewandte Chemie - International Edition* **2011**. DOI: 10.1002/anie.201006062.

(198) Chen, T.; Dai, L. Flexible and wearable wire-shaped microsupercapacitors based on highly aligned titania and carbon nanotubes. *Energy Storage Materials* **2016**, *2*, 21-26. DOI: 10.1016/j.ensm.2015.11.004.

(199) Liu, C.; Zhao, S.; Lu, Y.; Chang, Y.; Xu, D.; Wang, Q.; Dai, Z.; Bao, J.; Han, M. 3D Porous Nanoarchitectures Derived from SnS/S-Doped Graphene Hybrid Nanosheets for

Flexible All-Solid-State Supercapacitors. *Small* **2017**, *13* (12), 1603494. DOI: 10.1002/smll.201603494.

(200) Liu, S.; Xie, J.; Li, H.; Wang, Y.; Yang, H. Y.; Zhu, T.; Zhang, S.; Cao, G.; Zhao, X. Nitrogen-doped reduced graphene oxide for high-performance flexible all-solid-state micro-supercapacitors. *Journal of Materials Chemistry A* **2014**, *2* (42), 18125-18131, 10.1039/C4TA03192J. DOI: 10.1039/C4TA03192J.

(201) Islam, M. R.; Afroj, S.; Beach, C.; Islam, M. H.; Parraman, C.; Abdelkader, A.; Casson, A. J.; Novoselov, K. S.; Karim, N. Fully printed and multifunctional graphene-based wearable e-textiles for personalized healthcare applications. *iScience* **2022**, *25* (3), 103945. DOI: 10.1016/j.isci.2022.103945.

(202) Ghasemi, F.; Jalali, M.; Abdollahi, A.; Mohammadi, S.; Sanaee, Z.; Mohajerzadeh, S. A high performance supercapacitor based on decoration of MoS2/reduced graphene oxide with NiO nanoparticles. *RSC Advances* **2017**, *7* (83), 52772-52781, 10.1039/C7RA09060A. DOI: 10.1039/C7RA09060A.

(203) Cai, F.; Tao, C.-a.; Li, Y.; Yin, W.; Wang, X.; Wang, J. Effects of amount of graphene oxide and the times of LightScribe on the performance of all-solid-state flexible graphene-based micro-supercapacitors. *Materials Research Express* **2017**, *4* (3), 036304. DOI: 10.1088/2053-1591/aa65fb.

(204) Beidaghi, M.; Wang, C. Micro-Supercapacitors Based on Interdigital Electrodes of Reduced Graphene Oxide and Carbon Nanotube Composites with Ultrahigh Power Handling Performance. *Advanced Functional Materials* **2012**, *22* (21), 4501-4510. DOI: 10.1002/adfm.201201292.

(205) Noh, J.; Yoon, C.-M.; Kim, Y. K.; Jang, J. High performance asymmetric supercapacitor twisted from carbon fiber/MnO2 and carbon fiber/MoO3. *Carbon* **2017**, *116*, 470-478. DOI: https://doi.org/10.1016/j.carbon.2017.02.033.

(206) Gao, W.; Singh, N.; Song, L.; Liu, Z.; Reddy, A. L. M.; Ci, L.; Vajtai, R.; Zhang, Q.; Wei, B.; Ajayan, P. M. Direct laser writing of micro-supercapacitors on hydrated graphite oxide films. *Nature Nanotechnology* **2011**, *6* (8), 496-500. DOI: 10.1038/nnano.2011.110.

(207) Wang, H.; Lu, Z.; Kong, D.; Sun, J.; Hymel, T. M.; Cui, Y. Electrochemical Tuning of MoS2 Nanoparticles on Three-Dimensional Substrate for Efficient Hydrogen Evolution. *ACS Nano* **2014**, *8* (5), 4940-4947. DOI: 10.1021/nn500959v.

(208) Lin, J.; Zhang, C.; Yan, Z.; Zhu, Y.; Peng, Z.; Hauge, R. H.; Natelson, D.; Tour, J. M. 3-Dimensional Graphene Carbon Nanotube Carpet-Based Microsupercapacitors with High Electrochemical Performance. *Nano Letters* **2013**, *13* (1), 72-78. DOI: 10.1021/nl3034976.

(209) Winchester, A.; Ghosh, S.; Feng, S.; Elias, A. L.; Mallouk, T.; Terrones, M.; Talapatra, S. Electrochemical Characterization of Liquid Phase Exfoliated Two-Dimensional Layers of Molybdenum Disulfide. *ACS Applied Materials & Interfaces* **2014**, *6* (3), 2125-2130. DOI: 10.1021/am4051316.